

**Histories and Mechanisms of Change in the Development of Shore
Platforms at Kaikōura and Rodney, New Zealand:
Application of Cosmogenic Nuclides and Numerical Modelling on Exposed Coastal
Surfaces**

Aidan Duart McLean

A thesis submitted to Victoria University of Wellington
in partial fulfilment of requirements for the degree of

Master of Science

In

Physical Geography



School of Geography, Environment and Earth Sciences

Victoria University of Wellington

2018

This thesis is dedicated to my Nana and Grandad, Lorraine and Ian Falgar

Abstract

Global sea level rise is contributing to the acceleration of cliff erosion rates in New Zealand, where it surpasses rates of uplift. A significant challenge facing scientists and managers is that we have no method for reliably extracting past rates of coastal erosion along harder rock cliffs over the time-scales that significant sea level change occurs (100s-1000s of years). This gap in knowledge is limiting efforts to model and understand the relationship between sea level rise and cliff erosion rates and what the form of that relationship is.

Cosmogenic Beryllium-10 analysis has been applied on two low angle shore platforms in New Zealand to produce chronologies of sea cliff retreat during the late-Holocene. Surface exposure ages were attained on a tectonically active platform at Kaikoura, Canterbury and a tectonically quiescent platform at Cape Rodney, Auckland. This is the first application of cosmogenic nuclides to a shore platform study in New Zealand and adds two new data-sets to the very small group of global shore platform chronologies.

Exposure ages show New Zealand platforms have developed in the late-Holocene. Long-term platform surface erosion rates at Kaikoura ($<0.2\text{mm a}^{-1}$) were found to be significantly slower than modern erosion rates ($>0.4\text{mm a}^{-1}$), potentially due to uplift driven positive feedback such as altered sea level position, driving up weathering rates on the tidally inundated platform. Nuclide concentrations at Okakari Point, Rodney, reveal a significant role of recent sea level fall after $\sim 4000\text{yrs BP}$, driving surface denudation (0.1mm a^{-1}). The long-term cliff back-wearing rate at Okakari point was found to be 24.66mm a^{-1} . Patterns in cosmogenic nuclide concentrations in New Zealand's shallow platforms differ from global examples recorded on steeper platforms. Exploratory numerical modelling was applied with the coupled Rocky Profile CRN model (RPM_CRN) to identify process relationships between key drivers within platform coastal systems and scenarios of sea level change and active tectonics.

This combined geochemical and numerical modelling study has shown that shore platforms in New Zealand have complex histories, with different potential driving forces at Kaikoura and Okakari. This highlights the local variability in platform development and cliff retreat, suggesting that estimates of future shoreline erosion will need to take local contingencies into account.

Acknowledgements

Firstly, the biggest thanks goes to my two great supervisors Kevin Norton and Mark Dickson. Kevin, your relaxed attitude, great advice and morning espressos have been hugely appreciated over the last two years. I am thankful for your guidance through this thesis and the opportunity to be your student. Mark, I am extremely grateful for the faith you put in me in allowing me to take on this project, your guidance and regular visits have been invaluable to me throughout this thesis, not to mention the funding you provided for various bits of work and conference attendance. I would also like to specially thank Hironori Matsumoto for providing me with his model, showing me the ropes and being available to help when it was needed. Further thanks to Martin Hurst for allowing me to use your model code and for the assistance in the field. And to Wayne Stephenson, thank you for assisting me with field work at Kaikoura and for the opportunity for me to help out with your re-surveying. This was a very memorable experience and your enthusiasm out in the field was motivating! Also for the ongoing contact and ideas you have helped me to realise in my thesis. I would also like to thank the Cosmo lab users, Ross Whitmore, Richard Jones, Jamie Stutz and Claire Lukens who helped me through working out lab procedures and for having great chat on those long days in the lab.

A big thanks to all my buddies in CO421, you guys made this time fun and rewarding and encouraged great excursions and adventures outside of the office. Without you guys the days would have been much longer and harder. Also, thanks to all the staff and students around the cotton building who have been great friends, helpers, advice givers and colleagues. To my wonderful partner, office mate and all round best friend Alicia Taylor, you have been the one who got me through, kept me in good spirits, and have always been there through it all, so thank you. To Mum and Dad, thanks for the support and encouragement in me perusing another degree. To my little brother, thanks for being such a cool bro and always telling me to keep at it! And finally, thanks to my Nana and Grandad, to whom I have dedicated this thesis, you have been huge supporters in my life and have always encouraged me to do the best I can, even though I know you're still not happy I moved out Nana.

Contents

Chapter 1: Introduction and Background	1
1.1 Introduction	1
1.2 Coastal Systems	6
1.3 Climate Forced Morphodynamic Change of Coastal Landforms	7
1.4 The Rocky Coast	9
1.5 Shore Platforms	10
1.5.1 Platform Development	11
1.5.2 Recent Research Developments	14
1.5.2 ii Micro-Erosion Meter Erosion Studies.....	15
1.5.2 ii Wave Breaking Studies.....	16
1.5.2 iii Scarp Investigations.....	17
1.5.3 Knowledge Gaps	18
1.6 Cosmogenic Analysis.....	19
1.6.1 Beryllium-10 Dating on Shore Platforms	20
1.6.2 Interpreting ¹⁰ Be Concentrations	23
1.7 Aims and Objectives.....	24
1.8 Thesis Structure	24
Chapter 2: Cosmogenic Nuclides	25
2.1 Cosmic Rays and Nuclide Production.....	25
2.2 Beryllium-10 production	28
2.3 Applications	30
2.3.1 Surface Exposure Dating.....	30
2.3.2 Dating of Eroded Surfaces	31
Chapter 3: Study Areas.....	34
3.1 Wakatu Point, Kaikoura Peninsula.....	34
3.1.1 Geomorphology.....	35
3.1.2 Geology.....	37
3.1.3 Tectonics.....	40
3.1.4 Climate.....	41
3.2 Okakari Point.....	41
3.2.1 Geomorphology.....	43
3.2.2 Geology.....	44

3.2.3 Tectonics	46
3.2.4 Sea Level Fluctuations	46
3.2.5 Climate	47
Chapter 4: Methods.....	48
4.1 Sample Collection	48
4.1.1 Wakatu	48
4.1.2 Okakari	50
4.2 Laboratory Procedures	52
4.2.1 Physical Pre-treatment.....	52
4.2.2 Chemical Pre-treatment.....	53
4.2.3 ¹⁰ Be Isolation	55
4.2.4 Accelerator Mass Spectrometry.....	58
4.3 Modelling.....	58
4.3.1 RPM Model Framework	59
4.3.2 CRN Model Framework	60
4.3.3 Coupled Rocky Profile and Cosmogenic Radio-nuclide Model (RPM_CRN).....	62
4.3.4 Model Testing	62
Chapter 5: Modelling Results	64
5.1 Model Parameters and Sensitivity Tests	64
5.2 RPM Scenario Testing	73
5.2.1 Sea Level Changes	73
5.2.2 Tectonic Perturbations.....	77
Chapter 6: Wakatu Point, Results and Discussion	82
6.1 Results	82
6.2 Best Fit Model Result.....	92
6.3 Discussion	94
6.3.1 ¹⁰ Be Concentrations	94
6.3.2 Exposure Ages	96
6.3.3 Surface Erosion Rates.....	98
6.3.4 Erosion Rates Disparity	99
6.3.5 Reconciling the Lowering Rates Disparity	100
6.3.5 i Geomorphic Solution.....	101
6.3.5 ii Effect of Timescale.....	102
6.3.6 Interpreting Best Fit RPM Simulation	105
Chapter 7: Okakari Results and Discussion	106
7.1 Results	106
7.2 Best Fit Model Results	114
7.3 Discussion	116

7.3.1 Concentrations	117
7.3.2 Exposure Ages	118
7.3.3 Surface Erosion Rates	120
7.3.4 The Role of Rock Strength	121
6.3.6 Interpreting Best Fit RPM Simulations	123
Chapter 8: General Discussion.....	134
8.1 Assumptions and Validity of the Rocky Profile Model	134
8.2 Insights from Platform Driver Sensitivity Analysis	134
8.3 Insights from Scenario Based Testing	134
8.4 Linking to Previous Cosmogenic Platform Investigations	134
8.5 Future Work.....	134
Conclusion	133
Reference List	135

Figures

Figure 1.1 Coastal cliff failure in Auckland.....	2
Figure 1.2 Coastal Morphodynamics	7
Figure 1.3 Shore Platform Types	11
Figure 1.4 Bartrum’s Platform Development Model	12
Figure 1.5 Relationship of Platform Gradient and Tidal Range	13
Figure 1.6 ‘Hump-shaped’ Nuclide Distribution	20
Figure 1.7 Nuclide Concentrations with Tidal Range.....	21
Figure 2.1 Cosmic Particle Cascade	27
Figure 2.2 ¹⁰ Be Production with Depth in Rock.....	30
Figure 2.3 Erosion Rates Plot	32
Figure 2.4 Shielding Ratio Plots.....	33
Figure 3.1 Satellite Image of Wakatu Point	35
Figure 3.2 Kaikoura Marine Terraces.....	36
Figure 3.3 Kaikoura Geological Map.....	38
Figure 3.4 Wakatu Point Platform Photos	39
Figure 3.5 Satellite Image of Okakari Point.....	42
Figure 3.6 Overlook of Okakari Point Platform	43
Figure 3.7 Okakari Point Sea Cliff	45
Figure 4.1 Wakatu Point Overview with Sample Locations	49
Figure 4.2 Okakari Point Overview with Sample Locations	51
Figure 4.3 Physical Sample Preparation for Okakari Samples.....	53
Figure 4.4 Wakatu Samples Under Microscope	54
Figure 4.5 Beryllium Isolation	58
Figure 4.6 Shielding by a Single Rectangular Obstruction	61
Figure 5.1 Model Outputs for Material Resistance	68
Figure 5.2 Final Modelled Profiles for Material Resistance	69
Figure 5.3 Model Outputs for Weathering Rate	70
Figure 5.4 Final Modelled Profiles for Weathering Rate	71
Figure 5.5 Model Outputs for Wave Efficacy	72
Figure 5.6 Final Modelled Profiles for Wave Efficacy	73
Figure 5.7 Model Outputs for Sea Level Fall Scenarios	74
Figure 5.8 Final Modelled Profiles for Sea Level Fall Scenario	75
Figure 5.9 Model Outputs for Sea Level Rise Scenario	76
Figure 5.10 Final Modelled Profiles for Sea Level Rise Scenario	77
Figure 5.11 Model Outputs for Uplift Step Size Test	78
Figure 5.12 Final Modelled Profiles for Uplift Step Size Test	79

Figure 5.13 Model Outputs for Uplift Recurrence Interval Tests.....	80
Figure 5.14 Final Profiles for Modelled Uplift Recurrence Interval Tests.....	81
Figure 6.1 Wakatu Point Shore Profile	84
Figure 6.2 Wakatu Point Nuclide Concentrations	86
Figure 6.3 Wakatu Sample Shielding Plots	87
Figure 6.4 Wakatu Point Exposure Ages	90
Figure 6.5 Wakatu Point Erosion Rates Plot	91
Figure 6.6 Model Output Wakatu Best Fit Scenario	92
Figure 6.7 Final Profile for Modelled Best Fit Scenario	93
Figure 6.8 Wakatu Point Terrace Erosion.....	97
Figure 6.9 Micro Erosion Meter Bolt Sites Wakatu Point.....	100
Figure 6.10 Schumer and Jerolmack 09 Erosion Rates Plot.....	103
Figure 6.11 Wakatu Erosion Rates over Averaging Time	104
Figure 7.1 Okakari Point Profile	107
Figure 7.2 Okakari Point Nuclide Concentrations	109
Figure 7.3 Okakari Sample Shielding Plots	110
Figure 7.4 Okakari Point Exposure Ages.....	113
Figure 7.5 Okakari Point Erosion Rates Plot	114
Figure 7.6 Model Output for Okakari Best Scenario	115
Figure 7.7 Final Profile for Modelled Best fit Scenario.....	116
Figure 7.8 Evidence of Surface Weathering at Okakari.....	122
Figure 8.1 Platform Gradient vs Tidal Range With NZ Platforms	130

Tables

Table 5.1 RPM_CRN Model Parameters	66
Table 6.1 ¹⁰ Be/ ⁹ Be Ratios and Total Nuclide Concentrations at Wakatu Point	85
Table 6.2 Exposure Ages Wakatu Point.....	88
Table 6.3 Exposure Ages, Time Averaged Scaling Schemes Wakatu Point.....	88
Table 7.1 ¹⁰ Be/ ⁹ Be Ratios and Total Nuclide Concentrations at Okakari Point.....	108
Table 7.2 Exposure Ages Wakatu Point.....	112
Table 7.3 Exposure Ages, Time Averaged Scaling Schemes Wakatu Point.....	112

Chapter 1: Introduction and Background

1.1 Introduction

The 15000km long coast of New Zealand is made up of globally representative morphologies (Bell & Gibb, 1996). It is a highly valued and marketable aspect of the national identity. Around the globe, coastlines exhibit the most significant accumulations of human population, due to many benefits associated with proximity to the coast. The primary drivers of this trend are the abundance of resources and the significant trading opportunities that exist at the coast (McGranahan et al., 2007). Wheeler, *et al.* (2012) also finds that there is evidence to suggest that living in close proximity to the ocean can have benefits to health and wellbeing. In New Zealand this trend is apparent, with sixty-five percent of the population living within 5km of the coast as of 2006 (Statistics New Zealand, 2009) and this proportion has likely increased further in the last decade.

This agglomeration at the coast, however, exposes people and infrastructure to a range of direct, natural and indirect, artificial (human caused) hazards, which are associated with coasts. This necessitates the need to identify and understand the hazards that people are exposed to, in order to manage and mitigate these hazards. Natural hazards occur at the coast when the pace of coastal change outstrips the ability for humans to react to the change, thus posing a danger to human life or infrastructure and causing environmental degradation. According to Gornitz (1991), the accentuated erosion of coastal cliffs results in increased instances of mass failure. Other hazards come in the form of episodic flooding from storm waves and surges and saltwater intrusion into aquifers and estuaries (Gornitz, 1991).

On rocky coasts the single, dominating coastal hazard is coastal landslides (mass failures). These occur on the rock coasts where there are coastal cliffs, as movements of large masses of rock, earth or debris, down a coastal slope (Bird, 2011). They are usually sudden, but infrequent and occur due to the concomitance of a range of complex factors, such as: seasonal variation in erosion processes; and the interaction between geo-mechanical factors and geomorphological factors (Budetta *et al.*, 2008). Mass failures result in the landward retreat of coastal cliffs, posing a significant risk to

coastal property which is often concentrated near coastal cliffs or bluffs due to their aesthetic value (Moore *et al*, 1999) see *figure 1.1*.



Figure 1.1: Residential property in Auckland (NZ) at risk of being undermined from cliff erosion after a mass failure event during Cyclone Debbie 2017. Photo Credit: NZ Herald

In New Zealand, cliffed coasts occur along approximately 23% of the total coastline (Kennedy and Dickson, 2007); thus they account for a large portion of coastal hazard in New Zealand. However, determining the degree of the hazard posed from coastal cliff erosion becomes challenging when accounting for changes to climate in the present day and into the future. One of the major controls on environmental boundary conditions on cliffed coasts is climate and therefore sea level. Walkden and Dickson (2008) find that increasing the rate of sea level rise results in an increase in the equilibrium rate of shoreline erosion of a soft rock coast. Given this relationship, it is clear that the rate of shoreline erosion along many erosional coasts must have already increased. This is down to the change in the rate of sea level rise that has already occurred over the last century. At the end of the twentieth century the rate of global mean sea level (henceforth GMSL) rise was between 1.5-2.0mm/yr this had already increased to between 2.4-3.8mm/yr by the beginning of the twenty-first century (Church *et al.*, 2013). Most projections of future sea level indicate that this rate will continue to increase, however, by how much depends of many factors. GMSL is currently projected to rise between 10-90cm by the end of the century (Church *et al.*,

2013), affected primarily by eustatic increases and thermal expansion. The problem this poses for geomorphologists is working out what the new cliff erosion rates will be, in order to equate these to the level of hazard that is posed to people and infrastructure along cliffed coasts.

Over the last century a great deal of research and debate has been conducted to understand the various processes on cliffed coasts. Despite this the processes remain poorly defined in terms of their relative influence in the development of the features over time. Also the rates of landform change along these coasts remain vague. In the past, research has focussed heavily on qualitative and exploratory descriptions of shore platforms and little attempt has been afforded to quantifying processes or measuring erosion rates (Stephenson, 2000). Because of this, many of the processes described on shore platforms have been inferred based on the form of the features (Mii, 1962). Stephenson (2000) argues that arguments tend to become circular as the processes, which are inferred from the form, are then used to evaluate further morphology. According to Woodroffe (2002) the lack of research in quantifying processes is due to the timescales involved with erosion of rocky coasts. They are so long that it has been too difficult to collect data to determine accurately which processes have produced the morphology.

Historical records, usually in the form of aerial photography, have been used in the past to determine cliff recession rates. Stephenson (2001) identifies that this method can be limited, in that there can be difficulties in pairing older imagery with newer images. There are also few historical records of coastal cliff retreat around the world that span longer than a few decades. Drawing erosion rates from these short-term data sets does not provide sufficient evidence to determine which processes dominate the erosive action at that coast. For example, a 10 year dataset may indicate imperceptible erosion until a single mass failure removes several meters from the coast at once. This does not provide any information about the regularity of mass failure or a reliable erosion rate.

A key aspect in the assessment of natural hazards is the analysis of the frequency of recurrence of hazardous events of differing magnitude, such as landslides and floods. Often this is assessed using short term datasets, as these are all that is available.

Extrapolating out trends of events from short term dataset can lead to drastic underestimation of event size and frequency. The only way to produce long term data sets which provide more precise indications of event frequency, is to use geologic markers, usually features in the system which mark out particular points in time. These markers include, but are not limited to: marine terraces, shore platforms, tephras in a sedimentary facies and nuclide concentrations in rocks.

This problem has led a number of coastal geomorphologists to take different approaches to work out longer-term erosion rates on cliffed coasts (e.g. Bell, 2007; Bradley & Griggs, 1976; Brooke *et al.*, 1994; Choi *et al.*, 2012; de Lange & Moon, 2005; Hurst *et al.*, 2016; Kirk, 1977; Porter *et al.*, 2010; Regard *et al.*, 2012; Rosser *et al.*, 2005; Stephenson *et al.*, 2010; Stephenson, 1997; Stephenson & Kirk, 2000a; Stephenson & Kirk, 2000b; Stephenson & Kirk, 1996). Shore platforms, a common feature along cliffed coasts, have been used as a record of sea cliff retreat and represent one of these geologic markers. Shore platforms are relatively flat intertidal rock features which form as a sea cliff retreats. The width of these features has been used to determine the rates of sea cliff recession in New Zealand (de Lange & Moon, 2005). However, this method involved using local sea level proxies to determine the likely initiation time of platform development. Assuming the initiation age can leave a significant margin for error, for this reason it is necessary to employ new measures to directly determine the ages of points on shore platforms.

Geochemical approaches which have existed for decades, but have not until recently been applied to the study of cliffed coasts, can be utilised in the pursuit of such data (Regard *et al.*, 2012). Absolute dating of shore platforms would enable the unravelling of long-term (10^3 - 10^5 year) histories of sea cliff retreat. Attaining such information would assist in determining the natural rates of cliff retreat and their possible responses to alterations in the pace of GMSL rise.

The approach referred to here is exposure age dating of shore platforms using the in-situ produced (produced in the matrix of the bedrock, i.e. not transported or deposited) cosmogenic radionuclide, Beryllium-10 (^{10}Be). The accumulation of the radionuclide ^{10}Be over time, which initiates when a surface is exposed to atmosphere, occurs at a known rate (Dunai, 2010). This enables workers to calculate the time when

the surface was first exposed, from the total concentration of the radionuclide in a sample collected from that surface. On shore platforms the initiation of that accumulation occurs as the cliff is eroded, exposing the platform surface. A collection of samples of the surface taken across a platform can be used to pinpoint the time of platform initiation and identify the chronology of its development, throughout the lifetime of the feature.

So far this approach has been applied in three separate studies, which have begun to develop the method towards a framework which can be applied in rocky coast settings. (Choi et al., 2012) carried out ^{10}Be dating on a shore platform along the western coastline of the Korean Peninsula in a macro-tidal coastal setting. This initial study focused around establishing an age for the platform and identifying any signal of complex exposure history. The study established that it was possible to apply the method ^{10}Be dating to shore platforms. Regard et al, (2012) produced the first framework for modelling exposure ages and erosion rates in the coastal setting, where a complexity of attenuating factors such as weathering and erosive processes can add significant error to the surface exposure ages if not properly modelled. This framework was then applied to a chalk shore platform in Northern France, another macro-tidal setting.

Most recently Hurst *et al*, (2017) further improved the method to account for additional sources of cosmic ray attenuation and thus lower rates of ^{10}Be production on shore platforms. These included topographic shielding from the sea cliff, beach or talus cover on the platform and water cover due to tides or changes to relative sea level (Hurst *et al.*, 2017). Additionally, they were able to better integrate the suite of erosive processes and styles of platform development into their framework. In Hurst *et al*, (2017) this framework was applied to another chalk shore platform along the coast of southern England. This study demonstrated the onset of rapid shoreline erosion during the late-Holocene (Hurst et al., 2016).

There now exists a relatively robust framework for assessing shore platform development over long time-scales using ^{10}Be exposure dating; however, it has not yet been widely applied to different coastal settings. The three existing applications of the method focus on regions where the tidal regime is macro-tidal and where there is

stable regional tectonics. Applying this method in regions where the tidal regime is different would allow the framework to be tested to see how it performs in places where platform development may have occurred in a different style. Also, as many coastlines occur in regions of tectonic dynamism, it would also be useful to test the framework along an active coastline, to determine the role of seismic events on platform development. For these reasons applying an updated version of this framework to New Zealand shore platforms would prove useful, not only in providing new chronologies to assess the development of New Zealand shore platforms and coastal hazards, but also to help to identify what further limitations this framework is still subject to; as well as identifying trends in shore platform development in settings analogous to many other coastal regions around the globe.

1.2 Coastal Systems

Features within the coastal zone can be related to the geological formations that are present at the coast such as outcrops of granite or rhyolite or they are related to erosion and the movement and deposition of sediments. Geologically controlled features might be cliffs, stacks, platforms or other hard coastal features (Bird, 2011). Soft sediment features can be beaches, estuaries and barriers. All coastal features in the shore zone are constantly being modified by wind and water associated processes, and this extends to all features of the wider coastal zone over variable timescales. It is the constant changing of coastal landforms and features which lead to their conceptualization as 'morphodynamic systems', systems which change over time due to erosion and sedimentation (Carter & Woodroffe, 1997). This approach to thinking about the coast as a morphodynamic system was first applied by Wright and Thom (1977), who viewed the coastal environment as a dynamic geomorphic system with identifiable inputs and outputs of energy and material, driven and controlled by environmental conditions (Masselink & Hughes, 2003). *Figure 1.2* shows their general conceptualisation of the coastal system.

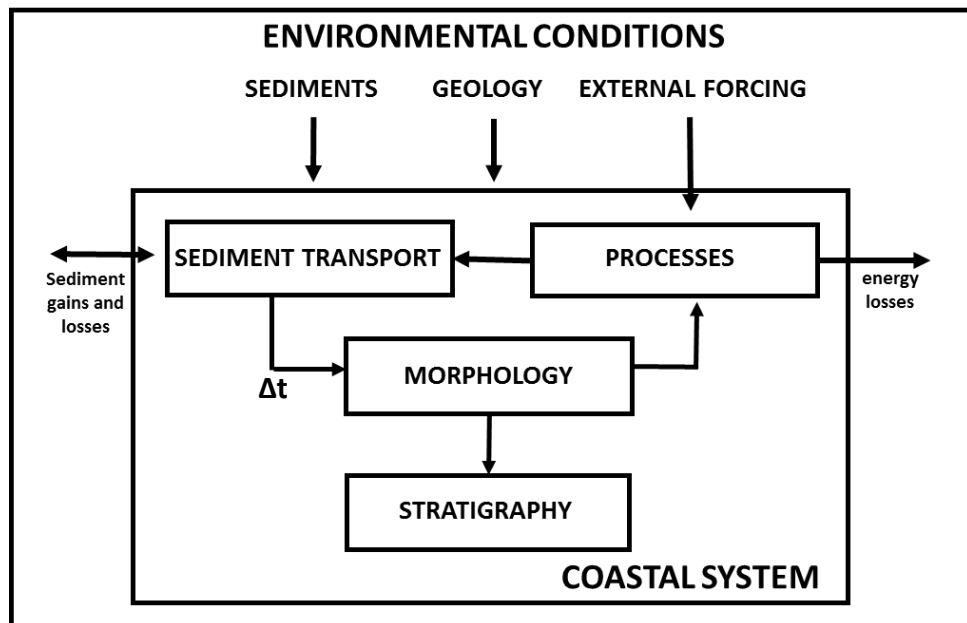


Figure 1.2: The primary components of coastal morphodynamics. The feedback loop present between morphology and process is responsible for the complexity of coastal evolution. The time component Δt signifies the inherent time dependence in the evolution of coasts. Source: Masselink and Hughes (2003)

Coastal morphodynamic systems are governed by a few fundamental properties. These properties are key to the interpretation of coastal features and include positive and negative feedbacks, equilibrium and relaxation time. Positive feedbacks push a system away from equilibrium through significant modifications of the system (Masselink & Hughes, 2003) such as a prolonged, rapid rise in sea level. This drives systems towards a new equilibrium state when natural thresholds are breached (Schumm, 1979). Negative feedbacks are dampening mechanisms, which act against departures from a particular state, maintaining equilibrium. Relaxation time relates to the morphological adjustment to perturbations and usually involves the redistribution of sediment, requiring a finite amount of time (Masselink & Hughes, 2003). The amount of time for adjustment is called the relaxation time. Coastal systems are controlled by further properties, however, these three are key in the interpretations in this thesis.

1.3 Climate Forced Morphodynamic Change of Coastal Landforms

Masselink & Hughes (2003) define two broad types of sea level change; relative sea level change and eustatic sea level change. Relative sea level change refers to the changes in sea level position relative to the land. This can be brought about by changes to the level of the sea or changes to the level of the land. Eustatic sea level refers to a

global change in sea level, due to change in the volume of water in the ocean and the volume of the ocean basins. In New Zealand most change in sea level is attributed to eustatic sea level change, especially throughout the early Holocene when sea level rose rapidly post-glaciation (Chappell, 1974). At local scales uplift histories need to be accounted for as parts of New Zealand are highly tectonically active.

Eustatic sea level fluctuates naturally with the glacial and inter-glacial cycle, dependent on the abundance of ice on the globe at any point in time (Lambeck & Chappell, 2001). The recent glacial maximum lasting from about 25ka to 18ka exhibited global mean sea level (GMSL) around 125m below present, while the last inter-glacial exhibited GMSL slightly higher than present day sea level (Lambeck & Chappell, 2001). These Quaternary records have been calculated through the use of a combination of geochemical, isotopic, and physical records. One such commonly cited record uses oxygen isotope ratios from ice cores and pairs them with the Huon Peninsula raised coral reef terrace record of sea level (Chappell et al., 1996).

The global oceans are strongly coupled with the atmosphere, meaning that any significant change in the atmosphere (most importantly, a temperature change) will drive changes in the ocean, which are usually alterations to GMSL (Manabe *et al*, 1991). The variation in sea level correlates well with global mean atmospheric temperature, indicated by paleo records (IPCC 2013). Present day GMSL trajectory is rising. Since the instrumental record began, a recorded 12cm sea level rise has occurred in the last century, mainly attributed to thermal expansion (Gornitz, 1991). The pace of this change in sea level is greater than the natural fluctuation speeds of the glacial/inter-glacial cycles (IPCC, 2013). In response, coastal features are being altered at higher rates than in the past.

Sea level change is not the only climatic driver of morphological change at the coast. There are also direct climatological impacts that can accelerate or decelerate coastal erosion. Most notably, changes in rainfall can alter the rates and quantities of terrestrial sediment transported to the coast (Coelho *et al*, 2009). Changes in the storminess of a coastal region can also influence upon regimes of erosion and aggradation.

For New Zealand it is projected that westerly wind flow will increase in frequency by 20% during spring and 70% in winter, but decrease by ~20% during summer and autumn (Mullan *et al.*, 2011). It is also projected that there will be a 3-6% increase in conditions conducive to storm development by 2070-2100 (Mullan *et al.*, 2011). These trends will contribute to enhanced erosive conditions along the east coast of New Zealand, where wave climates have typically been passive by comparison to the west coast. Fyfe (2003) also reports that there is likely to be a ~30% decrease in the number of extra-tropical cyclones which effect New Zealand. However cyclone intensity is expected to increase within the mid-latitudes (Fyfe, 2003). The impact of greater cyclone intensity would be marked on the New Zealand Coastline and may have significant implications on the rocky coast.

1.4 The Rocky Coast

Emery and Kuhn (1982) made the distinction that rocky or cliffed coasts make up around 80% of the global coastline, and that they occurred at all latitudes. This abundance estimate has largely been accepted in its reproduction in various later literature, however there has not been any substantial evidence to support this estimate (Naylor *et al.*, 2010). Naylor *et al* (2010) make the distinction that rocky coasts are those which are predominantly erosional, as opposed to depositional (beaches or dunes, etc.). Features associated with erosional coasts are steep sea cliffs, rocky headlands, sea stacks and islands, which are very different from the typical features of depositional coasts, i.e. beaches, dunes, estuaries and deltas.

Inman and Nordstrom (1971) investigated the importance of tectonic setting on coastal morphology, they found that at active margins, where collision between two tectonic plates occurred more mountainous coasts form. They state that along these coasts more erosional features are abundant. This is the categorization applies to most of the New Zealand coast, as New Zealand sits along an active margin (Inman & Nordstrom, 1971), however, there are significant variations from this classification. For example, much of the North Island exhibits depositional features such as estuaries, dune sequences and barriers. This is indicative that simple broad classification of coastal regions often does not capture the complexity of geomorphological processes and morphologies which occur in a region or locality.

Other coastal morphologies which generally appear on active margins are deep-sea trenches, narrow continental shelves and marine terraces (Griggs & Trenhaile, 1997). These are all present around the New Zealand coastal zone. Rocky coast features are not exclusively associated with active margins and there are many examples of rocky coast morphology along passive margins. These, however, are usually controlled by the structural grain of the landscape (Griggs and Trenhaile, 1997). For example, certain hard or high density lithologies favour the development of erosional features such as shore platforms, or plunging cliffs.

The processes which modulate the changes that occur along the rocky coast are well defined in the literature. The main processes which occur in the shore zone to erode rocky coastal features are: mechanical wave erosion, chemical and salt weathering, solution of limestones, bioerosion, frost and related mechanisms, and mass movements (Trenhaile, 1987). The role each of these processes play in the erosion of substrate along the coast varies significantly depending on the features present, their lithology and the environmental factors present. The erosive processes above fall into two categories: sub-aerial weathering and wave induced erosion (simply, above water processes and below water processes) (Trenhaile, 2002).

1.5 Shore Platforms

Shore platforms have been the focus of a century long debate around the processes (sub-aerial or wave induced) and environmental parameters which allow this feature of the rocky coast to form (Trenhaile, 2002). Despite the length of time this debate has been considered in the coastal science community, these features and the processes and interactions which form them, are still not as well classified or understood to the extent that depositional coast features and processes are. This is a reflection of the modern process oriented coastal literature focus, where greater emphasis is placed on beaches and other systems which respond rapidly to changing environmental conditions (Griggs & Trenhaile, 1997). This emphasis on depositional coasts is due to the fact that processes and changes on 'soft' coastal systems are easily observed and measured. 'Hard' coastal systems are less well suited to process studies as they are difficult to measure. However, a suite of new research into shore platform morphodynamics has stimulated new emphasis on understanding the longer-term

process relationships that occur on rocky coast features. Some of this research has likely been stimulated by the concern within the scientific community that there is need to understand the response of coastal morphodynamic systems to climate change (Naylor *et al.*, 2010).

1.5.1 Platform Development

Shore platforms are ubiquitous features of the rocky coast that form as a sea cliff retreats landward, leaving a nearly flat platform of rock within the intertidal zone. Shore platforms develop towards either of two end member states: sloping platforms and near-horizontal platforms; Sunamura (1992) gave these platform members designations, type-A (sloping) and type-B (near-horizontal)(*Figure 1.3*). Most platforms sit somewhere along a continuum between either end member state, reflecting the dominant processes that have formed that feature and the lithology of the parent rock.

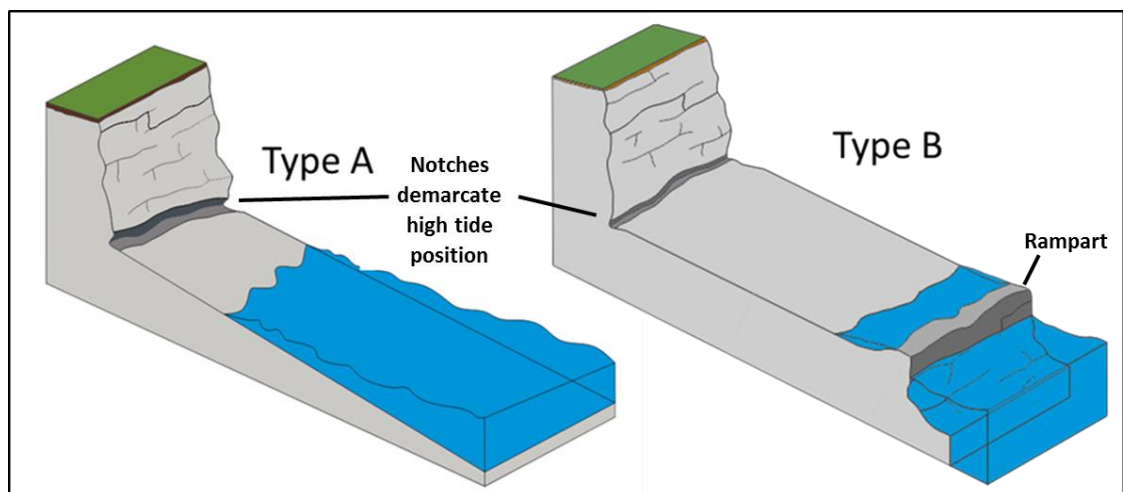


Figure 1.3: Schematic of the two end-member states of shore platforms as designated by Sunamura (1992). The type A platform slopes into the sea, so that the water column is deeper towards the outside of the platform. The type B platform terminates abruptly in a seaward scarp. At lower tides (as depicted) the platform can be free of water, save for rock pools. Both of these platforms have notches at the base of the cliffs, which form due to wave erosion.

Platform morphology was first described by Dana in 1849, when he discussed the ‘Old Hat’ platform (Bartrum, 1926). The ‘Old Hat’ (Mill Island or Kaiaraara Island, Northland, NZ) is a small island surrounded mostly with a type B shore platform. Dana did not prescribe a clear description of the causal process which led the platform to develop, however, he did suggest that it was not a structural feature, instead presenting the

idea that forces of erosion had cut into the bedrock to form the platform (Kennedy *et al.*, 2011). Recent work by Kennedy *et al.* (2011) validated this claim finding that most platforms in the same area were cut into the Greywacke parent rock.

The early work of Dana ignited a long-lasting debate as to which processes dominated the development of these features on erosional coasts: sub-aerial weathering or wave mechanical erosion (Trenhaile, 1987). Much of the early work around shore platforms went into categorizing the various forms which were identified around the world and contributing to the debate around process dominance (Ashton *et al.*, 2011). Bartrum (1926), proposed a theory that these 'Old Hat' (now type B) platforms form through the subaerial weathering of rock, allowing for failure of the slope to occur, driving the

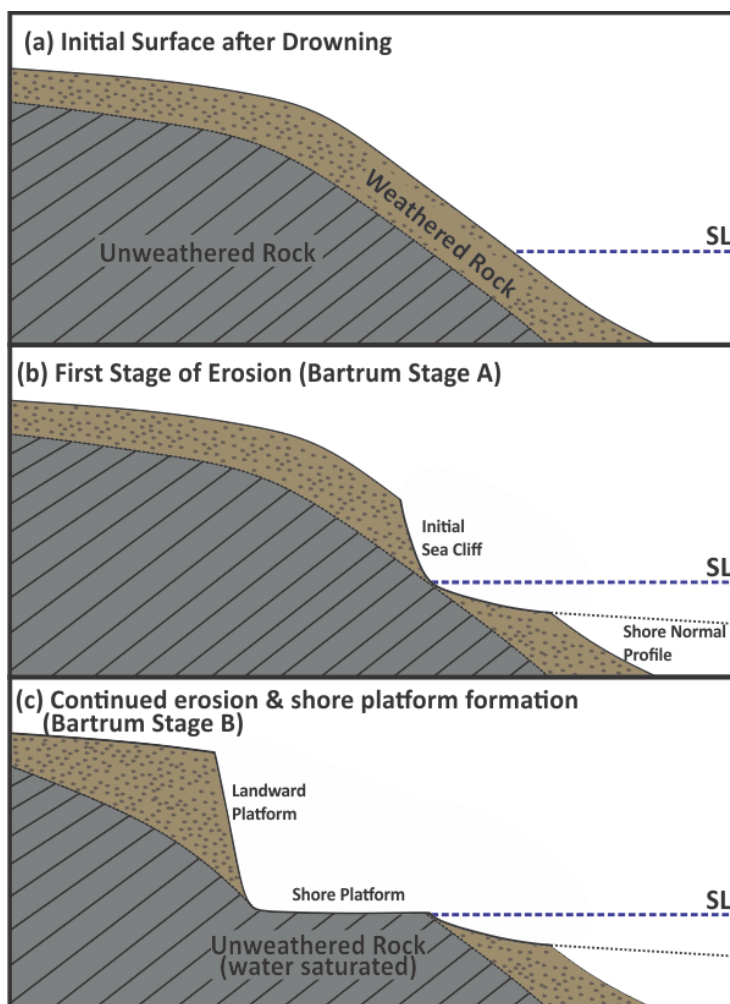


Figure 1.4: Bartrum's shore platform development model adapted into each progressive stage of shoreline truncation from the initial flooding surface, driving the first stage of erosion, through to creation of a shore platform as increasing weathering of the parent rock occurs. After Kennedy *et al.*, 2011.

retreat of the slope inland. Through the action of waves, slope debris are removed from the platform. This process is outlined in *Figure 1.4*. The theory states that the flat platform surface is the upper limit of the zone of permanent saturation, beneath which rock is sufficiently shielded from sub-aerial weathering (Bartrum, 1926). This explanation is useful when considering the development of type B platforms, but for type A platforms this is not a sufficient explanation of the processes.

The counter to Bartrum's theory is the theory that mechanical wave erosion causes wear in the weaker, weathered rock at the base of the cliff at the 'level of greatest wear' (Trenhaile, 1987), this theory is supported by a number of workers (Bradley & Griggs, 1976; Dana, 1894; Sunamura, 1978). The level of greatest wear, as Dana (1894) described, is located a little above the half-tide mark, this is the area most exposed to the action of waves. However, this position depends significantly on the energetics of the waves 'attacking' the shoreline. In a high-energy wave climate, the level of greatest wear would be higher, and in a low-energy wave climate, it would be lower. The typical sign of this type of erosive action would be a notch in the base of the cliff, marking the level at which the cliff is being preferentially eroded. It is the formation of a notch in the cliff base which can eventually undermine its structural integrity and cause the

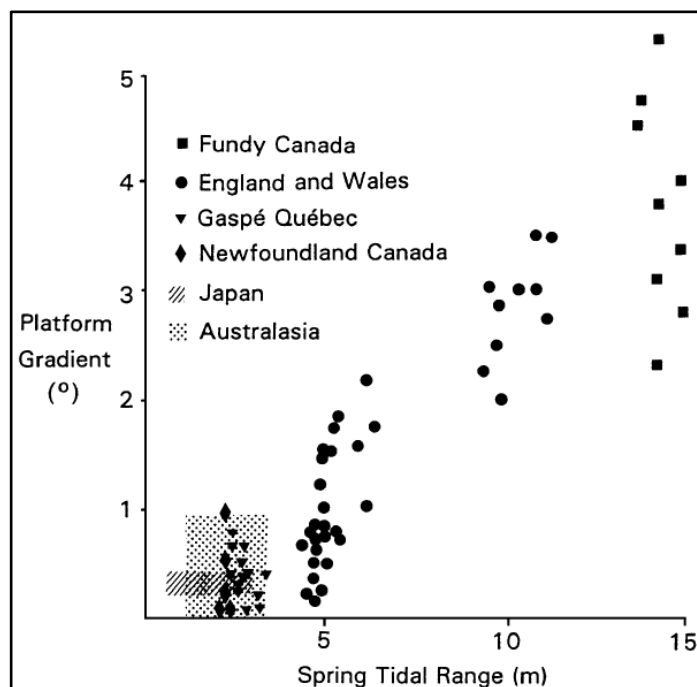


Figure 1.5: The relationship between shore platform gradient and tidal range. Each point represents the local mean of a large number of surveyed profiles. Source: Trenhaile (2002).

slope to fail. This theory describes the likely process through which the type B shore platforms along Auckland's (NZ) west coast formed. These platforms exhibit a high elevation platform, with the level of most wear, well above the mid-tide position (Bartrum, 1926).

Even considering both original theories for platform development, neither one successfully explains the formative process of type A platforms. The work of the various early workers on shore platforms had been conducted largely in ignorance of the fundamental role of tidal range (Trenhaile, 2002). A series of works by Trenhaile outline the relationship between tidal range and platform width and geometry (Trenhaile, 1974, 1987, 1999). There is a linear relationship between tidal range and platform gradient (*Figure 1.5*), which show that in regions with small (large) tidal range platforms usually develop into type B (type A) platforms (Trenhaile, 1999). This relationship occurs because, with a large tidal range the wave energy on shore is highly distributed throughout the tidal period, so that no point on the platform is worn to a significantly greater extent than another. This favours the development of a sloped platform profile. The occurrence of the mean water surface is increasingly concentrated between the mean high and low water neap tidal levels as the tidal range decreases (Trenhaile, 2002). As a response, the shore platform surface exhibits a lesser gradient, and terminates in a low tide cliff or scarp. Finally, the relationship between tidal range and platform width is debated, with some early workers suggesting there is a positive correlation (e.g. Flemming, 1965; Wright, 1969) and others a negative correlation (Trenhaile, 1999). This inconsistency between authors indicates that it might not be possible to identify a simple relationship between tidal range and platform width, meaning other factors must be at play in controlling the width of platforms.

1.5.2 Recent Research Developments

Most of the recent work outlined here is focussed on New Zealand literature and as such, much of this work has focussed on understanding type B platforms. Type B platforms are prominent around the New Zealand coastline; it is likely that this is due to the relatively low tidal range around most of the country. Bartrum (1926) stated

that New Zealand was an ideal place to study shore platforms due to their prevalence along parts of the coastline.

The recent geomorphological study of shore platforms has moved away from attempting to classify platforms into various sub-morphologies. The present focus is on examining the suite of processes at work on shore platforms and attempting to understand how these processes interact over as yet undefined timescales to build these coastal features. The recent body of work has focussed on modelling approaches to provide insights into the rates of platform development. Griggs and Trenhaile (1997) discussed how the slow rates of change on shore platforms made it very difficult for workers to study shore platform processes. Modelling approaches can be used to identify the transient responses of shore platforms to changes in boundary conditions and assess the long-term morphology forming processes, driving the development of the features. These approaches require information about how the processes at work on the platforms affect the various components of the system. This has in turn stimulated a lot of process-based investigation recently (Kennedy & Dickson, 2007).

1.5.2 i Micro-Erosion Meter Erosion Studies

The first of these process based investigations are micro-erosion meter (MEM) studies. These have been used to measure the small-scale denudation processes which occur atop the platform surface. Early work had interpreted the platform surface as undergoing negligible erosion, but through the employ of MEMs (and the more modern traversing MEM), it is possible to quantify these down-wearing rates and their contribution to the sediment budget (Stephenson, 2010). Early use of this device to measure denudation processes usually involved around a two-year deployment. This short period of time resulted in the requirement to extrapolate denudation rates out over longer time-scales (Hemmingsen *et al.*, 2007). While short-term measurements are useful for understanding the processes responsible for rock weathering, the extrapolation of these processes over time creates significant uncertainty. Stephenson & Kirk (1996) found that extrapolating out 2 year deployment denudation rates, resulted in the under-prediction of erosion at a decadal scale. Extrapolations of these trends to >100 year timescales becomes speculative, as the room for under or over-prediction of the rates of denudation become too great.

Deployment of MEM bolts on the Kaikoura peninsula shore platforms has more recently allowed for a greatly improved interpretation of the role of tectonic activity on shore platform development. Stephenson *et al.* (2017) conducted a resurvey of the Kaikoura shore platforms following the November 2016 7.8 (Mw) Kaikoura earthquake, which caused the uplift of 1.1m along that section of coast. Due to the significant change in the position of the platform within the tidal range, an increased number of wetting and drying cycles now occur on the outer platforms and are likely to result in higher rates of platform surface erosion in the coming years (Stephenson *et al.*, 2017). This idea was based on previous indications that sections of the platform surface exposed to more frequent wetting and drying cycles showed increased rates of this type of erosion, when compared to supra-tidal or sub-tidal sections of the platform (Stephenson & Kirk, 2000). The implication of this new work is that tectonic events have a significant impact on process regimes on shore platforms and should be considered a major morphological control when interpreting or modelling these coastal features.

1.5.2 ii Wave Breaking Studies

Another area that is being pursued in process based investigations are recent works on wave dynamics on shore platforms. These have led to greater understanding of the wave conditions that drive erosion of the sea cliffs. Ogawa *et al.* (2012) found that on wide type B platforms, different wave types dominate along different parts of the platform. Nearer the seaward terminus gravity waves were responsible for the wave conditions present. Gravity waves are depth limited, so they are attenuated significantly along the platform profile (Ogawa *et al.*, 2012). At the cliff toe, infra-gravity wave frequencies were dominant. These waves are not depth limited, allowing wave energy to be translated up to the cliff, with potential implication for rates of erosion. Ogawa *et al.* (2011) also demonstrated that there are different hydrodynamic zones across platforms and that these shift with the tidal cycle. These zones also correspond with wave heights, which diminish towards the cliff toe. This recent evidence suggests that insignificant wave energy reaches the cliff toe on type B platforms, suggesting that sub-aerial processes may be the dominant factor driving erosion on these platforms.

The use of tri-axial seismic sensors to measure high-frequency ground motions in a shore platforms and sea-cliffs have been undertaken in a few studies (Adams et al., 2002; Adams et al., 2005; Lim et al., 2011; Young et al., 2011; Dickson and Pentney, 2012). One of these investigations was carried out by Dickson and Pentney (2012), the purpose of which was to identify the impact of the wave climate on the shore platform and cliff. They found that at their study site at Okakari Point, Auckland, sea waves break on or against the shore platform causing seismic waves to pass through the platform and cliff rock. The frequency of the seismic waves increases with increasing wave height and the largest wave heights occurred with the falling tide (Dickson & Pentney, 2012). This type of measurement allows workers to determine the relative importance of wave action on the erosion of the cliff and platform. Similar work carried out in Kaikoura found that seismic waves influencing the sea cliff were too low to have any implication for the geomorphic structure of the feature, thus concluding that wave action was unimportant for erosion at that location (Stephenson & Kirk, 2000). Work by Stephenson and Thornton (2005) found that on an Australian shore platform a significant proportion of the wave energy as measured by its seismic signal was able to impact upon the geomorphology. These works have helped to identify the impact of wave breaking on shore platforms, the implication being a better understanding of why some platforms are wave dominated and others weathering controlled.

1.5.2 iii Scarp Investigations

One problem posed by the morphology of many shore platforms is determining the origin of the scarps at the seaward edge of type-B platforms. These features are present on most platforms around New Zealand. Bartrum (1926) proposed that this was a hillslope feature drowned by sea level rise and re-worked by sub-tidal erosion. This theory has been largely invalidated in recent times, as modelling carried out by Trenhaile (2010) showed that the accelerated Holocene sea level rise, from 9000 to 6500yrs BP would only have been able to produce slopes of 5° to 15°. This slope is not representative of the near vertical scarps on most shore platforms around New Zealand. It is possible that these scarp features formed because of lowering sea level since the mid-Holocene when sea level may have been around 5m above present day. Dickson and Pentney (2012) find that based on their data from Okakari point, it is likely

that platform formation occurred mostly under a higher sea level than at present. So, that now the present sea level height results in much of the wave energy being dispersed on contact with the seaward edge of the platform, developing the scarp. This evidence from Dickson and Pentney (2012) supports the idea that platforms develop under a negative feedback regime, put forward in Ashton et al. (2011). Where the action of waves creates a low-gradient platform geometry that effectively dissipates wave energy, the system eventually reaches a point where wave energy no longer affects the cliff stability, dampening the change.

1.5.3 Knowledge Gaps

While there has been a wide range of new research into shore platforms since 2000, the fundamental debate about process dominance on shore platforms is ongoing (Dickson & Stephenson, 2014). Process-based research is aiding in the development of shore platform process models, the aim of which is to quantify the rates of change on shore platforms and to unravel the histories of cliff erosion in various regional settings. One of the biggest obstacles to understanding shore platforms is the limited record of reliable long-term data that are available. Stephenson and Kirk's (2000a) work on shore platforms utilised MEM measurements over 30 years, one of the longest records of data available on a shore platform. This lack of long-term data makes it difficult to reconcile any understanding of the process at work on a platform with the rates at which they operate, to determine how much they influence platform morphology. Some recent work has been applied to date platform surfaces and sediments, to work out the time-spans through which they formed.

Brooke et al. (1994) employed three techniques to date coarse-grained deposits atop shore platforms along the Illawarra coast, New South Wales. Carbon-14 dating, Amino Acid Racemization (AAR) and Thermo-luminescence (TL) dating of deposited quartz sand and shells revealed a chronology for the formation of the deposits. They use the record of deposition as a record for platform formation. These techniques have been applied to the dating of marine terraces, the uplifted counterparts of shore platforms. The techniques, however, are subject to high uncertainty as they use deposits as a proxy for platform development, so they do not measure the platforms themselves.

Another recent technique used in Stone et al. (1996), measured in-situ Chlorine-36 accumulation in rock on a prominent 10-20m wide shore platform in western Scotland. Early work in the region suggested that the platform was Holocene in age, however, other workers had proposed the platform may have been cut over a longer time interval. This was theorised, as the erosion rates required to cut the surface during the Holocene would be in the order of 10-20mm per year, which is a much greater rate than on most present day platforms. The results of Stone et al. (1996), however, did suggest Holocene cutting during the late-glacial stadial, a period of cold climate and stable sea level which lasted ~1ka. They suggest that rapid shoreline erosion during this time could have occurred as a result of various freeze thaw processes acting upon the coastline. This indicates that platform cutting may not occur slowly and over drawn out periods, but instead may occur due to rapid bursts of incision. This is a particular example where a longer term dating technique has led to the identification of processes and erosional patterns that occur over long time scales, which may not be replicated under present climate and sea level conditions.

These dating techniques represent a possible new direction for the study of shore platforms. Attaining exposure ages for the rock on shore platforms would facilitate the calculation of long-term platform widening rates and surface erosion rates. Information about the speed of platform development and the timing of the development can help to determine which process are more important on different platforms. The application of the relatively new method of in-situ cosmogenic ¹⁰Be dating to shore platforms builds off the work of Stone et al.,(1996). In New Zealand applying this method would help to fill in significant gaps surrounding long-term platform development. This would be particularly useful on the east coast of New Zealand, where population densities are higher and the impacts of changing climate are likely to affect a greater number of people.

1.6 Cosmogenic Analysis

Cosmogenic nuclide analysis is a widely-used tool to address questions in Earth surface sciences. The use of this analysis was made possible by significant advances in analytical sensitivity, accuracy and precision in the late 1980s (Dunai, 2010). Since this time cosmogenic nuclides have been applied in a range of settings to develop

understanding about various geomorphic process which occur on the surface of the Earth. The application of terrestrial cosmogenic nuclides (TCN) has been revolutionary in the field of geomorphology through its use in determining surface exposure ages, burial ages, erosion/denudation rates and uplift rates. Cosmogenic nuclide analysis is being applied to new settings every year; one of these new settings is the rocky coastline, where shore platforms have been analysed. Only three studies have been conducted which have utilised cosmogenic nuclide dating on shore platforms (Choi *et al.*, 2012; Regard *et al.*, 2012; Hurst, *et al.*, 2016), none of which were in New Zealand. The method still requires further refining and the calculation of exposure ages requires more attention to increase precision and accuracy.

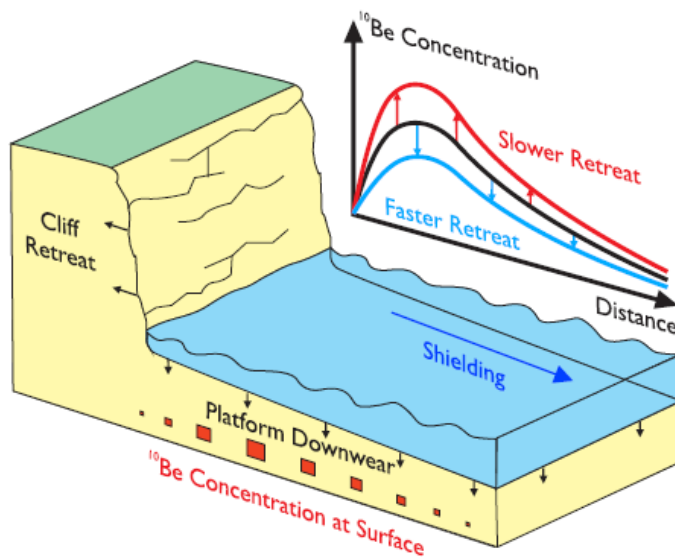


Figure 1.6: Schematic diagram showing the concentration of ^{10}Be across a shore platform. Cliff retreat exposes rock to cosmogenic rays; over time ^{10}Be accumulates in the exposed rock. Platform down wearing removes ^{10}Be rich rock, lowering the total accumulated ^{10}Be towards the seaward edge. Source: Hurst *et al.* (2016)

1.6.1 Beryllium-10 Dating on Shore Platforms

The three recent studies, noted above, are the first instances of this technique being applied in dynamic coastal settings. However, the application in a highly changeable environment introduces new complications to the calculation of ^{10}Be production rates, thus there is still a large degree of uncertainty in interpreting ^{10}Be concentrations and using these interpretations to understand the development histories of shore platforms. Regard *et al.* (2012) measured ^{10}Be concentrations on the flint-bearing chalk coastline near Mensil-Val, France. In this study, they developed a numerical model for

the prediction of concentrations of ^{10}Be on shore platforms as a function of the rate of cliff retreat. From model this they were able to estimate long-term average retreat rates, however, Hurst *et al.* (2016) note that the uncertainties in their analysis were large, reducing the resolution and confidence in their results.

The theoretical distribution of ^{10}Be concentrations across a shore platform (*Figure 1.6*), was estimated by Regard *et al.* (2012) and Hurst *et al.* (2017) to increase from the cliff base and then decrease towards the seaward edge of the platform. The decreasing trend towards the platform edge is due to the role of partial attenuation of the cosmic ray flux, from water cover and the erosion of the platform surface or seaward edge.

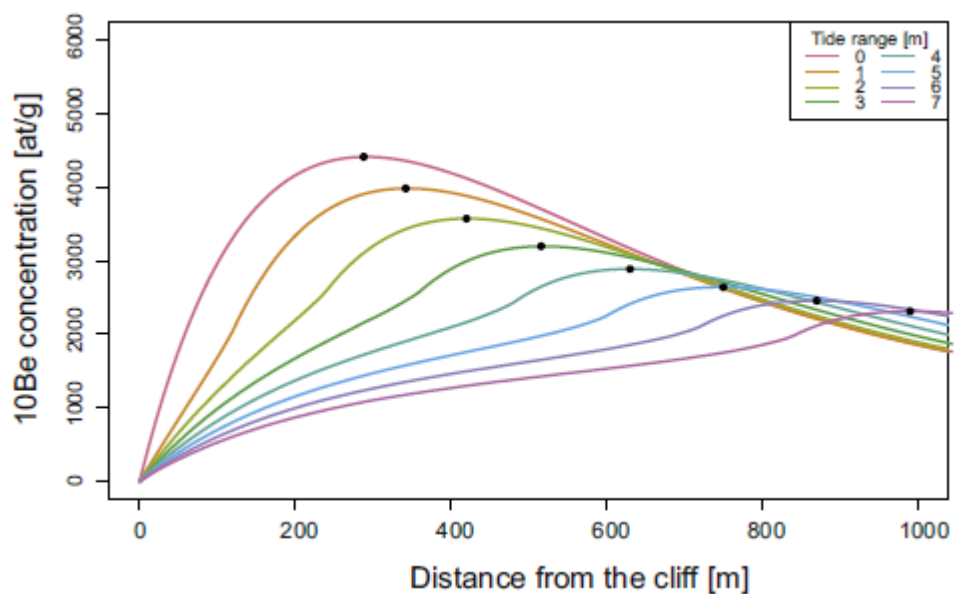


Figure 1.7: Predicted ^{10}Be concentration on rocks on the platform depending on the tide range. Cliff retreat rate is 0.1 m/yr, peak locations are shown by black dots.

Source: Regard *et al.* (2012)

This is described as a ‘hump-shaped’ distribution, because the largest concentrations are centred slightly seaward of the eroding cliff. The speed of cliff retreat inversely determines the magnitude of the humped distribution; if there is faster retreat then there is less time for nuclides to accumulate. However, this theoretical distribution is idealized and optimised for a type A (sloping) shore platform and there may be deviations from this distribution due to platform geometry, tidal range, or other complicating factors. One of the goals of this work is to explore the potential distributions of cosmogenic nuclides in non-sloping type B platforms.

The presence of water on shore platforms results in the attenuation of the cosmic ray flux. Water attenuates cosmic rays in a similar way to rock, however water is less dense and therefore is not as effective at attenuating the flux. The idealised distribution model (*Figure 1.6*) accounts for the depth of water across the platform, however it does not account for the harmonic fluctuation of tides, altering the depth of water cover on the shore platform though the duration of the tidal cycle (Hurst *et al.*, 2016). Regard *et al.* (2012) found that tidal range has a net effect of reducing the concentration of accumulated ^{10}Be on the landward portion of a sloping platform, due to periodic cover. At the same time, this tidal effect increases the concentration at the seaward portion of the platform, due to periodic exposure. The extent of this effect is illustrated in *Figure 1.7*, which shows how the tidal range can alter the position where the maximum accumulation will likely occur on the shore platform. The other factor which influences the accumulation in the seaward portion is denudation or platform erosion; this process lowers the measured TCN concentrations in samples from surfaces, by bringing material to the surface that had been previously shielded from cosmic rays (Dunai, 2010).

Another consideration for the modelling of ^{10}Be concentrations on shore platforms is the tendency for beaches to form on their more landward portions. Beach formation on platforms can be stimulated by supply of talus sediment from cliffs, or from sediment being transported from other parts of the local coastline (Hurst *et al.*, 2016). Naturally the presence of beach sediments atop a platform results in the partial attenuation of the cosmic ray flux; beach cover may be periodic and as such needs to be accounted for as a potentially dynamic factor in regulating accumulation of nuclides. The last major factor that plays a potentially significant role in altering the attenuation factor associated with water, is relative sea level change. Regard *et al.* (2012) noted an interesting relationship between the rate of nuclide accumulation and relative sea level rise: As RSL increased, accumulation rates also increased when the cliff was driven by a steady state retreat model. This is because less vertical down-wear of the platform is required to maintain the equilibrium state and there is also less loss of ^{10}Be enriched rock from the platform surface.

A final added complexity that may inhibit the ability to accurately model accumulation ages across a shore platform is the role of complex exposure histories. This role refers to instances when the actively accumulating platform has been exposed previously to the cosmic ray flux, but was subsequently buried during a period of lowered sea level. A realistic scenario of this may be a platform that developed during the last interglacial, followed by a period of burial during the glacial and then exhumation during the recent Holocene high-stand. Choi *et al.* (2012) proposed this process as an explanation for some of the exposure ages they measured on a shore platform in South Korea. It is difficult to prove such an occurrence using only ^{10}Be concentrations, as this only gives the minimum ages of the samples. This means the upper bound or maximum age would be unconstrained. To overcome this potential problem a coupled CRN approach could be used, measuring concentrations of both ^{10}Be and ^{26}Al . By plotting the $^{26}\text{Al}/^{10}\text{Be}$ ratio of a sample as an isotope ratio plot (colloquially known as a banana plot), the exact nature of the exposure can be determined, including instances of prior exposure and burial. This approach has been applied on various surfaces to uncover complex exposure histories (Gosse & Phillips, 2001).

1.6.2 Interpreting ^{10}Be Concentrations

The Cosmogenic Radio-Nuclide (CRN) model developed by Hurst *et al.* (2016) to predict ^{10}Be concentrations across a dynamic shore platform is applicable to shore platforms anywhere in the world. This model is coupled with a 'shore platform processes' model titled the 'Rock and Bottom Coastal Profile' (RoBoCoP) model, which simulates platform development. This coupling allows the user to alter platform development parameters to interpret the effects that different processes have on the ^{10}Be concentration profile. However the RoBoCoP model is limited in its ability to simulate the suite of processes which act to develop platform morphology, as discussed in the previous section. A new shore platform processes model, after Matsumoto *et al.* (2016) can be applied to this framework in place of RoBoCoP to formulate a new coupled CRN and platform processes model. The applicability of these two models will be discussed in detail in Chapter 4. This coupling produces a powerful tool for use in interpreting ^{10}Be concentrations measured across a shore platform profile.

1.7 Aims and Objectives

Wolman & Miller (1960, p.73) argued that “the evaluation of the relative importance of various geomorphic processes in a given region, as well as the relative effectiveness of events of different frequency, will require more detailed observations of the landforms themselves and of the processes operative on them”. The purpose of this work in accordance with this statement is to unravel the histories and the timescale through which shore platforms have developed at the Kaikoura Peninsula and Cape Rodney, and gaining a deeper understanding of the mechanisms of change driving the development of these platforms. The knowledge gained from these two case studies which share similarities with shore platforms around the globe will enable comparisons to be drawn between the development of shore platforms in active and quiescent tectonic regimes.

In order to conduct this research, the aims of this thesis are separated into two parts:

- First, to determine the developmental histories of shore platform evolution at Kaikoura and Rodney.
- Second, to assess the relative roles and importance of different processes/drivers in the formation of these shore platforms.

To address these aims the following objectives apply to each of the two aims respectively:

- To address the first aim, an analysis of the age and rates of erosion on the shore platforms was applied through cosmogenic ^{10}Be surface exposure dating at both localities.
- To address the second aim, exploratory numerical modelling will be carried out to simulate platform development and the associated ^{10}Be concentrations across the simulated platforms. This modelling will test for the impacts of different drivers on platform formation and extent.

1.8 Thesis Structure

The second chapter of this thesis, details the theory of cosmogenic nuclides and how they are applied to the dating of exposed surfaces. Chapter three of the thesis sets out the two study areas that are the subject of the cosmogenic analysis; their geological,

geomorphological, tectonic and climatic settings. The fourth chapter outlines the methodologies applied to investigating the shore platform case studies, including the field work and laboratory procedures. This chapter also covers the numerical modelling work that is conducted. Chapter five presents the results of the modelling work, including sensitivity analysis and scenario based testing. In chapter six, the results of the field and laboratory investigation of the Wakatu Point shore platform are reported and discussed, along with the best fit model scenario for this platform. Chapter seven presents the results and discussion for the Okakari Point shore platform case study. Finally, chapter eight is a general discussion of the exploratory modelling and the findings of both of the case studies.

Chapter 2: Cosmogenic Nuclides

2.1 Cosmic Rays and Nuclide Production

The production of cosmogenic nuclides occurs through the reactions of cosmic rays (atomic particles produced outside our solar system) with elements and molecules within Earth's atmosphere and lithosphere. Cosmic rays are particles (mostly protons, but also muons and alpha particles) which are accelerated to relativistic speeds; they are the signature of supernovae explosions and carry significant kinetic energy (Ackermann et al., 2013). The vast majority of the cosmic rays which encounter the Earth are produced within the Milky Way galaxy (Lingenfelter & Flamm, 1964), but some ultra-high energy, cosmic rays are produced outside of our galaxy. The energy associated with these cosmic particles can range from a few MeV (Mega-electron Volts, one MeV is equal to 10^6 eV) to 10^{20} eV; energy levels that are important at Earth's surface are those between 10MeV and 20GeV (one GeV is equal to 1000 MeV), as these are responsible for supporting secondary particle production (Masarik & Reedy, 1995). The mean cosmogenic energy spectrum and integrated cosmogenic ray flux is considered to be constant over the last 10Ma (Dunai, 2010), meaning that the rate of production of cosmogenic nuclides has not been altered by changes to the galactic cosmic ray flux. Cosmic rays, after spiralling through the terrestrial magnetic field, interact with the nuclei of atoms in the atmosphere to produce a cascade of

particles and reactions, with net energy being lost to the atmosphere and lithosphere (Gosse & Phillips, 2001).

The cosmic rays that reach the Earth's atmosphere are considerably affected by the earth's geomagnetic field. Low energy particles are more likely to be deflected by the field or otherwise take a complex pathway to reach the atmosphere usually being directed to the poles; high energy particles follow less complex pathways, as the abundant kinetic energy reduces the effect of magnetic deviations from their trajectory (Smart et al., 2000). Modulation of the cosmic particles with charge less than 10GeV occurs due to interaction of the solar wind cycle with the Earth's magnetic field. Consequently particles with 'rigidity' (momentum per unit charge) of, on average less than 0.6GV do not reach the Earth's atmosphere (Michel et al., 1996). Due to the strength of the geomagnetic field at low latitudes, the flux of cosmic rays entering the atmosphere is of higher energy. While at higher latitudes the overall cosmic ray flux is higher as more rays are able to pass into the atmosphere at parallels to the magnetic field, allowing more low energy particles through (Gosse & Phillips, 2001). Therefore the production of meteoric (produced in atmosphere) and in-situ (produced in lithosphere) cosmogenic nuclides is greater at high latitudes.

Upon contact with the atmosphere, cosmic rays react with atomic nuclei in primary spallation reactions. These occur when the incoming proton impacts the nucleus, sputtering off nucleons, mesons, pions, etc. (Dunai, 2010). These nucleons generally maintain the trajectory of the protons, depending on the energy of the nucleon; those with the highest energies show the lowest standard deviation for the angular distribution of scattered neutrons (Dorman et al., 1999). These scattered nucleons in turn react with other target nuclei in secondary cosmogenic reactions. This produces the cosmic cascade (*figure 2.1*) which is propagated through the atmosphere and into the first few meters of the surface rock.

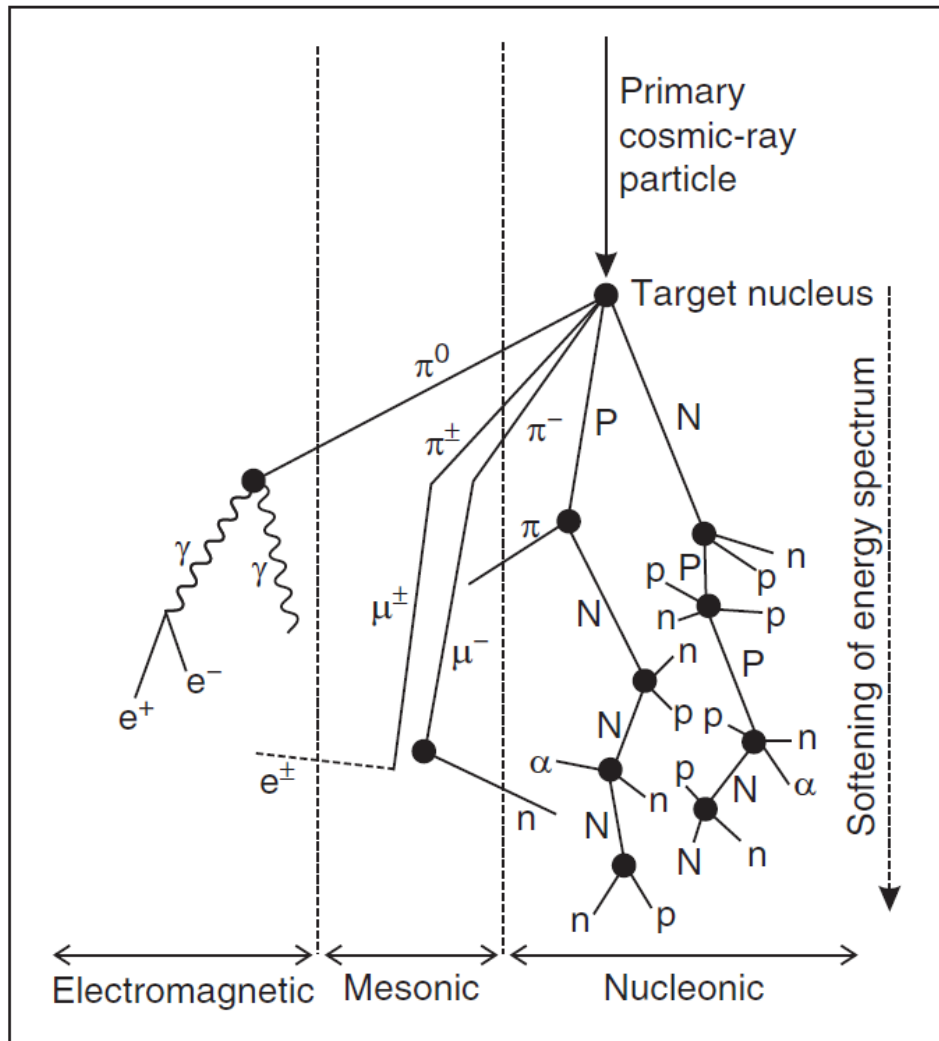


Figure 2.1: The major components of a cosmic-ray extensive air shower (cascade), showing secondary particle production in the atmosphere and rock. Abbreviations used: n, neutron, p, proton (capital letters for particles carrying the nuclear cascade), α , alpha particle, e^\pm , electron or positron, γ , gamma-ray, π , photon, ρ , pion, μ , muon.

Source: Dunai (2010).

Spallation also produces cosmogenic nuclides, as the atomic mass of nuclei is altered during the reaction. If this occurs in the atmosphere they are termed meteoric, while nuclides produced in rock are terrestrial cosmogenic nuclides (TCNs) (Gosse & Phillips, 2001). In rock the production rate of cosmogenic nuclides is attenuated at depth, so that spallation usually only produces measurable concentrations of nuclides within several centimetres of the surface. Spallation is not however, the only pathway through which TCNs are produced; negative muon capture causes muogenic reactions, which also produce cosmogenic nuclides. Negative muons, once stopped can be

captured by the electron shell of an atom; if this occurs they cascade to the lowest shell, where they are captured by the nucleus. This results in the one proton being neutralised, thus producing a cosmogenic nuclide. Muons decay rapidly (lifetime $\sim 10^{-6}$ seconds) and they do not have high reactivity like other secondary cosmic particles, as such they penetrate much deeper into rock, up to several 10s of meters or more (Gosse & Phillips, 2001).

2.2 Beryllium-10 production

One of the 'useful' cosmogenic nuclides that is produced in quartz (SiO_2) is Beryllium-10 (^{10}Be). This is an alkali earth metal which is part of a group called the cosmogenic radio nuclides (CRNs), meaning that they undergo radioactive decay (Dunai, 2010). Beryllium has one stable nuclide, ^9Be and two radio nuclides, ^{10}Be and ^7Be . Beryllium-7 is not useful for the dating of geologic events, due to its short half-life of 57 days (Nishiizumi et al., 2007). ^{10}Be is considered a useful TCN because it is long-lived, with regard to most modern morphologies, with a half-life of $1.36 \pm 0.07\text{Ma}$ (Chmeleff et al., 2010). It also has low background concentrations in rock due to its radio-active decay, meaning that old ($>1.38 \pm 0.07\text{Ma}$) ^{10}Be is removed from the system through extinction. There are several reaction pathways through which ^{10}Be is produced in-situ. The primary pathways are: spallation reactions with the target elements O and Si (96.4% of production), and negative muon capture in the target elements (3.6% of production) (Heisinger et al., 2002). Meteoric ^{10}Be is also produced in the atmosphere at much greater rates than in rock (Gosse & Phillips, 2001); this can be problematic for measuring in-situ produced ^{10}Be , as samples can become contaminated from the meteoric portion being absorbed onto and deposited in rock from meteoric waters. The component of meteoric ^{10}Be in rock is termed 'garden variety' by Nishiizumi *et al.*, (1986).

Beryllium-10 can be used in Earth Sciences to determine the exposure ages of rock. Rock does not contain any cosmogenic ^{10}Be prior to its exposure to the atmosphere. Once a rock or surface does become exposed to the cosmic ray flux, cosmogenic nuclides begin to accumulate. In exposed rock ^{10}Be is accumulated at a known rate (which does vary with time), this is because of the constant flux of cosmic rays bombarding every point on the Earth at any given time. There are two primary controls

on the accumulation rates of ^{10}Be in rock, these are: attenuation and energy. Gosse and Phillips (2001) demonstrated that the production rate of ^{10}Be in rock is depth-dependent, given in *figure 2.2*; production attenuates rapidly with depth. The energy of cosmic rays determine a particle's ability to penetrate through the geomagnetic field, as discussed earlier. Thus, there is latitudinal variation in the production of ^{10}Be . Finally, because the cosmic ray flux losses energy further down the cascade, surfaces at higher altitude are exposed to a larger flux of cosmic rays. So, at higher altitudes accumulation of ^{10}Be is faster than at low altitudes (Stone et al., 1998). The production rate of ^{10}Be is referenced to sea-level high latitude (SLHL) and scaled to the elevation and latitude of the sample site (*figure 2.2*). The production rate for ^{10}Be at the surface, at SLHL is $3.92 \text{ }^{10}\text{Be atoms g}^{-1} \text{ yr}^{-1}$ (Borchers et al., 2016).

Scaling factors are used to account for various sources of attenuation or shielding of the cosmic ray flux at a given position on the Earth's surface. These scaling factors need to be applied in the calculation of accumulation rates, otherwise the exposure age estimates will be incorrect. The spatial scaling factor accounts for the variations in production at geomagnetic latitude and altitude; the most widely used scaling model is that of Lal (1991), however this model overestimates the contribution of muon capture to the production rate of TCNs (Gosse & Phillips, 2001). Topographic shielding has the most potential to alter the cosmic ray flux at a given position, and topographic scaling is used to account for this factor. For a flat, horizontal and un-shielded surface, the production rate is attenuated with depth, but when there is an obstruction to the cosmic ray flux the effect is expressed in two ways: firstly, there is a decrease in the overall rate of production of nuclides due to some portion of the spectrum being blocked by the higher surrounding topography; secondly, there is a change in the effective attenuation length because the shielded particles tend to be those approaching at shallow angles and be of lower energy (i.e. attenuation length increases with shielding) (Dunne et al., 1999).

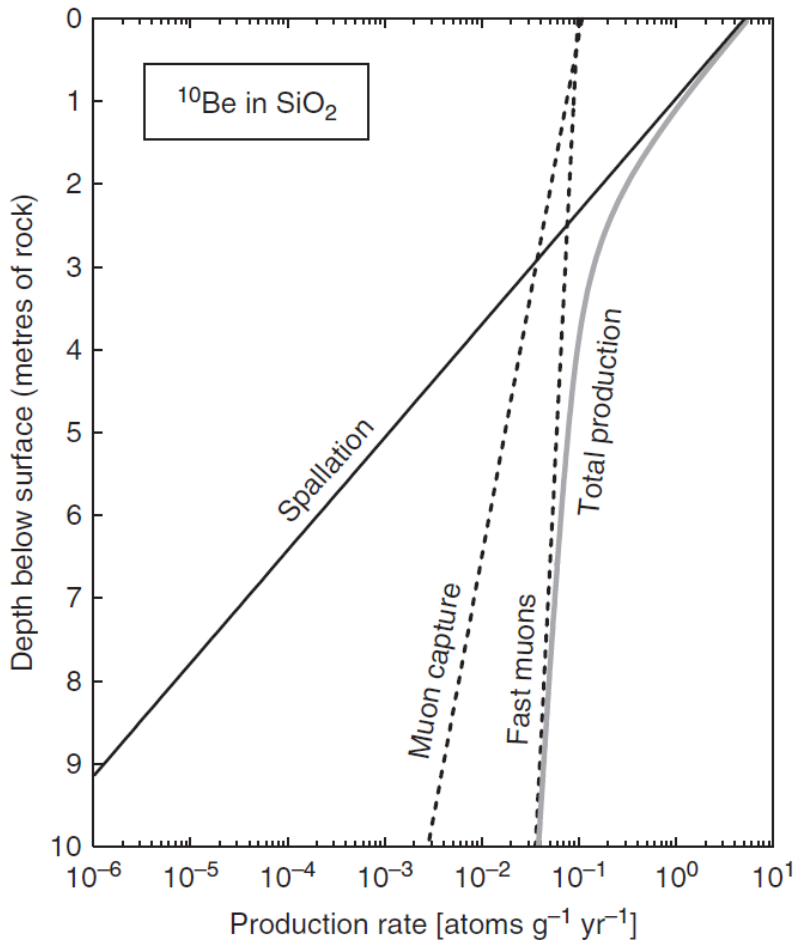


Figure 2.2: ^{10}Be production as a function of depth below surface at sea level and high latitude. Calculated using a rock density of 2.7 g cm^{-3} . Source: Dunai (2010).

2.3 Applications

2.3.1 Surface Exposure Dating

Beryllium-10 concentrations and the concentrations of other cosmogenic nuclides are measured for the application of surface exposure dating on a diverse range of landforms to understand geomorphic evolution (e.g. Owen et al., 2006; Stone et al., 1998; Wells et al., 1995). As long as a surface remains relatively stable and is continuously exposed at the surface then the concentration of accumulated cosmogenic nuclides can be used to date the surficial rock (Dunai, 2010). The method of surface exposure dating can be applied across the full range of climate settings and a wide range of lithologies (Gosse & Phillips, 2001). Some diverse examples of the application surface exposure dating include: the dating of rock slide debris, to assess

the timing a possible causes of major rock slide events following de-glaciation in Graubünden, Switzerland (Ivy-Ochs et al., 2009). The method has been used to constrain horizontal translational slip rates along the San Andreas fault by dating offset surfaces (van der Woerd et al., 2006). Locally, surface exposure dating has been used to date exposed boulders on glacial moraines to determine the timing and extent of glacial advance and retreat in New Zealand and associated regional climate fluctuations (Schaefer et al., 2009).

2.3.2 Dating of Eroded Surfaces

On any given surface that is dated with the exposure dating method the surface may have been eroded since its exposure. Erosion on an exposed surface impacts upon the calculation of exposure ages due to the removal of nuclide enriched material from the surficial rock (Dunai, 2010). Lal (1991) introduced this equation to accurately describe the accumulation of cosmogenic nuclides in a surface with a constant erosion rate ε :

$$C_{total}(t, z) = C_{inh}(z)e^{-t\lambda} + \sum_i \frac{P_i(z)}{\lambda + \rho\varepsilon/\Lambda_i} e^{-\rho(z_0 - \varepsilon t)/\Lambda_i} \left(1 - e^{-(\lambda + \rho\varepsilon/\Lambda_i)t} \right) \quad (2.1)$$

Where C_{total} is the concentration of the radionuclide in the material. The first term $C_{inh}(z)e^{-t\lambda}$ gives the inherited nuclide concentration (if this can be determined); t is the time of exposure (years); i represents the different nuclide production pathways; P is the nuclide production rate at the target surface (atoms $g\ yr^{-1}$) (with relation to latitude and altitude); λ is the decay constant of the measured nuclide; ρ is the density of the material ($g\ cm^{-3}$); Λ is the mean free path for cosmic rays ($g\ cm^{-2}$) and z_0 is the initial shielding depth (cm).

The second term in the equation is accumulation through time of an eroding surface. With faster erosion C_{total} is reduced. If the erosion rate is high enough it will eventually reach an equilibrium with accumulation, where the erosion is equal to the production of the TCN; this is called secular equilibrium (Figure 2.3). Z in this equation is sample depth. It shows that occasional burial will reduce C_{total} . On platforms this can be either water or sediment. If a sample is buried at any depth below a column of water or a

layer of sediment or rock for any period of time, the attenuation of the cosmic ray flux (P_z) is increased. As a result the shielding ratio for that sample will increase, this relationship is shown in *figure 2.4*.

By using equation 2.1 it is possible to use the total number of accumulated nuclides in a sample to calculate surface exposure ages. The community of cosmogenic nuclide researchers have developed resources for use in calculating cosmogenic exposure ages from total concentration, location and shielding information. The most commonly used tool is the CRONUS Earth online calculator (Balco et al., 2008). This is the tool used in this thesis for the calculation of exposure ages from ^{10}Be concentrations across shore platforms.

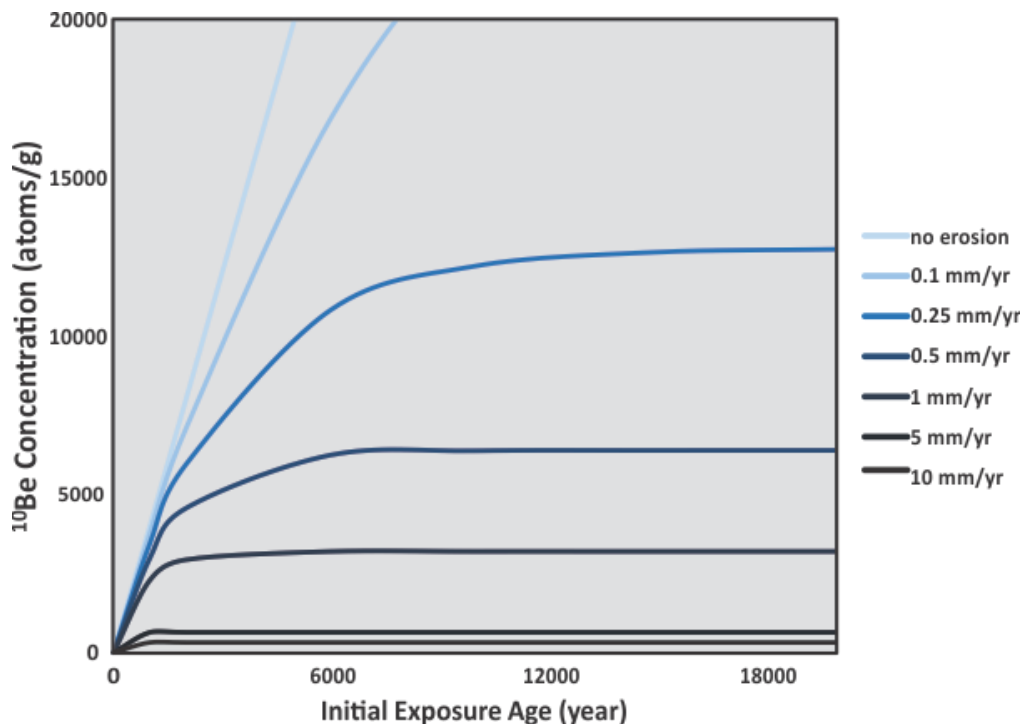


Figure 2.3: The plot shows the impact of erosion on exposure age. Faster erosion rates reduce the total concentration of atoms in a sample. The curves representing higher rates of erosion reach secular equilibrium in less time. Once secular equilibrium is reached no age information can be gained from a sample. The curves shown here are based on sea level at a latitude of 42° S .

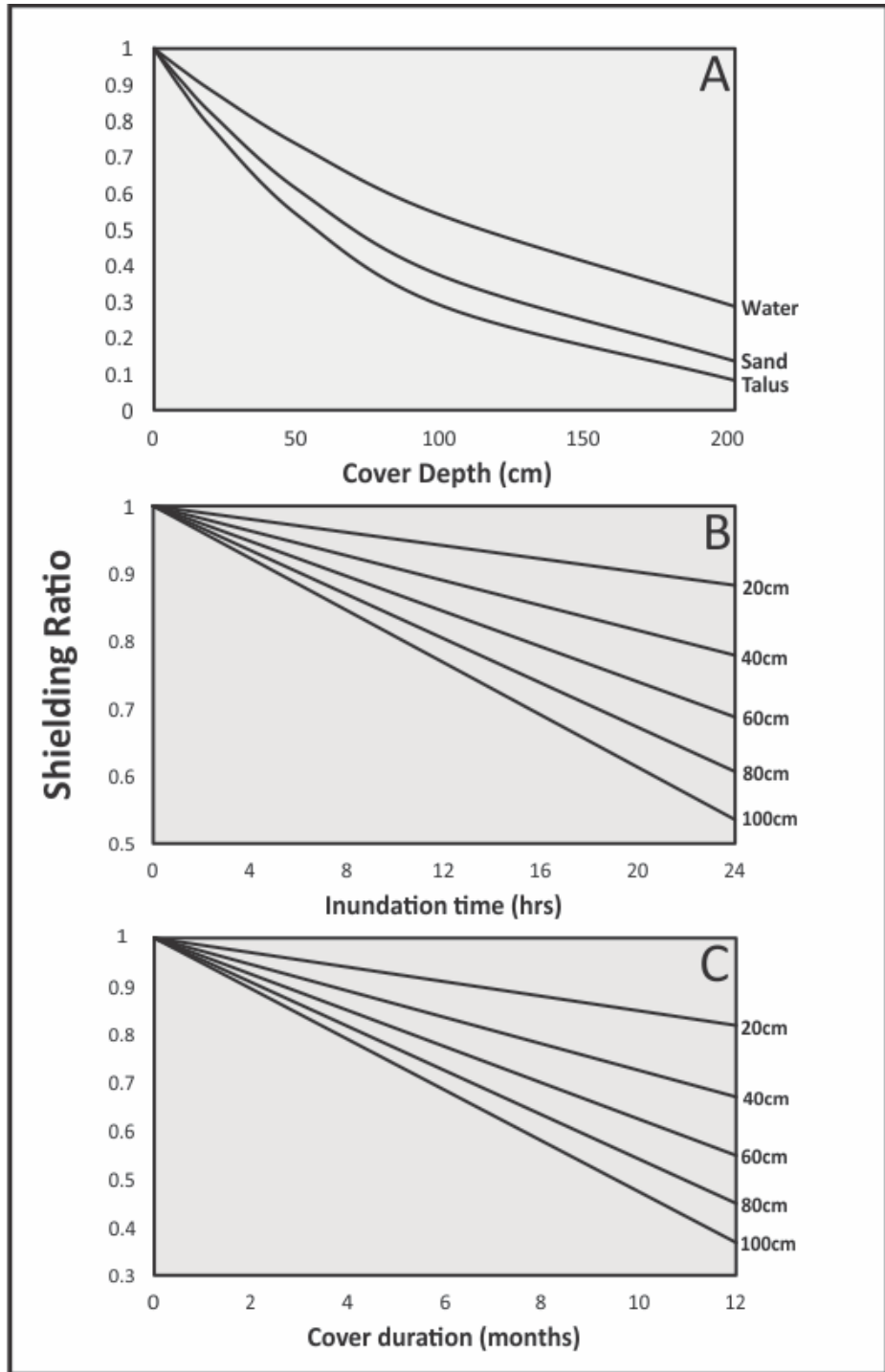


Figure 2.4: Plots demonstrating the impact of material cover depth through time on shielding. (a) shows the change in shielding value for increasing depth of cover with three different cover types of varying density, water (1g/cm^3), sand (1.6g/cm^3) and talus (2g/cm^3). Shielding value of 1 means there is no shielding, value of 0 means the position is fully shielded. (b) Change in shielding over the course of a day for water of increasing depths. Shown over 1 day due to the short duration ebb and flow of water cover from tides. (c) Change in shielding over the course of a year for sand cover of increasing depth. Shown over 1 year due to the long period oscillations in beach formation and removal on shore platforms.

Chapter 3: Study Areas

The following chapter reviews the two study areas investigated for the purpose of this research, both of which are located on the coast of the two main islands which make up New Zealand, the North and South Islands. New Zealand is located in the Pacific South East and sits within the Zealandia micro-continent (Mortimer et al., 2017). The exposed land-mass and its geography are the result of the obliquely converging Pacific and Indo-Australian tectonic plates, which also drive abundant volcanism and tectonism across the country.

3.1 Wakatu Point, Kaikoura Peninsula

Wakatu Point located at 42°24'53.0"S 173°42'20.0"E is one of three flat protrusions into the sea on the north east facing side of the Kaikoura peninsula in North East Canterbury in the South Island. The Kaikoura peninsula extends 4.5 km seaward, perpendicular to the predominant northeast-southwest strike (Kirk, 1977). Of the 5.2km² area that the peninsula covers approximately 0.77km² is intertidal (Kirk, 1977). The peninsula has been the subject of much scientific interest due to the geological and biological changes which have occurred in response to the recent 7.8M_w Kaikoura Earthquake (Little et al., 2018; Stirling et al., 2017). However, the peninsula coast has also been the subject of much long-term geomorphic investigation by Kirk (1977) and later by Stephenson (1997). Due to the prior coastal research at the site and the ideal lithology; notably the presence of chert nodules within the limestone shore platform, the site at Wakatu Point (*figure 3.1*) was chosen as an ideal location for exposure dating on a shore platform. Some of the major features near the Kaikoura Peninsula include the Seaward Kaikoura ranges, the Kowhai and Hapuku River catchments which deliver sediment south and north of the peninsula respectively, and a number of known active faults. These include the Hope fault (seaward section) which is one of the major splays off the Alpine Fault, the Hundalee Fault, Point Kean Fault and the Upper Kowhai Fault. The remainder of this section deals with the geomorphology, geology, tectonics and the climate of the study area.



Figure 3.1: Satellite image of the Wakatu Point shore platform, the central of the three points. The image is captured at a high tide, therefore the full extent of the platform (shown by the black line) is not visible beneath the water level. The built up area behind the platform may be a raised, sediment covered portion of the same platform. The box in the inset image shows the location of Wakatu point on the Kaikoura Peninsula, east of the main town belt.

3.1.1 Geomorphology

There are three main physiographic units at Kaikoura as identified by Chandra (1968); the peninsula block; beach ridges and raised beach ridges; and hard rock areas and alluvial fans. On the peninsula block there is a flight of five marine terraces; uplifted shore platforms, which comprise much of the surface area of the peninsula, rise to the highest point on the peninsula at 108m (Stephenson, 1997). There are a number of

shallow depressions or dolines within the surface of some of the terraces, which are notable mainly within terrace II. Stream channels have also heavily incised the terrace sequence toward the south eastern block of the peninsula, causing the development of the numerous alluvial fans depositing on the modern surfaces. Ota *et al.* (1996) identified the elevations and positions of the five terraces (Figure 3.2). The elevations reported were:

Terrace I at 95-108m,

Terrace II at 75-83m,

Terrace III at c. 64m to the west and 35-55 to the east,

Terrace IV between 46 and 58m and

Terrace V at c. 38m

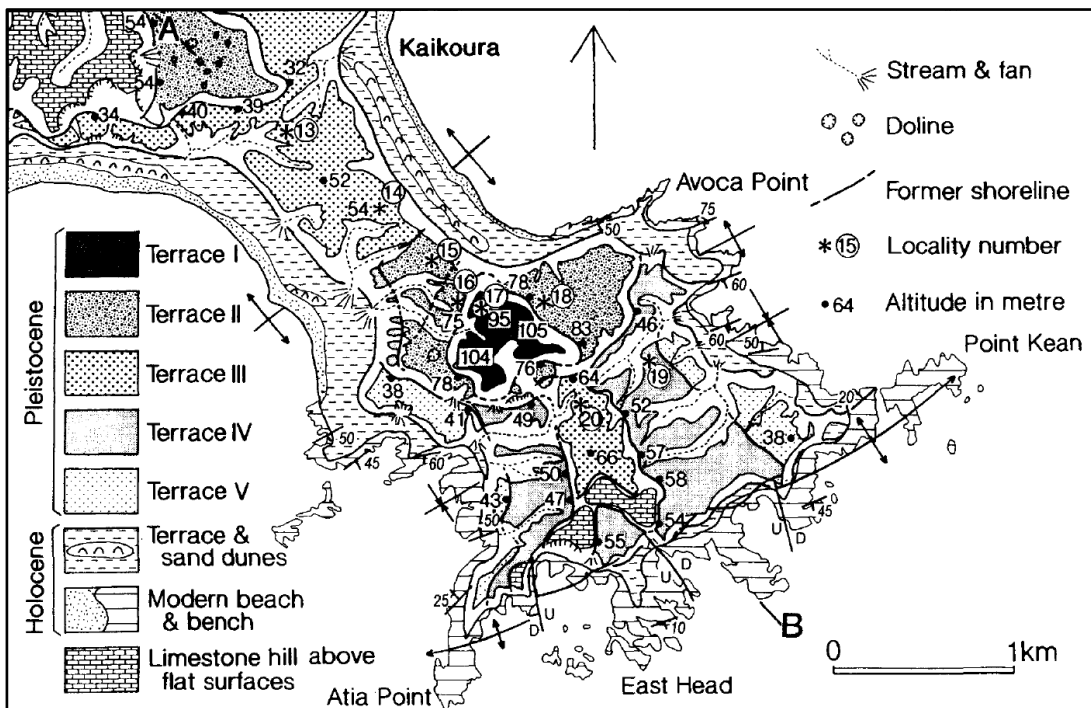


Figure 3.2: The major geomorphological features on the Kaikoura peninsula. The extent of the five Pleistocene marine terraces is shown, along with younger features. Shore platforms are shown all around the peninsula. The area behind the Wakatu Point shore platform, next to Avoca Point is represented as a Holocene terrace. Locality numbers refer to auger hole positions taken from each terrace from Ota *et al.* (1996).

Source: Ota *et al.* (1996)

Westward tilting of the peninsula surfaces accounts for the elevational variation of the terraces. Terrace I was dated using amino acid racemisation of molluscs from a sandy shell bed at 6m depth in an auger hole. This placed the terrace age at $110\text{ka} \pm 20\text{ka}$,

forming during either oxygen isotope stage 5c or 5e (Ota et al., 1996). Dates for the remaining terraces were attained from correlation to sea level high-stands from Chappell and Shackleton (1986). This places terrace II at 96 ± 5 ka; terrace III at 81 ± 5 ka; terrace IV at 72 ± 3 ka; and terrace V at 59 ± 3 ka (Ota et al., 1996).

Most of the 'hard rock and alluvial fan block' falls into the coastal margin of the peninsula, with shore platforms backed by cliffs surrounding all of the southeastern area of the peninsula. There are also a number of raised sea caves around the peninsula and two lagoons developed behind sandy barriers at Wairepo and Mudstone Bays (Stephenson, 1997). Wakatu Point, located on the northern shore of the peninsula is a 160m wide shore platform with a gently sloping relief, facing northeast. The platform is not continuous alongshore as it narrows immediately to the north west and southeast. To the northwest of the platform lies Avoca point, a similar protrusion to Wakatu point, there is another similar platform feature immediately to the south east next to Armers Beach. These three platform features make up a larger three pronged intertidal trident that protrudes out from an undated, likely Holocene in age terrace. Between each of the prongs are shallow bays where waves have been concentrated and funnelled up to the shore line, where there is evident shoreline erosion into a grassy bank. The shore flanking the south-eastern side of Wakatu Pt. has been partially armoured with rip rap to protect against this erosive wave action.

3.1.2 Geology

The sedimentary rocks which make up the Kaikoura peninsula are upper-Cretaceous to middle-Miocene in age. Starting from lower to upper series the peninsula consists of the Mata series rocks, which are late-Cretaceous in age; these are the Bluff sandstone which is overlain by the Seymour Group, which is also largely made up of sandstone. The Bluff sandstone, however, contains conglomerates, the clasts of which consist of chert, vein quartz and a range of volcanics (Rattenbury et al., 2006). Next are the Paleocene to Eocene Dannevirke series rocks; at Kaikoura these form part of the Muzzel group rocks, which are made up of the Mead Hill formation and the Amuri limestone. The older Mead Hill formation consists of limestone with abundant nodular chert, which is overlain by the younger Amuri limestone. The Amuri limestone is made up of hard siliceous limestone, micritic limestone or interbedded limestone and marls

(Rattenbury et al., 2006). The Landon series, formed during the Oligocene, contains the Spyglass formation, which is another limestone. Finally there are the early to middle Miocene Pareora-Southland Series, which contain the Waima Formation, consisting of sandstone and mudstone.

As seen in *figure 3.3*, the oldest rocks of the Bluff sandstone and the Seymour group occur at the isthmus; moving southeast there is a narrow band of the Mead Hill formation which outcrops at Avoca point and at South Bay. The Amuri limestone crops out in a thick band next to the Mead Hill Formation from Avoca point to South Bay, and in another band along the seaward-most flank of the peninsula. The Oligocene limestone which overlies the Amuri occurs in two thin bands, one from Armers Bay to South Bay and the other slightly seaward of the Amuri at East Head. The rest of the peninsula is made up of the Waima formation.

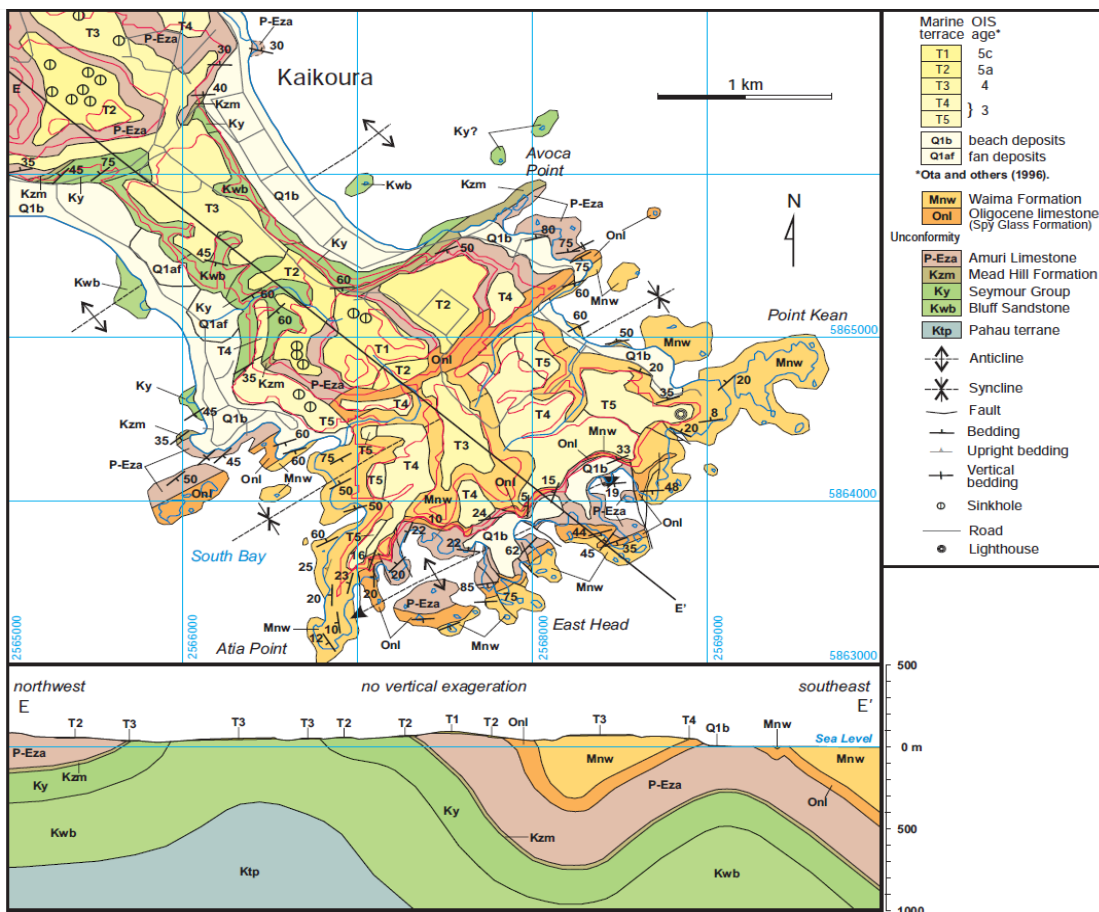


Figure 3.3: Geological map of the Kaikoura Peninsula indicating where the different units outcrop and the structural grain of the landscape. As in figure 3.2 the terrace positions are also noted. Source: Rattenbury et al., (2006)

The shore platforms surrounding the peninsula are formed primarily in the Amuri limestone and the Waima formation sand and siltstones. The Amuri limestone is distributed with a number of minor strike-slip and dip-slip faults and is subject to localized folding (Duckmanton, 1974). The structure of the peninsula consists of two anticlines bounding either side of an asymmetrical syncline aligned north-east to south-west (Stephenson, 1997). As a result, the shore platforms around the Kaikoura

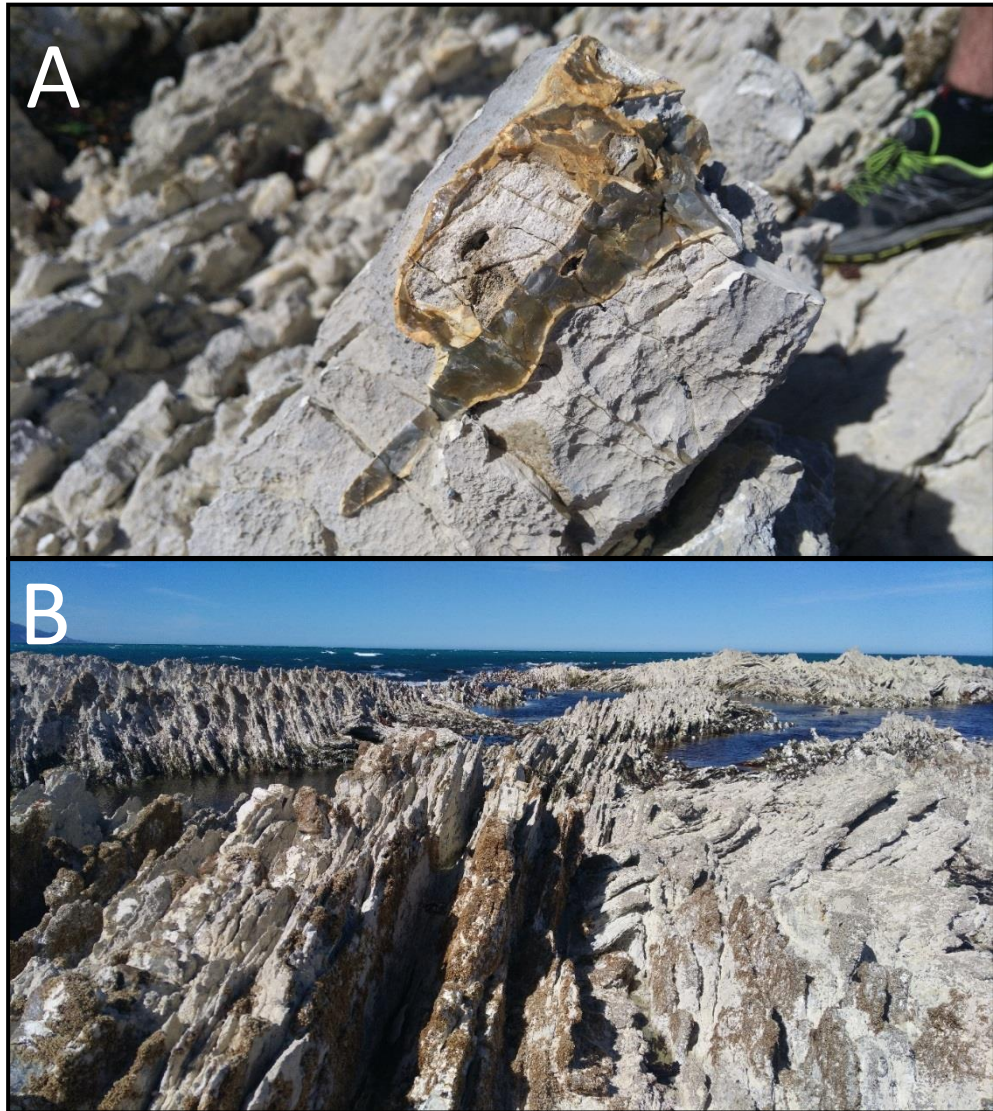


Figure 3.4: Photographs of the Wakatu Point shore platform high tide: (a) Nodular Chert in Amuri limestone at Wakatu Point. (b) Irregular platform shape at Wakatu Point, caused by tight folding in exposed Amuri limestones (high tide).

peninsula are heavily controlled by the geology present. The shore platform at Wakatu point is cut into Amuri limestone and contains abundant nodular chert (*Figure 3.4a*).

The Amuri at this locality appears to be interbedded limestone and marls that is tightly folded, causing an irregular platform shape (*figure 3.4b*).

3.1.3 Tectonics

The sequence of Quaternary marine terraces making up the Kaikoura peninsula suggest a strong tectonic control exists in the development of the Kaikoura peninsula and its surrounding shore platforms. Ota et al. (1996) found that the Holocene uplift rate along the Kaikoura coastline is $\sim 1\text{mm a}^{-1}$, a rate that is fairly consistent throughout the Pleistocene. The two uppermost marine terraces in the sequence (terraces I & II) exhibit a northwest tilting about 20m/km. The extent of this tilting is not consistent with the other younger terraces indicating a change in the axes of warping. The fault which may have driven this uplift and tilting is the seaward section of the Hundalee Fault roughly 5km southeast of the Peninsula (Ota et al., 1996). However, seismic mapping since the recent 2016 Kaikoura earthquake has revealed the previously unmapped, offshore Point Kean Fault which ruptured along 2.1km $\sim 10\text{km}$ northeast of the peninsula (Stirling et al., 2017). This Point Kean Fault may be the dominant driver of uplift at Kaikoura; if not, it is still likely to be an important component of the uplifting of Kaikoura.

Uplift at the Kaikoura Peninsula appears to be intermittent, with significant uplift events occurring between periods of slow subsidence, equating to an overall uplifting trend. This has caused the rapid stranding of shore platforms, forming the raised marine terraces. While the youngest marine terrace (terrace V) is attributed an age $\sim 60\text{ka}$ (Ota et al., 1996), Duckmanton (1974) reports on numerous identifiers of continued uplifting through the late Pleistocene and Holocene. Surveys of raised beaches at localities around the peninsula showed consistent elevations between the raised and modern beach heights with a difference of $\sim 2\text{m}$; this illustrates a recent uplift event of around 2m. Duckmanton (1974) dated this event using peat deposits from Wairepo lagoon cores taken behind the raised barrier beaches, attaining a minimum age of $360 \pm 90\text{yrs BP}$, placing an upper bound at around 1000yrs BP. If an event of this magnitude occurred within the proposed time period, it would have had some impact on the development of the modern shore platforms around the peninsula.

3.1.4 Climate

The climate at Kaikoura is temperate as the area is largely sheltered from the prevailing westerly air flow over New Zealand by the mountains immediately west of Kaikoura. Winds are predominantly southerly, with secondary flow from the north-east (Kirk, 1977). Climate data from an automated weather station at 105m elevation on the Kaikoura peninsula are collected by the National Institute of Water and Atmospheric Research (NIWA) The average annual rainfall for the years 1981-2010 is 710mm a⁻¹ with 16 ground frost days annually. The warmest monthly average temp occurs in January at 16.4°C, with the coldest average month being July with 8.1°C. Swell and storm waves affect the peninsula from south, southeast and northeast (Stephenson & Kirk, 1996). Stephenson (1997) reports that wave conditions throughout most of the year (48%) are smooth with maximum wave heights of 0.5m. Waves 0.5-1.25m occurred 17% of the year, this represents slight waviness, while 4% of the year waves in excess of 1.25m occurred. The upper bound of significant wave heights around Kaikoura is 2.44m (Kirk, 1975). Ocean conditions at Kaikoura tends to be calm throughout most of the year, punctuated with short periods of intense storm wave activity, driven by the progression of cyclonic disturbances tracking southwards along the east coast (Kirk, 1977). Seasonality appears to have no influence on the occurrence of storms. Tides at Kaikoura are semi-diurnal with up to 20% diurnal inequality in the magnitude of high water, with the daytime high usually being larger (Kirk, 1977). The mean tidal range is from 1.36m to 2.57m (Kirk, 1977), which makes it a meso-tidal regime.

3.2 Okakari Point

Okakari point is a largely dissimilar site to Kaikoura, which offers up points of comparison for surface exposure dating on different shore platforms within a different coastal and geological setting. Located at 36°15'37.0"S, 174°15'04.0"E, the platform at Okakari Pt. is a perfect example of a sub-horizontal shore platform. Okakari Point (*figure 3.5*) which sits on the Cape Rodney coast roughly mid-way between Pakiri and Leigh in Auckland's northeast, is part of a mainly rocky coastal section which spans roughly 15km around the Cape Rodney headland. Immediately east of the shore platform at Okakari Pt. is the well-known Goat Island-Okakari Point Marine Reserve. The site has been previously examined by Dickson and Petney (2012), as discussed in

section 1.5.2. This site exhibits a fairly classic example of a shore platform and exists near a large metropolitan area which also has a number of similar shaped platforms. It is useful to use this shore platform for the purpose of this research in order to offer a contrasting analysis to that of the platform at Wakatu Pt. Understanding about the



Figure 3.5: Satellite image of Okakari Point showing the wide type B shore platform. The Image is captured during low to mid-tide, however almost all of the platform is fully exposed. The inset image shows cape Rodney, with Leigh on its southeast and Whangateau Harbour in the South. Okakari point is shown in the box at the top of the inset.

development of this platform can also be used to examine the level of the coastal hazard along rock coasts in the Auckland area. The rest of this section deals with the geomorphology, geology, tectonics, sea level fluctuations and climate in the region.

3.2.1 Geomorphology

The Okakari point shore platform site sits about 1.5km east of Pakiri beach. The site is immediately backed by a 14m cliff, behind which the terrain rises steeply up to 280m. Immediately west of the site, cliffs rise over 100m from the coast; land sliding is apparent along this section of the coast due to build-up of talus along the base of cliffs (this is not the case at Okakari Pt where very little talus is present at the base of the 14m cliff). Around the small headland at the north-east margin of the platform is a small pocket beach, with sand which spills around onto the platform (*figure 3.6*). Sediment supply for this beach is likely sourced from westward longshore drift off Pakiri beach. While all of the coastline around Cape Rodney has near continuous wide sub-horizontal shore platforms, Okakari point is where the platform is widest, at 135m. Water depth off of the outside edge of the platform plunges ~11-13m, therefore the platform is exposed to unbroken incident wave action (Dickson & Pentney, 2012). Dickson and Pentney (2012) also noted the platform is elevated 0.8m above the local mean sea level (MSL) and features a discontinuous rampart along the seaward edge which is elevated to approximately to mean high water. Elevated ~2m above the main platform surface, at the base of the cliff is another planation that is 3m wide, the base



Figure 3.6: Photograph of the Okakari Point shore platform from the top of the 13m cliff, looking north. Sand from the small pocket beach (out of frame around the western side of the headland) has been transported onto part of the platform surface. This may indicate periodic washing of sediment onto the platform surface. Photo Credit: Martin Hurst 2017.

of which is notched. It may be the case that this higher elevation surface was cut during a period of slightly higher sea level than today.

3.2.2 Geology

The sedimentary and volcanic rocks of the Auckland region are upper-Oligocene to middle-Miocene in age. The region is made up predominantly of the Waitemata Group flysch, which sits over a basement of metagreywacke-metaargillite (Ballance, 1974). The Warkworth subgroup makes up most of the Auckland area and is separated into three distinct flysch facies. These are the northern volcanic-rich flysch facies, a mixed flysch facies and the southern volcanic-poor flysch facies (Bell, 2007). These facies were generated around the period of the Kaikoura Orogeny, when the Auckland area was undergoing a period of subsidence. This formed the Waitemata basin. During the late-Oligocene to the early-Miocene two volcanic arcs formed to the east and west of the basin (Allen, 2004), depositing sediments into the basin. The andesitic volcanism of the eastern volcanic arc continued through to the Pliocene (Ballance, 1974). The northern volcanic-rich facies of the Warkworth subgroup are known as the Pakiri Formation. These facies outcrop along the coast around Cape Rodney. The shore platform and cliff at Okakari Point are made up of these Pakiri Formation facies.

The best description of the Pakiri Formation facies comes from Ballance (1974): the sandstones of the formation are normally graded, with beds which tend to be very thick and coarse grained. Sandstones are lithic with a predominance of argillaceous rock fragments with mudstone clasts up to 30cm long occurring. They also have varying quantities of lava throughout. There is a relatively low proportion of quartz and feldspar, making up ~20% of the coarse grained material and up to ~30% of the fine grained (Ballance, 1974). There also occur in small quantities plagioclase, augite and hypersthene. The relatively low proportion of quartz in the material and the abundance of volcanic minerals present a challenge in separating out quartz for cosmogenic analysis.

The beds at Okakari Point tend to be parallel laminated throughout (*Figure 3.7a*), dipping gently landward. The beds are made up of sandstones that are fine, medium and coarse grained and sandy mudstones (Dickson & Pentney, 2012). Structurally, the cliff line and platform orientation is controlled by the orientation of dominant joints

and faults. This includes some steep (50-90° dip) normal faults, oriented NW-SE and NE-SW and low angle (20-40° dip) thrust faults oriented NW-SE (Dickson & Pentney, 2012).

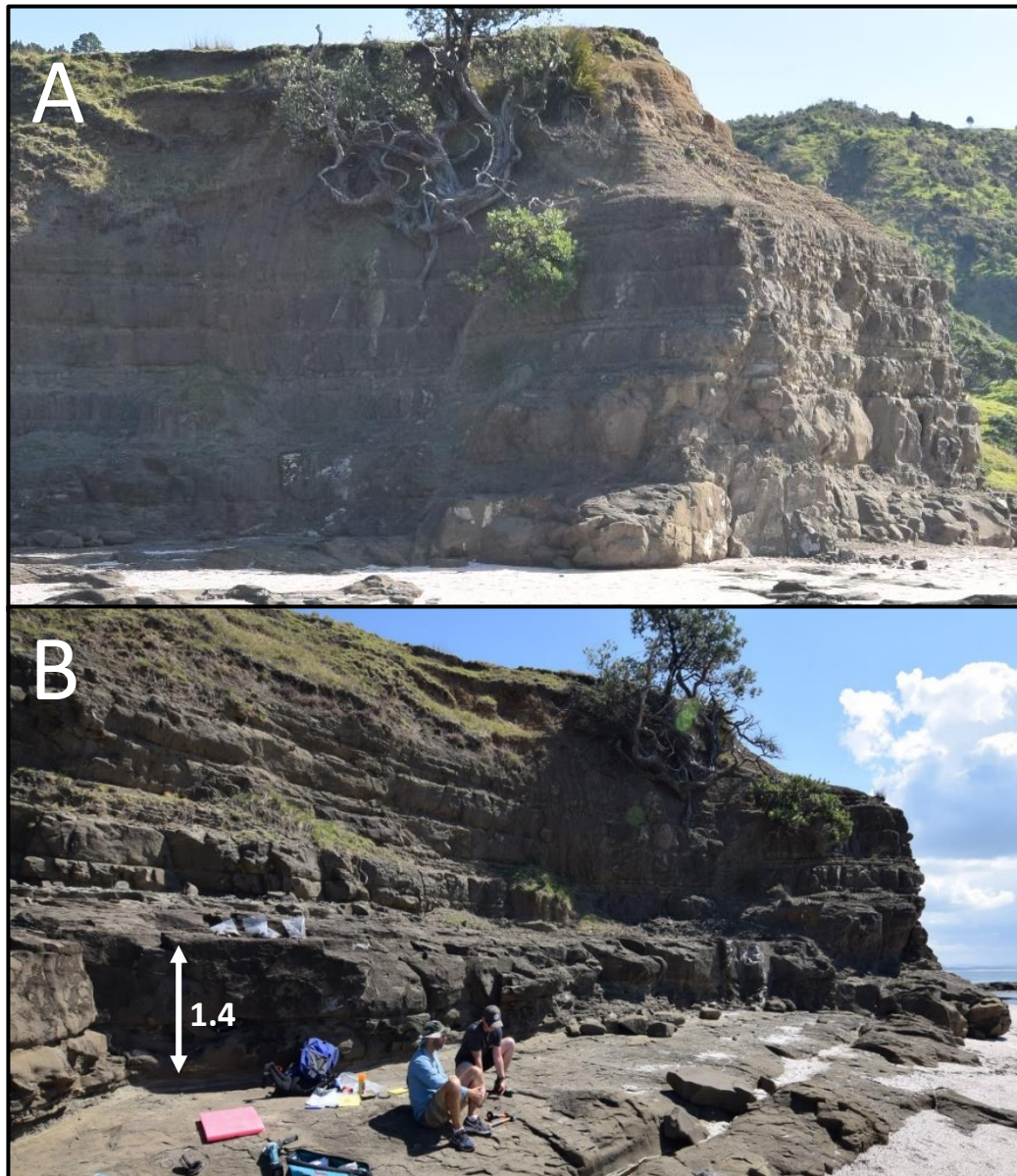


Figure 3.7: Landward facing photographs of the platform and cliff at Okakari Point: (a) shows the parallel lamination of the bedding in the Pakiri formation outcropping along the coast at Okakari. (b) is an image of the back of the shore platform, showing the ~1.4m elevated ledge which extends 3m out from the cliff base. Parts of the base of this ledge appear to have notching. Photo Credit: Martin Hurst 2017

3.2.3 Tectonics

Generally tectonism in the Auckland and Northland regions is quiescent. Being far from the subduction zone out to the east of the North Island, there is little crustal warping in the area. However, the Auckland region does exhibit features indicative of long-term uplift in the form of marine and fluvial terraces. Claessens *et al.*, (2009) surveyed 12 marine and 13 fluvial terraces near the Waitakere Ranges, Auckland, identifying an acceleration in the regional uplift rate from 0.278mm a^{-1} to 0.42mm a^{-1} since the late-Pleistocene. They achieved this through tephra age controls found within the overlying sediments on the terraces. The most likely driver of this uplift is an isostatic response to higher erosion rates of the continental crust (Claessens *et al.*, 2009). Bell (2007) notes that slightly elevated platform ledges (1-3m) are common features where there are shore platforms around the Auckland coast. As noted above in 3.2.1 there is a slightly elevated ledge at the back of the Okakari Point platform (*figure 3.7b*). It is possible that recent tectonic uplift during the Holocene still-stand could be responsible for these raised features. However, lack of evidence for recent uplift would indicate that due to the stability in the region, these features have developed in response to changes in eustatic sea level.

3.2.4 Sea Level Fluctuations

Around the world eustatic sea level has risen substantially and rapidly since the initiation of the post-glacial marine transgression (technically termed the Flandrian Transgression) at the termination of the Pleistocene. According to Gibb (1986) this trend is observed in New Zealand, with a period of rapid sea level transgression culminating at near present day sea levels around 6500yrs BP. Gibb (1986) was able to attain a more precise sea level response for the Auckland area: one of the 8 analysed sites in the study was the Weiti River in Auckland, where there was no influence of tectonic uplift. Chenier deposits at the mouth of the river were dated using radio-carbon to reveal a calibrated calendar age of $7120 \pm 70\text{yrs BP}$. This date is taken as the time at which sea levels close to the present day in Auckland were established. Gibb (1986) also suggested that since this time sea levels in the region have not fluctuated

more than 0.5m. In de Lange and Moon (2005) they take this age from Gibb as the time at which the modern shore platforms began to form.

Another group of prograded cheniers, part of the Miranda chenier plain in the Firth of Thames, indicates a period of Holocene sea level fall in the Auckland area. Dougherty and Dickson (2012) conducted analysis of the chenier plain, finding evidence for progradation of the coast from ~4000yrs BP to ~1200yrs BP. This indicates that sea level fell ~2m during this time, down to the present day sea level. It is thus likely then that sea level reached a Holocene still-stand that was 2m above present sea level for the period roughly between 7120yrs BP and 4000yrs BP. The prolonged period of slightly higher sea level may have allowed for the development of the elevated platform benches observed at Okakari Point and at other sites around the Auckland Region.

3.2.5 Climate

The climate of the Auckland region is sub-tropical, being located 13° S of the Tropic of Capricorn (Chappell, 2013). The predominant wind flow is from the SW, however in summer the proportion of flow from the SE increases. The annual rainfall near Okakari point is 1117mm a⁻¹, with the wettest month, July, accounting for 12% of this rainfall. Extreme rainfall events are uncommon but do occur due to the sub-tropical cyclones propagating from the NW of New Zealand. The air temperature ranges from 14°C to 20°C (monthly average) from July to February respectively and ground frosts are very rare (Chappell, 2013). According to Hilton (1995) the dominant swell arrives from the NE and the mean wave height is 1.4m, rarely exceeding 3m. The highest wave activity is associated with the onshore winds driven by the aforementioned sub-tropical cyclones (Hilton, 1995). Finally the tides are semi-diurnal with a maximum range of 3m in springs and 1.5m in neaps.

Chapter 4: Methods

4.1 Sample Collection

Samples for cosmogenic analysis were collected at Wakatu Point and at Okakari Point during the 2016-17 austral summer. Two locations were chosen in order to apply the method to two different shore platform morphologies with different tectonic and sea level regimes. Samples were collected in accordance with previous work (Choi et al., 2012; Hurst et al., 2016; Regard et al., 2012) detailing sampling practice for cosmogenic analysis on shore platforms. The following two sections detail the sampling procedures that were carried out at each of the localities and other data that were collected on site.

4.1.1 Wakatu

Samples were collected along an across shore profile of the shore platform at Wakatu Point on the north-eastern side of the Kaikoura peninsula. The shore platform at Wakatu Point is a sloping type A platform, with jagged rock formations across its profile. The unevenness of the platform is due to the tight folding of the Amuri Limestone in which the platform is formed. The work was conducted over a week long period from 14/12/16 to 20/12/16, with the first few days spent prospecting the platforms around the peninsula for ideal sampling material. Wakatu point was found to have favourable amounts of nodular chert across the platform and sampling took place on the 17th. A platform profile survey was conducted on the 19th. This period was one month after the Kaikoura Earthquake in November 2016, which had uplifted the coast at Kaikoura by 1.1m. As a result the tidal stage had little effect on the ability to collect samples across the entire profile of the shore platform.

Figure 4.1 shows the positions of the 10 samples which were collected on the outer platform surface at Wakatu point. Samples were only collected from the platform surface and not the raised terrace as no bedrock was exposed on that surface. This lack of exposed bedrock is due to the build-up of terrestrial sediment and emplacement of roads and other man-made structures on the terrace. The samples collected were nodules of Chert in a matrix of the Amuri Limestone. These are similar in composition to the samples collected in Regard et al. (2012) and Hurst et al. (2016) who demonstrated successful extraction of ^{10}Be from samples of chert. Of the 10 samples collected from Wakatu Pt, 3 were later discarded after being found to contain

insufficient mass of chert from which to extract ^{10}Be . The discarded samples were WP7, WP9 and WP10. The samples WP9 and WP10 were both from the outer edge of the platform on a structurally controlled high point.

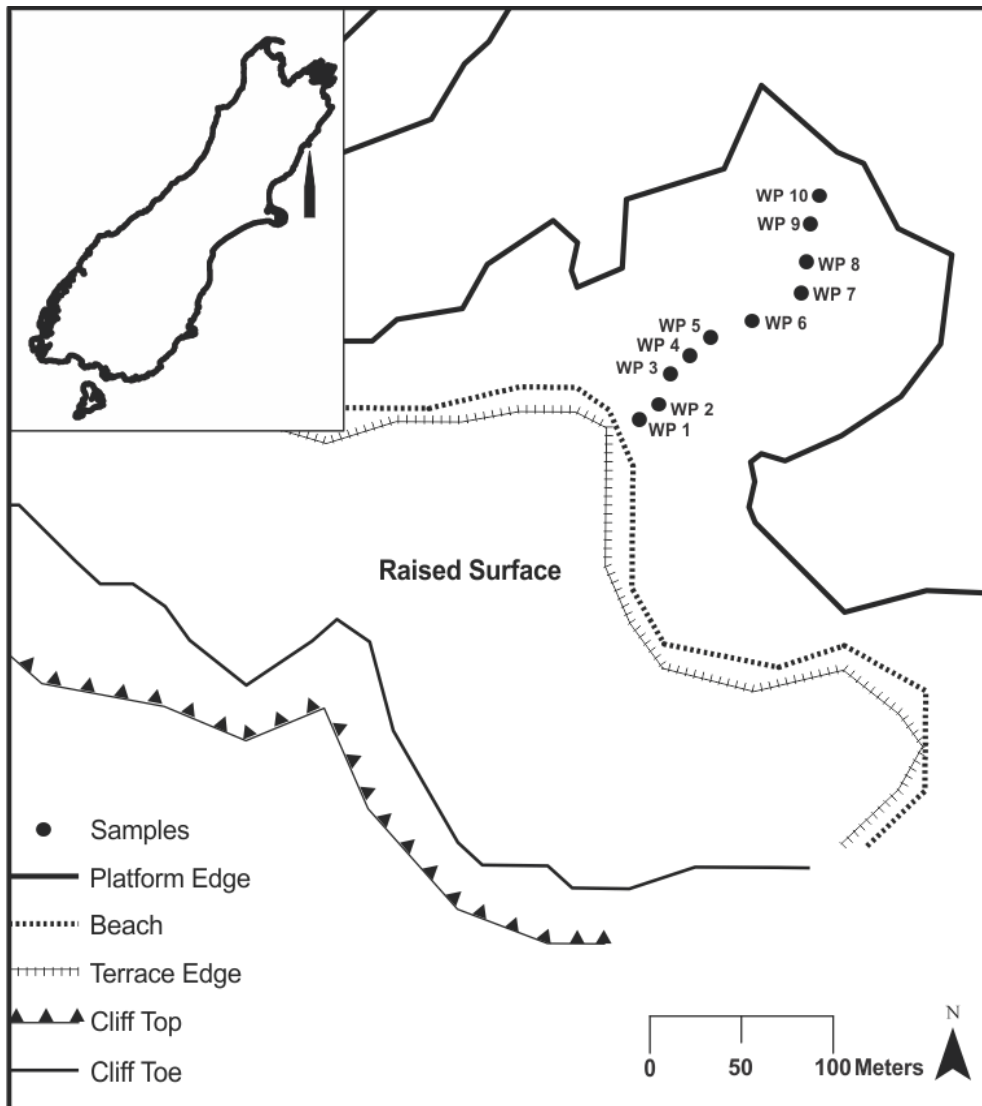


Figure 4.1: Image demarcating the positions of each terrestrial surface at Wakatu Point, showing the extent of the platform and its raised portion. The positions of each sample that was collected is indicated on the platform surface. Samples 7, 9 and 10 were not dated.

During sampling, positions were chosen if they were not obstructed from the sky in any significant way by the topography and if the surface did not look to be heavily weathered. Sampling positions were also selected based on a visual assessment of the content of chert and the ease of removing the sample from the bedrock. The amount of material collected was also based on the visual assessment of chert content; sample masses range from 0.5-2kg of material. Samples were extracted with hammer and chisel and for the most part came away easily from the limestone bedrock. When it

was attempted to hack out a portion of a large chert nodule it was difficult to break the chert. At each sample position dip and strike measurements were taken, along with the angle of inclination to the horizon around eight different azimuths, 360° around the sample. These measurements were taken to later calculate the topographic shielding factor for each sample using the method of Dunne *et al.* (1999). Following sample collection a survey of the profile of the shore platform was conducted, using a total station. This covered the zone from the top of the beach surface at the landward side of the platform to the 'on the day' low tide extent of the outer shore platform. The positions of the samples along this profile were taken down during the survey. The survey of this platform was located on the peninsula relative to bolt site KM1C from Stephenson *et al.* (2010) The locations of Stephenson's bolts are surveyed in relative to the Trig Station atop the Kaikoura peninsula at 105m.

4.1.2 Okakari

Samples were collected at Okakari Point 1km due east of Pakiri Beach. Sampling was conducted largely in similar fashion to sampling at Wakatu Point, along an across shore profile. The Okakari Point shore platform is, however, a sub-horizontal shore platform which terminates at the seaward edge in a seaward scarp, to a depth of greater than 10 meters. The platform is also backed by a steep 13m tall cliff which acts as a significant source of shielding. The sampling took place with the falling tide on the afternoon of 2/3/17 and on the following morning 3/3/17. Samples were extracted from Pakiri Formation Sandstones with quartz being the target material. Visual inspection with a hand lens confirmed the presence of quartz within the matrix of the sandstone, however in low quantity.

The samples collected are located at points across the shore platform (*figure 4.3*), and there is a concentration of samples next to the cliff. At this landward side of the platform is a ramp elevating up from the main horizontal platform surface and just below the cliff is a raised platform surface. Six samples were collected from these surfaces in order to determine the development history of this unusual platform geometry. Fewer samples were collected across the middle of the platform due to the uniformity of the geometry. Also, due to the flatness of the surface on the mid platform it was necessary to extract some samples using a diamond tipped angle

grinder (the rest were able to be extracted with hammer and chisel). Another group of samples is located on the outer edge or rampart to capture the time of initial platform cutting. One difference from the sampling at Wakatu Point is that we were able to retrieve a sample (OK 0) from a small, shallow sea cave around the eastern point of the headland. Sea cave samples had been collected in Hurst *et al.* (2016), it was reasoned that any ^{10}Be measured in a sea cave sample must represent the inherited portion of ^{10}Be in the bedrock of that platform.

As with the Wakatu samples, some of the Okakari samples were eventually discarded due to low quantity of quartz. Of the 14 samples collected, 8 were dated. Fortunately these 8 samples were representative of the whole profile of the platform from the cliff base to the seaward edge, including the raised surface beneath the cliff. Samples OK1, OK5, OK7, OK8, OK9, and OK12 were not processed due to lack of quartz. The shielding data for each sample position were collected the same as at Wakatu Point, however, the exact GPS locations for each sample point were also taken at Okakari using

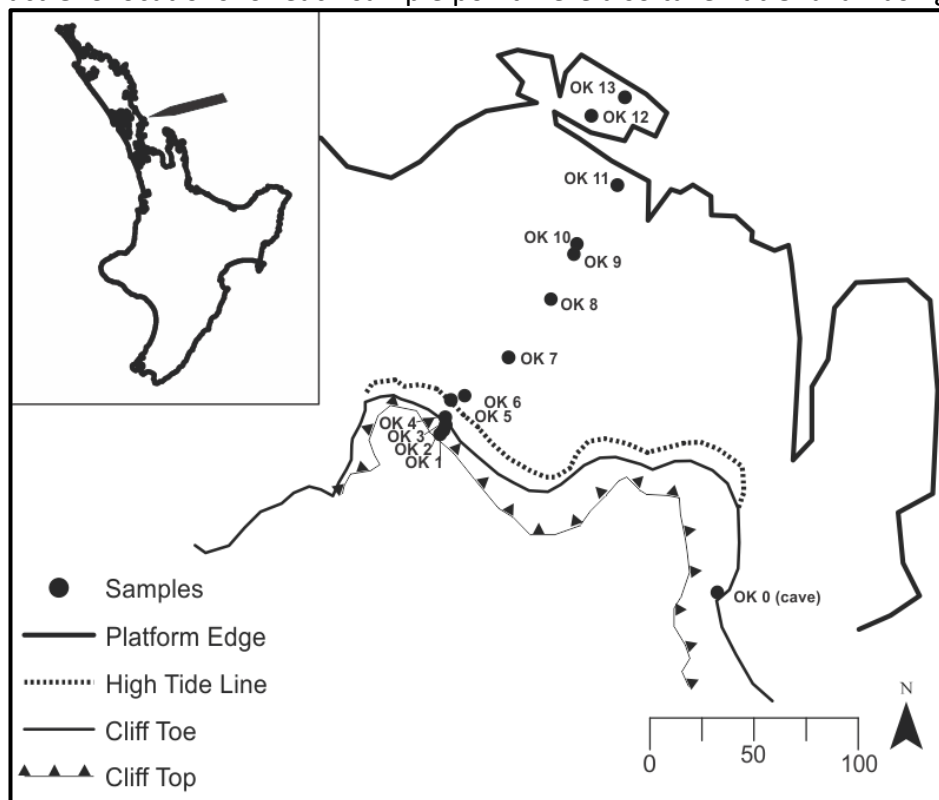


Figure 4.2: Image demarcates the positions of the main terrestrial surfaces at Okakari Point. The ‘cliff toe’ line sits along the base of the raised terrace surface described in section 3.2.3. This surface is discontinuous and is not well preserved either side of the main headland. The 14 sample positions are shown by the points. Samples 1-3 were collected from the raised terrace surface and sample 4 immediately at its base. Sample 0 SE of the main sample transect shows the location of the sea cave.

waypoint averaging. A survey was also conducted in the same way as at Wakatu, and this was located relative to an earlier survey from the Dickson and Pentney (2012) study. This was achieved by identifying bolt positions from a pressure transducer rig on the outer platform and taking a shot to that point with the total station.

4.2 Laboratory Procedures

The collected samples were processed in two sets at different times after each of the two sampling trips. Also due to the difference of the geology (limestone and chert vs sandstone and quartz) in the two sample sets, the physical and chemical pre-treatment steps were modified to account for these differences. However, generally the pre-treatment steps followed standard procedures (e.g. Gosse & Phillips, 2001; Kohl & Nishiizumi, 1992). The following outlines the various physical and chemical laboratory steps undertaken in this project.

4.2.1 Physical Pre-treatment

Wakatu samples - The Wakatu Point sample set were the first to be processed in the labs, following the scraping off of the majority of the biological material and allowing the remaining material to desiccate. Initially samples were weighed and photographed before being broken into smaller pieces with a sledge hammer. Samples were then crushed using a Boyd Crusher, sieved down to <1mm diameter and washed. Visual inspection under a microscope confirmed abundant chert content in most samples. Grains were then further crushed and sieved to <0.5mm to increase the surface exposure of the grains, then weighed again. Magnetic mineral separation was trailed with a small volume of sample; this yielded minimal separation as the non-chert material was mostly limestone and not magnetic. The samples thus were moved directly to chemical leaching.

Okakari samples - The Okakari Point sample set were similarly scraped and allowed to desiccate, followed by weighing and photographing in lab. The samples were crushed and sieved to <1mm, then a small volume of sample was washed and inspected under microscope. The visual inspection showed minimal quartz, with ~5% of the coarse material as pure quartz and ~20% of the finer material as quartz. It was apparent that much of the fine-grained quartz remained in agglomerations with other minerals. The samples were then washed and dried to remove dust. Grains were further pulverised

in a tungsten carbide ring-mill to break apart the mineral agglomerates. Sample material was then dry sieved with a sieve shaker to separate out the grain size fractions: $>500\mu\text{m}$, $500\text{-}250\mu\text{m}$, $250\text{-}112\mu\text{m}$, $112\text{-}106\mu\text{m}$ and $<106\mu\text{m}$. The $>500\mu\text{m}$ fraction contained only agglomerations of dust size particles and was discarded. Similarly the $<106\mu\text{m}$ fractions was deemed to fine and also discarded. At this point Sample OK-1 was discarded as almost all material fell into the $<106\mu\text{m}$ fraction. The

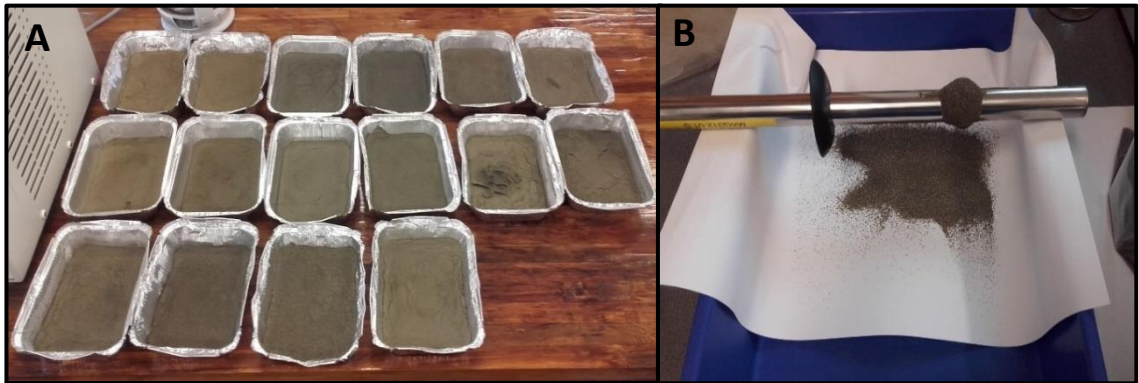


Figure 4.3: Images of physical pre-treatment steps for the Okakari samples. (a) Dried samples after wet sieving, in some of the trays biological materials rafted together while wet and dried into crusts which were easily removed. (b) Neodymium hand magnet, samples were poured over the magnet. Magnetic grains that stuck to the magnet were decanted into separate bags.

$500\text{-}250\mu\text{m}$ fraction was then labelled 'coarse' and the $250\text{-}112\mu\text{m}$ and $112\text{-}106\mu\text{m}$ fractions combined and labelled 'fine'. These two fractions were then processed separately afterwards. Samples were then wet sieved to remove any remaining dust before magnetic separation and dried (*figure 4.4a*). A large hand magnet (*figure 4.4b*) was used to pull out the most magnetic fraction of the samples followed by a low (0.2amp) pass, then a high (1.5amp) pass on the Frantz magnetic-separator. At this point the non-magnetic fractions contained primarily quartz after visual inspection. The fine and coarse non-magnetic fractions were then weighed again prior to chemical pre-treatment.

4.2.2 Chemical Pre-treatment

Wakatu samples -Initially a test of method was conducted to determine the appropriate procedure to leach the samples. Standard methods were not suitable due to the abundance of calcium-carbonate in the remaining material. Ten grams of material from sample WP-5 (sample with most abundant remaining material) was added with 50ml of concentrated hydrochloric acid to test the reactivity and effectiveness of dissolution. The sample was found to be highly reactive due to the

high content of calcium-carbonate in the samples. The test yielded good dissolution of the non-chert material, so all samples were leached in concentrated HCl. 200g of each sample was placed in 1L glass beakers. 100ml of conc. HCl was slowly added to the samples and once the reaction had subsided the beakers were swirled and left uncovered in a fume hood overnight. This process was repeated three times to achieve total dissolution of the carbonates. Samples WP-7, WP-9 and WP-10 remained vigorously reactive during the third leaches indicating they contained mostly non-chert material.

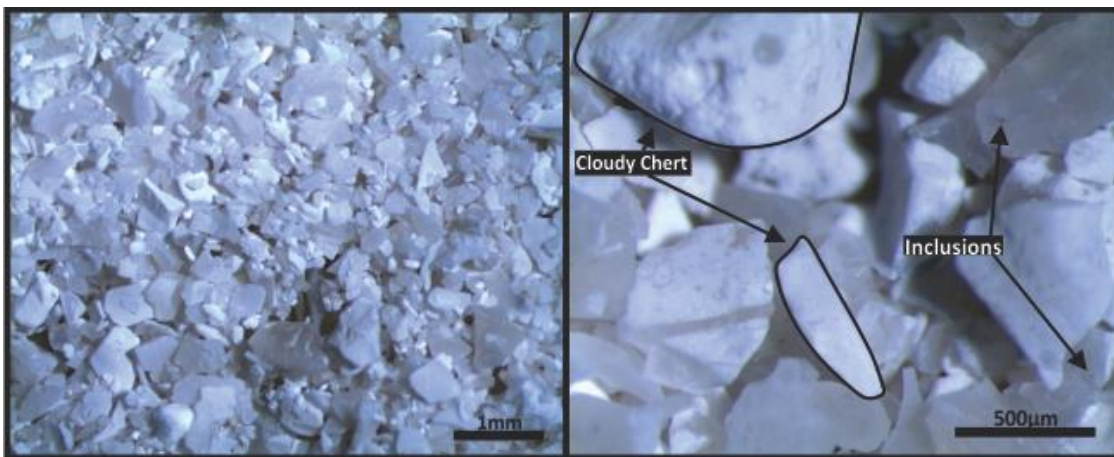


Figure 4.4: Microscope images of one of the Wakatu samples (WP-6) following leaching steps. The image on the left shows the majority of the grains are translucent chert. The zoomed in image of the right shows the cloudy white grains which are chert grains or cortex crusts in amongst the clear chert grains. Some of the grains are both translucent and cloudy indicating some colour banding. Most of the chert grains contain small inclusions, indicating some impurities in the rock.

The samples were then rinsed and transferred to large Teflon bottles. At this step the samples were moved into a clean lab for the remaining chemical procedures. All samples were covered with a small volume of 5% hydrofluoric acid solution, and left to leach, covered, on a hotplate at 50°C overnight. This HF acid leach is applied to release the grain absorbed meteoric ^{10}Be into aqueous solution without removing the in-situ produced ^{10}Be , while also dissolving any oxides and feldspars. This leach was repeated three times; each time sample WP-9 reacted notably. Following this step the samples were washed with H_2O and dried down for visual inspection. Sample WP-9 was discarded at this point as its remaining chert content was too low for further processing. Under the microscope it was noted that an unidentified cloudy white mineral (*Figure 4.5*), which was not a precipitate or calcite, persisted in some of the samples as whole grains or crusts around grains of chert. To remove this material, the

samples were placed back into weak HF for one further leach, after which the mineral still persisted. It was determined that this mineral was most likely either a white chert or a cortex crust (either of which are quartz based) and the samples were washed, dried and weighed.

Okakari Samples –Leaching of the Okakari samples followed normal standard protocols of Kohn and Nishiizumi (1992). The 13 remaining sets (coarse and fine) Okakari samples were placed into 1L Teflon bottles and leached two times overnight in 800mls of 10% HCl solution at 50°C in a hot water bath. After the second leach the acids were no longer coloured yellow, indicating that most carbonates and metal oxides had been removed. Samples were then moved into the clean lab for weak HF leaching. Bottles were filled roughly two thirds with the 5% HF solution and placed in a hot water bath at 50°C for overnight reactions. This was repeated three times, with H₂O rinsing between each leach. The third round was left in solution unheated for 72 hours. The material was then washed, dried down in an oven and weighed. All samples had lost ~50% of their mass by this point, several had lost too much material to continue processing. Samples WP-5, WP-7, WP-8, WP-9 and WP-12 were discarded at this point for this reason.

4.2.3 ¹⁰Be Isolation

Wakatu samples –The dried samples were added to large Savillex teflon beakers, which had been earlier weighed without sample. An extra clean beaker was also added at this point to be a blank, which would remain empty of sample. The blank is carried through all remaining steps including AMS in order to identify any unintentional contamination of the samples while they are being processed in the clean lab. The samples were also renamed with a lab ID in accordance with the protocol of the lab facility, these designations were AD01 through AD08. A final leach was conducted by adding in just enough 7M HF acid to cover all the material and leaving on a hot plate for one hour at 120°C. This is an aggressive leach which strips the quartz or chert of any remaining meteoric ¹⁰Be. The samples are then rinsed in 18.0MΩ Milli-Q H₂O four times before 14M Aqua Regia (HNO₃+3 HCl) was added to cover each sample. This is to remove any fluoride that is still stuck to the grains and to dissolve any remaining contaminants. The beakers were then left on a hot plate at 120°C for two hours,

before the lids were loosened and heat turned off and left overnight to degas. After degassing the samples were rinsed again five times with Milli-Q H₂O, and left to dry on the hot plate overnight. The beakers with samples in were then weighed again to get the precise weight of the samples remaining. All of the beakers (excl. Blank) had retained a large amount of material by this point and samples AD01, AD02, AD04, AD05 and AD07 had to have some material removed so not to over load the analytical scales. After removing some material from these samples ~50-70g of material remained in the beakers.

After weighing the ~0.9g (precisely weighed) of ⁹Be carrier was added to the samples. This known portion of ⁹Be is used to assess ⁹Be/¹⁰Be ratio after AMS processing; the ratio is used to calculate the total concentration of ¹⁰Be atoms in each sample. The samples were then completely dissolved in strong 28M HF acid over five days, where HF was refilled 5 times. Once dissolved, the material in the beakers had become fluoride cakes containing the Be and any contaminant metals, these were very delicate and flaky. This occurs as the Be in the samples bind with fluorides to form a water soluble solid BeF₂. According to Stone (Stone, 1998) the insoluble elements (Na, Al, Mg, Ca and Fe) are retained as solids in varying degrees. The cakes were leached in 15mls of Milli-Q H₂O and heated to 60°C for 20 minutes to ensure maximum Be extraction, then pipetted into 50ml centrifuge tubes and centrifuged for five minutes at 3500rpm. The supernatants were decanted back into the wiped clean beakers, and precipitants left in the centrifuge tubes, added with another 15mls of H₂O for a repeat centrifugation. The above two steps were repeated twice, maximising the yield of BeF₂. The precipitants were discarded. The supernatants in the beakers were then evaporated overnight at 120°C, cooled then added with 10mls of 6M HCl and left another night to re-dissolve. After dissolution the samples in solution were added into new centrifuge tubes and centrifuged again to ensure total dissolution.

The samples, in solution, were then put through Fe cation columns filled with 2ml Biorad AG1-X8 100-200 mesh (anion) resin. This step used cation exchange chemistry to remove any remaining Fe from the samples. The Be was eluted from the mesh and collected with 6M HCl, while the Fe was held in the resin. The Fe was later eluted from the mesh with 0.3M HCl and discarded. Samples were then evaporated on the hotplate

before re-dissolution in 0.4M oxalic acid at 60°C for 2 hours, followed by another round of centrifugation in fresh centrifuge tubes. This prepared the samples for the next run of Be columns.

The Be was eluted with 5ml Biorad AG50-X8 200-400 mesh (cation) resin in 15ml Eichrom columns. The columns were cleaned with 5M HNO₃ then conditioned with 0.4M oxalic acid. After addition of the sample in the 0.4M oxalic acid solution any Fe, Ti and Al still remaining in the sample were eluted with the oxalic acid and discarded. Milli-Q H₂O was used to wash out the oxalic acid, then Na was eluted with 0.5M HNO₃. Be was eluted with 1M HNO₃ and collected into the large Savillex beakers, then the columns were flushed with 5M HNO₃. This process was repeated a second time later on, due to low Be yields from the initial run. The second run was carried out using the smaller 2ml Biorad AG50-X8 200-400 mesh (cation) resin in 15ml Eichrom columns.

After the second run of Be columns the samples were dried down then re-dissolved in 5mls of 1M HNO₃ each at 60°C. The solution was pipetted into small 15ml centrifuge tubes, and 1ml of ammonia (NH₄OH) was added to each tube. These were thoroughly mixed, then centrifuged. After centrifugation it was clear that BeOH had been precipitated as a milky white substance at the bottom of each centrifuge tube. The supernatants were decanted into the beakers, then 15mls of Milli-Q H₂O was added to the centrifuge tubes, vortexed for one minute and centrifuged again. This was repeated twice to ensure that only the BeOH remained in the centrifuge tubes. 0.3mls of 5M HNO₃ was then added to the precipitates which were mixed to dissolve them once more. The solutions were pipetted into quartz crucibles, which were left on the hotplate at 120°C to evaporate overnight. The dried samples were finally oxidised over a flame for 30 seconds each burning off all of the H and leaving BeO. The BeO was mixed with 3mg of niobium powder and packed into AMS targets following the PRIME lab packing protocol.

Okakari Samples- As with the Wakatu samples the 8 remaining Okakari samples were transferred into large savillex beakers which had been pre-weighed. Another blank beaker was added to the sample set. All of the samples were also assigned new lab designations from AD09 to AD19. The final HF leach was conducted in the exact same fashion as the other sample set. However, due to the small amount of quartz in some

of the Okakari samples (AD13, AD15, AD17 and AD18), they were kept in the 7M HF for only 30 minutes (rather than one hour), to preserve the remaining quartz. Following the Aqua Regia step the ^9Be carrier was added to the samples. For the smaller volume samples only $\sim 0.8\text{g}$ of carrier was added; the larger volume samples received $\sim 1\text{g}$ of carrier. The following steps, dissolution, BeF_2 leaching and Fe columns all were carried out following the same methods as described for the Wakatu Samples. The Be columns differed from the Wakatu sample set, in that they were only run once, through the larger 5ml columns (figure 4.6a). BeOH precipitation was successful (figure 4.6b) and the samples were oxidised and packed into AMS targets according to the PRIME lab packing protocol.

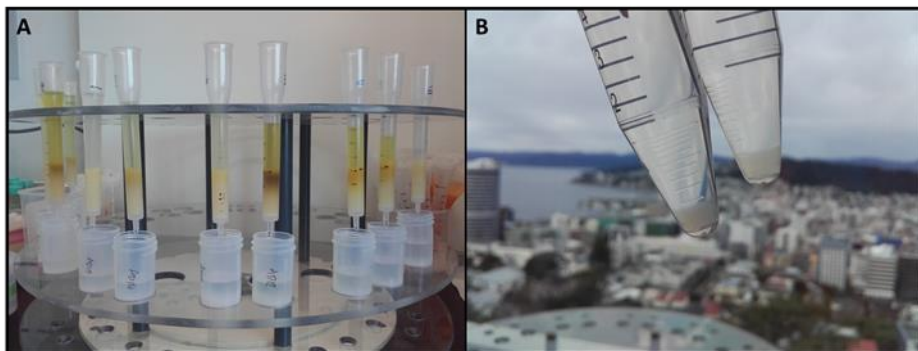


Figure 4.5: (a) running the 5ml columns. (b) BeOH precipitate is cloudy white substance in the bottom of the centrifuge tubes.

Photo Credits: Aidan McLean 2017

4.2.4 Accelerator Mass Spectrometry

The targets were sent to the Purdue Rare Isotope Measurement Laboratory (PRIME lab). The $^{10}\text{Be}/^9\text{Be}$ ratios were measured on their HVEC model FN tandem Van de Graaff accelerator modified for AMS (Sharma et al., 2000). The measured ratios were calibrated against the NIST (National Institute for standards and technology) SRM 4325 standard for normalization of radionuclides/stable nuclide ratios, with a $^{10}\text{Be}/^9\text{Be}$ ratio assumed to be 2.68×10^{-11} . The samples were also corrected for the laboratory blank AD09 (5.74×10^{-15}). Exposure ages for the blank corrected $^{10}\text{Be}/^9\text{Be}$ ratios were then calculated using the 07KNSTD (equivalent to S2007N) standardization on the former CRONUS Calculator version 2.3.

4.3 Modelling

The methodologies outlined in the above sections of this chapter are applied to address the first aim of this research to assess the development history of shore platforms at two study sites in New Zealand. The second main aim of this research is to

assess the relative role and importance of different processes acting to develop shore platforms and apply this assessment to the two case studies. In order to achieve this aim, an exploratory numerical modelling methodology is applied. The model is a coupled version of two separate and distinct models which perform separate tasks. The first is a rocky shore profile evolution model after Matsumoto *et al.* (2016a) called the Rocky Profile Model (RPM). The model code is available at the repository <https://github.com/hironorimatsumoto/RSPeM>. The approach used in this first model is relatively simple, whereby the modeller deliberately considers only a limited number of processes represented in simple terms (Matsumoto *et al.*, 2016b). According to Matsumoto *et al.* (2016b) the advantage of such an approach is to reduce computational demands of the model and enhance the clarity of potential insights the model can produce. The second model in this coupling is the Cosmogenic Radionuclide (CRN) model after Hurst *et al.* (2017), code available at https://github.com/mdhurst1/RoBoCoP_CRN. This model simulates the concentrations of a chosen radionuclide, in this case ^{10}Be (however, it can also simulate ^{14}C , ^{26}Al and ^{36}Cl) across a shore platform, as the platform evolves through simulated time. In Hurst *et al.* (2017), the CRN model is coupled with the ROck and BOttom COastal Profile (RoBoCoP) model, which is their version of the platform evolution model. The CRN model relies on a coupling with a platform evolution model, as it is from this evolution model that the CRN model retrieves the shore platform profiles. The CRN model is able to simulate nuclide accumulation while accounting for topographic shielding, water shielding, tides, block removal (or platform erosion) and beach cover. The coupling of these two models create the RPM_CRN model, the two components of which will be explained in further detail below.

4.3.1 RPM Model Framework

The model of Matsumoto *et al.*, (2016a) integrates the iterative dynamic interactions of various processes to drive cliff erosion on a 2 dimensional cellular grid. This model process produces varied platform geometries. Each grid cell is represented by a 0 or 1, sea/air and land respectively. A second value is assigned to each land cell as a rock resistance value between 0 and 1; this is the material resistance (F_R). This set up allows the process relationships to be operationalised in the model, with iterative time-steps

equivalent to 1 year (Matsumoto *et al.*, 2016a). This way the changes in the process framework represent annual changes.

Erosion by waves in this model operate in the same way as in Sunamura's (1992) conceptual rocky shore evolution model, where constant wave height is input and the hydraulic and mechanical actions are integrated into wave assailing force (F_W) (Matsumoto *et al.*, 2016a). Erosion occurs when F_W exceeds the material resistance F_R . F_W is split into two components: horizontal cliff backwearing and vertical downwearing. The flux of tides influence both of these components. Weathering processes are also included through the operation on the surficial rocks at each time-step, reducing the F_R value for that cell. This weathering only occurs in the intertidal zone where wetting and drying occurs. This restriction of weathering to part of the intertidal zone is based on the idea in Stephenson *et al.* (2017) that effective weathering of the surficial rock occurs in areas where wetting and drying is most common. Cliff erosion is represented only as a result of failure due to notch formation at the base of the cliff (Matsumoto *et al.*, 2016a).

4.3.2 CRN Model Framework

The CRN model from Hurst *et al.* (2017) simulates the production of ^{10}Be across the shore platform as it evolves. The production depends generally on the duration of exposure and the rate of removal of surface material through erosion. As mentioned above the model simulates the role of various factors which influence these two things. In this model topographic shielding is based on the framework of Dunne *et al.* (1999). Dunne and colleagues produced a model for the calculation of a scaling factor for topographic shielding. For a large rectangular obstruction, the shielding factor accounts for the portion of the cosmic ray flux that is shielded, using the angle of inclination (angle from a given position on the platform to the horizon) and the subtended azimuth angle (the portion of the horizon blocked by the obstruction). *Figure 4.7* shows the degree to which the shielding factor is affected by these two, three-dimensional coordinates. For a shielding factor of one, no portion of the cosmic ray flux is obstructed; complete shielding occurs at a factor of 0 (Dunne *et al.*, 1999). In calculating the production rate of TCNs the unobstructed production rate is multiplied by the shielding factor, so for a shielding factor of 0.5, the production rate would be

halved. The CRN model has shielding changing through time on the shore platform as the cliff is eroded back. The model simulates a cliff of fixed height that is straight in line with the platform (Hurst et al., 2017). The shielding factor S_{Cliff} is then based off the obstructed portion of the view shed to the horizon and iterated through time (Hurst et al., 2016). This simulates the change in topographic shielding factor for each iteration.

Hurst and colleagues (2016) simulate water shielding by predicting the level of attenuation of the cosmic ray flux by using the density of water ρ_w and the depth of the water column h_w . Tide modulates the depth of the water at points across the shore platform and changes on a $\sim 12\text{hr}$ harmonic timescale. The model makes predictions of the tidal inundation through the summing of the tide's harmonic constituents. The

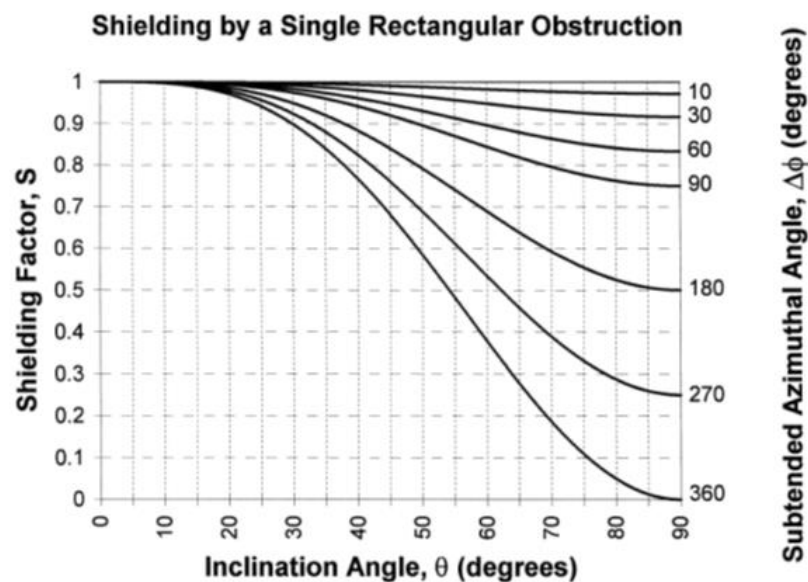


Figure 4.6: Shielding factor that results from a single, 'rectangular', cosmic-ray-blocking obstruction that subtends an azimuthal angle $\Delta\Phi$ through a constant zenith angle θ measured up from the horizontal. Source: Dunne et al (2001).

calculation for water attenuation and the prediction for the water depth across the platform through time, based on tidal flux, can be combined. This enables the calculation of the production rate for the TCN at the platform surface and can be averaged over the tidal cycle.

The model's treatment of beach cover simulates beach profile morphology by approximating it with the Bruun rule (Bruun, 1954):

$$z_b = z_{b0} - Ax_b^m$$

Where z_b is the elevation of the profile, z_{b0} is the elevation at the top of the berm, A is a scaling parameter for the size of the beach material and m is a dimensionless parameter for the dissipation of wave energy. The set up for this power law function in Hurst *et al.* (2017) has $A = 0.12$ which is a representation for gravel sediment and the shape exponent $m = 2/3$. The width of the beach is variable, changing with a sinusoidal function over decadal timescales. The wavelength of the sinusoid is 100 years, with an average width of 50m and an amplitude of 30m (Hurst *et al.*, 2017).

4.3.3 Coupled Rocky Profile and Cosmogenic Radio-nuclide Model (RPM_CRN)

In Hurst *et al.* (2017) the Cosmogenic Radionuclide component of the model is coupled with RoBoCoP, the platform evolution model. For this research the RoBoCoP component of that coupled model is excluded in favour of the model from Matsumoto *et al.*, (2016a). The model platform evolution framework from Matsumoto and others is able to simulate many and varied platform geometries based on a number of key process relationships. Coupling of the Matsumoto *et al.*, (2016a) evolution model and the CRN model allows the CRN model to retrieve shore profiles at time steps iterated through time and calculate the distribution of ^{10}Be concentration in atoms g^{-1} across the profile. With this coupling it is possible to set up the Matsumoto *et al.*, (2016a) model in various ways to simulate the different process relationships and assess their impact on ^{10}Be concentrations. The coupled version of these two models used in this research is called the Rocky Profile Model (henceforth RPM). This version has added capabilities to simulate scenarios of sea level rise/fall and tectonic uplift through step wise events. This is particularly important as the histories of the Wakatu Point and the Okakari Point shore platforms appear to be influenced largely by tectonics and sea level change respectively.

4.3.4 Model Testing

The model was set up for three different types of testing. First, models were set up for parameter sensitivity testing. This sensitivity testing is where the model was run multiple times with a set of parameters that would not change (things that were generally consistent for different platforms), and a set of parameters that would change from platform to platform in reality and are known to play important roles in the development of platforms. These changing parameters were: rock resistance, weathering rate and wave erosion efficacy. Each parameter was tested independently

for a range of three realistic values for each (see Table 5.1) based on Matsumoto *et al.* (2016a). While one parameter was being tested, the others were always set to their medium or middle values. This testing was carried out in order to assess how the different key parameters would impact the outputs of platform geometry and ^{10}Be concentrations.

The second set of testing was scenario based testing. These tests looked at the role of introducing sea level rise and fall into the model and the role of uplifting earthquakes in the development of shore platforms. The changing sea level tests were simply to assess the impact of continuous sea level rise and continuous sea level fall on the platform geometry. The earthquake uplift tests were conducted first to test the role of step size, i.e. the magnitude of the uplift event, (0.5m 1m or 2m per event). This approach addresses the potential for a threshold of event magnitude that causes preservation of platform surfaces as marine terraces. The uplift tests also examined the impact of the recurrence interval of uplift events on platform geometries, based on documented recurrence intervals of fault ruptures near Kaikoura.

The final model runs were tests of best fit between modelled profiles and measured ^{10}Be concentrations at Wakatu Point and Okakari Point. These tests were conducted in order to identify parameterizations and scenarios of sea level change and tectonic movement which produce outputs similar to the real life platforms measured in this thesis. These are used to help identify the more likely process relationships that have created these two shore platforms.

Chapter 5: Modelling Results

This chapter presents the results of the RPM_CRN model, which is a combination of the rocky profile model (RPM) by Matsumoto et al., (2016) and RoBoCoP CRN model by Hurst et al., (2017). This includes the first two types of model testing; parameter sensitivity tests and scenario based tests for the role of tectonics and sea level change. The third type of model tests, best fit modelling for sample sites, will be presented in the results and discussion sections of the respective site case studies.

5.1 Model Parameters and Sensitivity Tests

Sensitivity analysis of the various model parameters was conducted in Matsumoto et al., (2016a). Due to the exploratory nature of the RPM the model parameterisation is highly abstracted. This exploratory approach to the modelling is necessary because (i) the model was designed to simulate morphological evolution over long time scales, and (ii) the slow evolution of rock coasts has so far prevented a detailed process-based understanding of the mechanics of cliff erosion (see Murray (2007) and Matsumoto et al., (2016a) for a more detailed explanation of exploratory modelling in geomorphology).

For the sensitivity testing in this thesis, three critical variables were tested (outlined in 4.3.4). These parameters were set on the findings of the sensitivity analysis in Matsumoto et al., (2016a). For example, in Matsumoto et al., (2016a) the three values set for material resistance were 0.5 for soft rock, 5.0 for medium rock and 50.0 for hard rock. The hard rock value result in non-eroding, plunging cliff geometries, whereas the soft-rock value results in rapidly retreating, Type A platforms. The coupled RPM_CRN model discretizes the coast as 0.1m^2 cells, whereas in Matsumoto et al., (2016a), the RPM cell size was 1m^2 . Therefore, in this thesis, soft rock is given a value of 0.001, medium is 0.01 and hard is 0.1; values are 10 times smaller than those used in Matsumoto et al., (2016a) to account for the reduction in cell size. The values were also chosen due to slight differences in model behaviour between the RPM and the CRN models. The other two critical variables are weathering rate and wave erodibility, as are defined in *table 5.1*. All other parameters remain constant during the model run. All of the parameters related to producing the morphology used in this sensitivity testing are outlined in *table 5.1*. The only parameters which required setting for the

nuclide output were the nuclide production rate for the latitude and elevation that was required to be simulated and the rock density. Rock density can be based on the general rock type present.

The first test was of the material resistance. This is the resisting force based on the lithological control, one of the key determinants of platform geometry. Values of resistance (0.001, 0.01 and 0.1) were tested, where all other parameters were set to the medium values. The model was run three times, each with the different value of material resistance. The model outputs are shown in *figure 5.1*, all show that platforms have formed with some degree of incision on the seaward edge. The final profiles for each of the three runs is plotted in *figure 5.2*.

Table 5.1: Model parameters used for sensitivity testing.

Morphology Control					
Parameter Type	Parameter	Changing y/n	Setting(s)	Units (if applicable)	Description
Platform Gradient	Gradient	<i>n</i>	1		Gradient fraction 1/10, set for low angle type B platform.
Cliff Position	Cliff Height	<i>n</i>	20	meters	Denotes height of vertical cliff at 90 degree angle with shore platform.
Time Control	Total number of iterations	<i>n</i>	8000	years	Number of iterations the model runs.
	Time Interval	<i>n</i>	1	years	Iteration duration.
Printing	Print Interval	<i>n</i>	800	years	The model prints the profile after every 800 iterations, it will print 10 profiles.
Tides	Tidal Range	<i>n</i>	1.5	meters	Meso-micro-tidal range, representative of NZ tides.
	Tidal Period	<i>n</i>	12.25	hours	Semi-diurnal tidal period for NZ.
Waves	Mean Wave Height	<i>n</i>	2	meters	Set to represent normal incident wave activity.
	StD Wave Height	<i>n</i>	0	meters	Wave height remains constant to reduce complexity.
	Mean Wave Period	<i>n</i>	6	meters	Set to represent normal incident wave activity.
	StD Wave Period	<i>n</i>	0	meters	Wave period remains constant to reduce complexity.
Wave type	Standing Wave Coefficient	<i>n</i>	0.01		The different wave types are scaled to different orders of magnitude, based on the spatial distributions of pressures they exert across the platform.
	Breaking Wave Coefficient	<i>n</i>	10		
	Broken Wave Coefficient	<i>n</i>	1		

Geology	Cliff Failure Depth	n	1	meters	Controls the depth of notch formation into the base of the cliff. At the set depth the cliff will fail. This is the only mechanism for cliff failure in the model.
	Material Resistance	y	0.001, 0.01, 0.1		Unit-less values which control the degree of resistance of the rock cells to the assailing force. These values are based on model behaviours from sensitivity testing conducted in (Matsumoto et al., (2016a). Resistance value of 0.001 is soft rock, resistance value of 0.01 .is medium rock, resistance of 0.1 is hard rock.
	Weathering Rate	y	0.01, 0.001, 0.0001	meters/year	Efficacy of weathering, controls the rate of weathering of the platform rock. 0.01 is fast weathering, 0.001 is medium weathering and 0.0001 is slow weathering.
Wave Erodibility	Wave Attenuation Constant	y	0.01, 0.1, 1		Wave erodibility controls the exponential decay rate of wave height. Smaller decay rate, (0.01), causes wave height to decay very little so that the erosive force of the wave remains large. Larger decay rate, (1), causes the wave height to decay rapidly, so that the erosive force is significantly reduced.

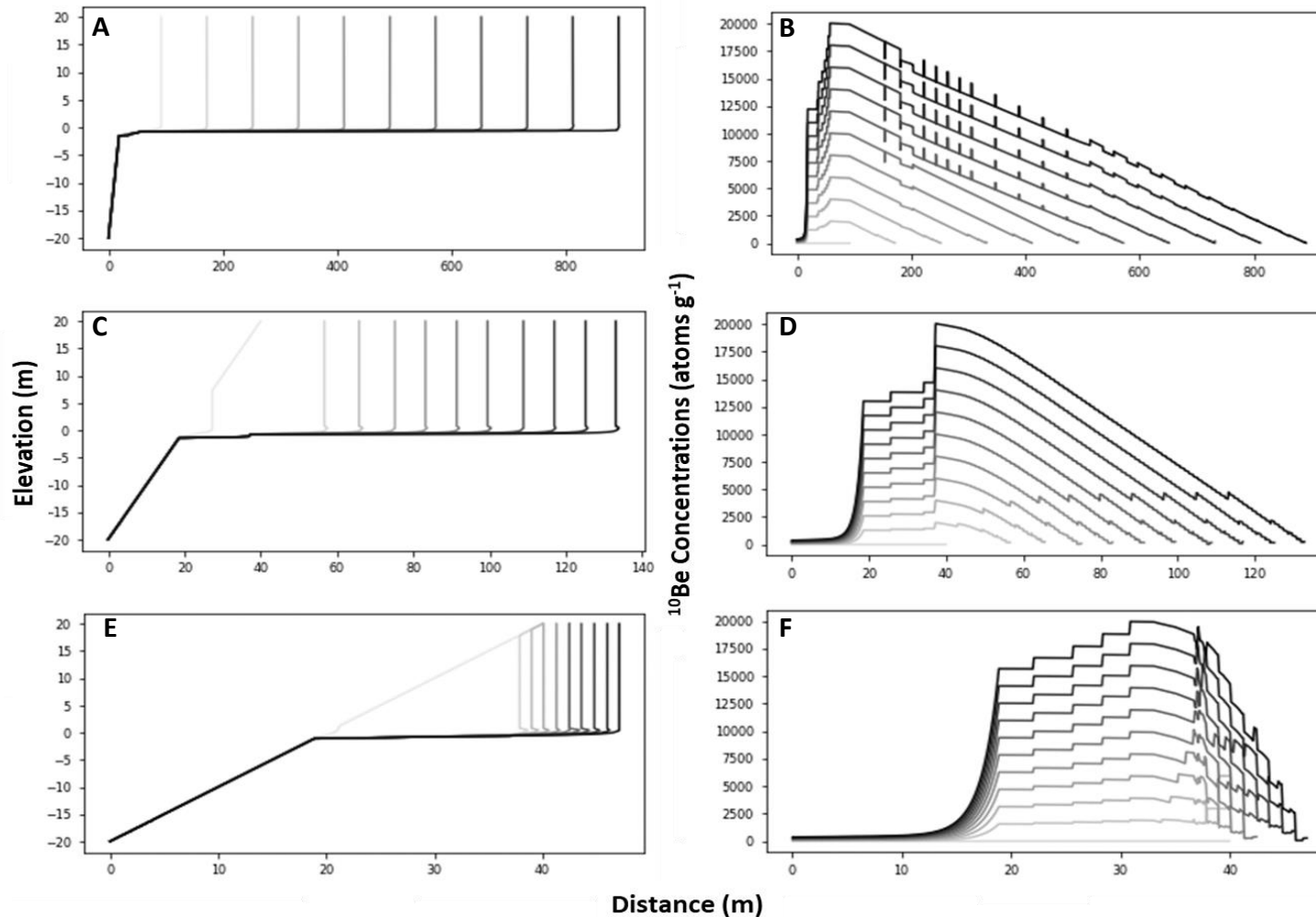


Figure 5.1: RPM model outputs for material resistance sensitivity test. The three plots on the left show the shore profiles and on the right are the nuclide concentration profiles for the platforms, the seaward edge is represented at 0 on the x axes on all plots. Each plot has 10 profiles printed at intervals of 800 iterations, lighter lines are earlier iterations, darker towards the end of the model run. (A) shows the morphological output for soft rock (0.001), (B) the output concentrations for soft rock. (C) morphological output for medium rock (0.01), (D) output concentrations for medium rock and (E) morphological output for hard rock (0.1), (F) output concentrations for hard rock.

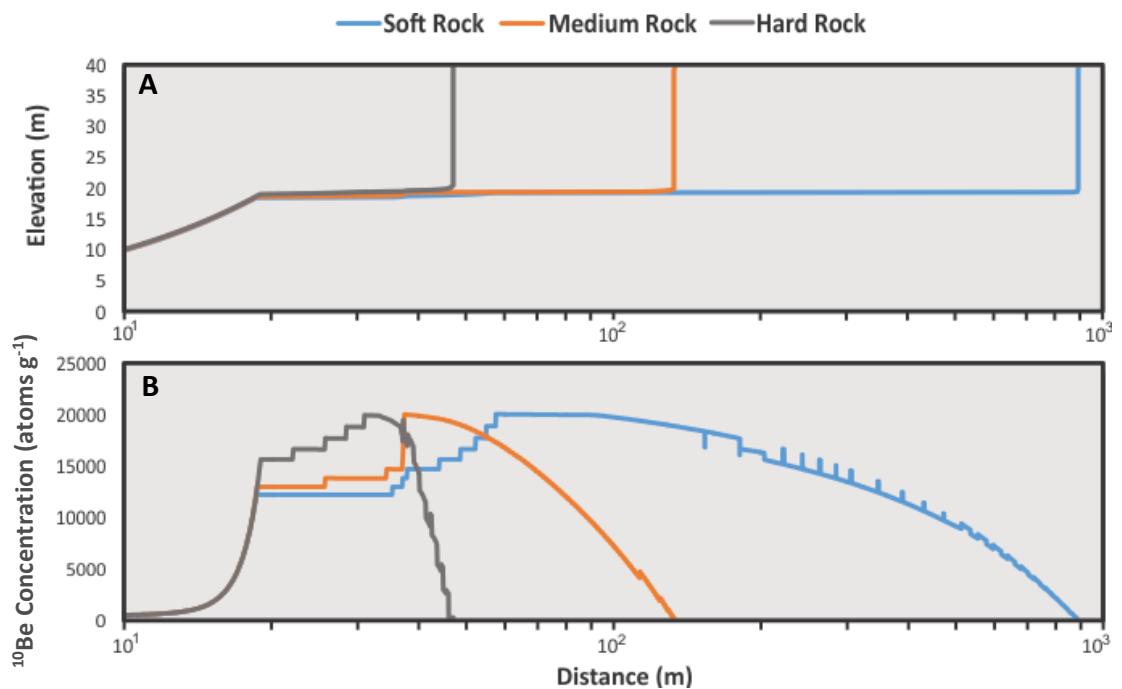


Figure 5.2: Final profiles after 8000yrs for the material resistance tests. (A) morphological outputs, (B) output concentrations. Profiles are compared on logarithmic scale horizontal axes. The profiles for Soft Rock are significantly longer than those for medium and hard rock. However all of the profiles show that nuclide concentration builds to similar levels. All the profiles also indicate that re-incision of the seaward edge has lowered concentrations on the outer platform. Note that all concentration profiles exhibit stepped reduction towards the seaward margins. These are associated with platform erosion, as physical steps in the platform profiles occur at the same positions that the concentrations peak. Sea level is positioned at 20m.

The next test was of the weathering rate, shown in *Figures 5.3 and 5.4*. This is an important driver to test as the weathering rate affects the pace of the breakdown of the rock material from year to year. These outputs emulate very closely the outputs of the material resistance test. There is a difference between the slow weathering rate profiles and the hard rock profiles. This difference comes from the depth of the re-incision on the seaward edge of the platforms profile. From this difference, it appears that material resistance controls the extent of the outer platform incision as the concentration trends in *Figure 5.4* all mimic the step down in ^{10}Be concentration on the outer platform, which is shown in the medium resistance output (*Figure 5.2*).

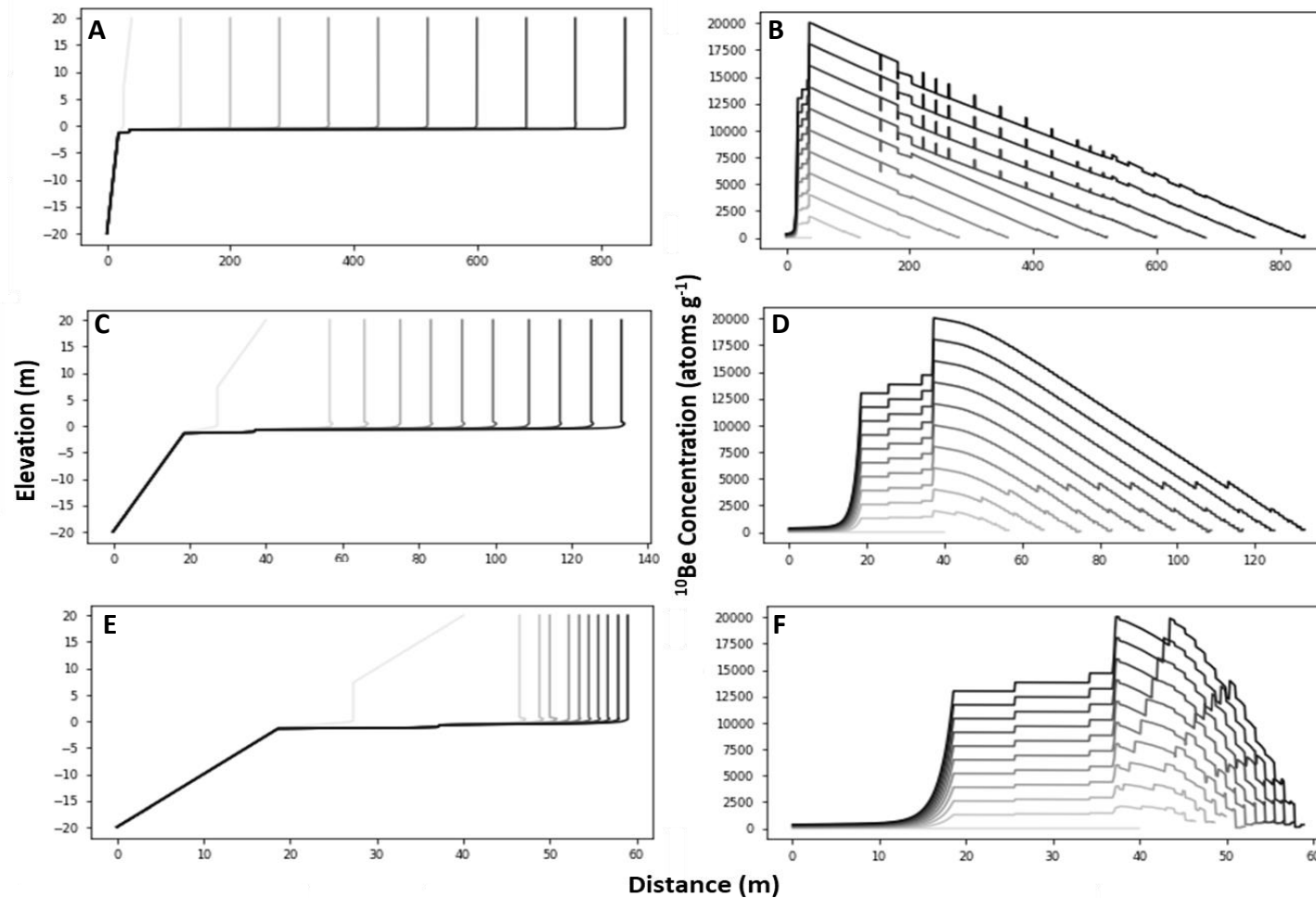


Figure 5.3: RPM model outputs for weathering rate sensitivity test, where other parameters (rock hardness & wave efficacy) are held constant. The three plots on the left show the shore profiles and on the right are the nuclide concentration profiles for the platforms. Each plot has 10 profiles printed at intervals of 800 iterations, lighter lines are earlier iterations, darker towards the end of the model run. (A,B) shows the output for fast weathering (0.01m^{-1}), (C,D) medium weathering (0.001m^{-1}) and (E,F) slow weathering (0.0001m^{-1}).

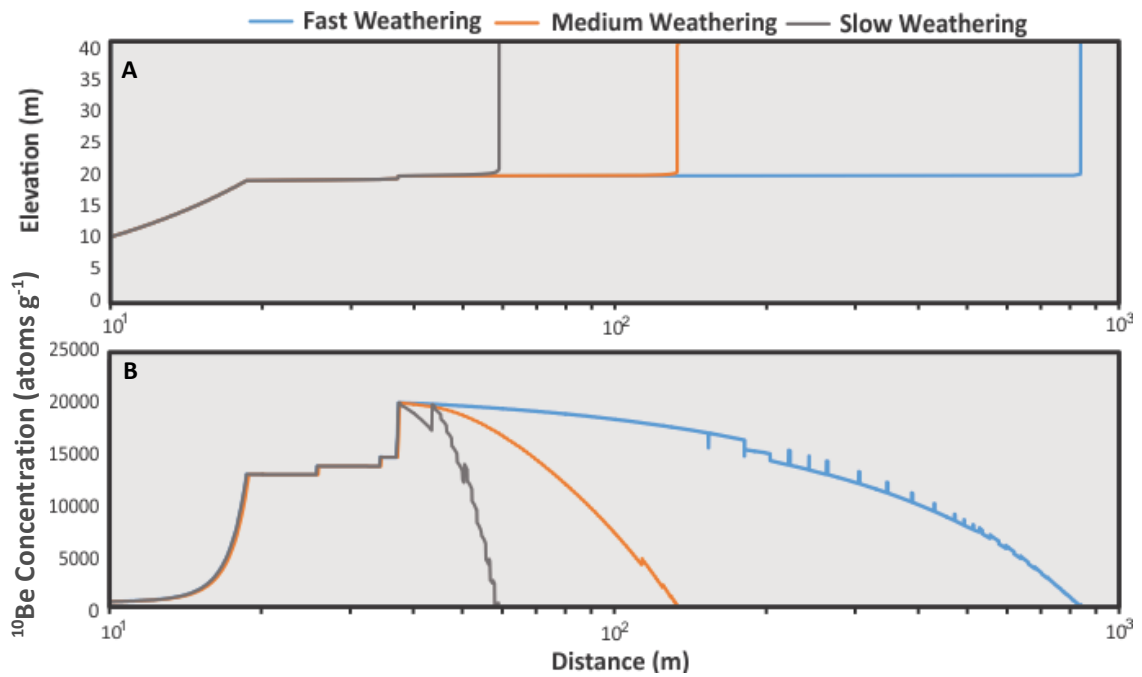


Figure 5.4: Final profiles after 8000yrs for the weathering rate tests. Profiles are compared on logarithmic scale horizontal axes. The profiles for fast weathering are significantly longer than those for medium and slow weathering. However all profiles reach similar nuclide concentrations. All the profiles also show re-incision of the seaward edge has lowered concentrations on the outer platform. All of the concentration profiles exhibit the same step down in concentration associated with the platform erosion for medium rock resistance. Sea level is positioned at 20m.

The final model runs were for the wave attenuation constant, and results are given in Figures 5.5 and 5.6. These runs produced outputs that are different from the previous two. High wave efficacy appears to produce narrower platforms than high weathering rate or low material resistance. The profile for high wave efficacy also shows re-incision to almost half-way across the platform. The profiles for low wave efficacy also produced a wider platform than low weathering rate or high material resistance. The concentration profile for low wave efficacy is relatively linear, with minimal incision at the seaward edge, in contrast to the other sensitivity tests.

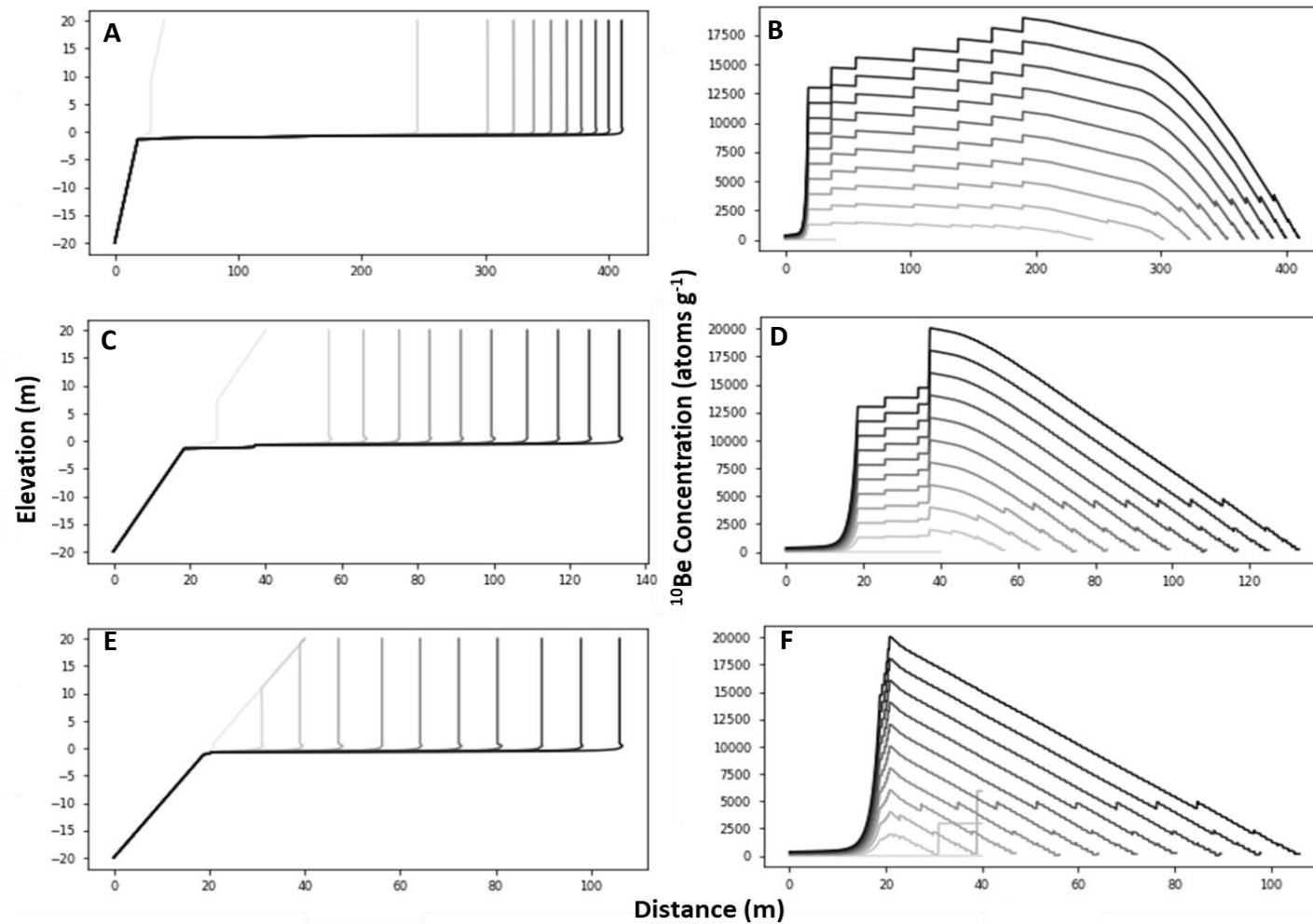


Figure 5.5: RPM model outputs for wave efficacy (erodibility) sensitivity test. The three plots on the left show the shore profiles and on the right are the nuclide concentration profiles for the platforms. Each plot has 10 profiles printed at intervals of 800 iterations, lighter lines are earlier iterations, darker towards the end of the model run. (A,B) shows the output for high wave efficacy (0.01), (C,D) medium wave efficacy (0.1) and (E,F) low wave efficacy (1).

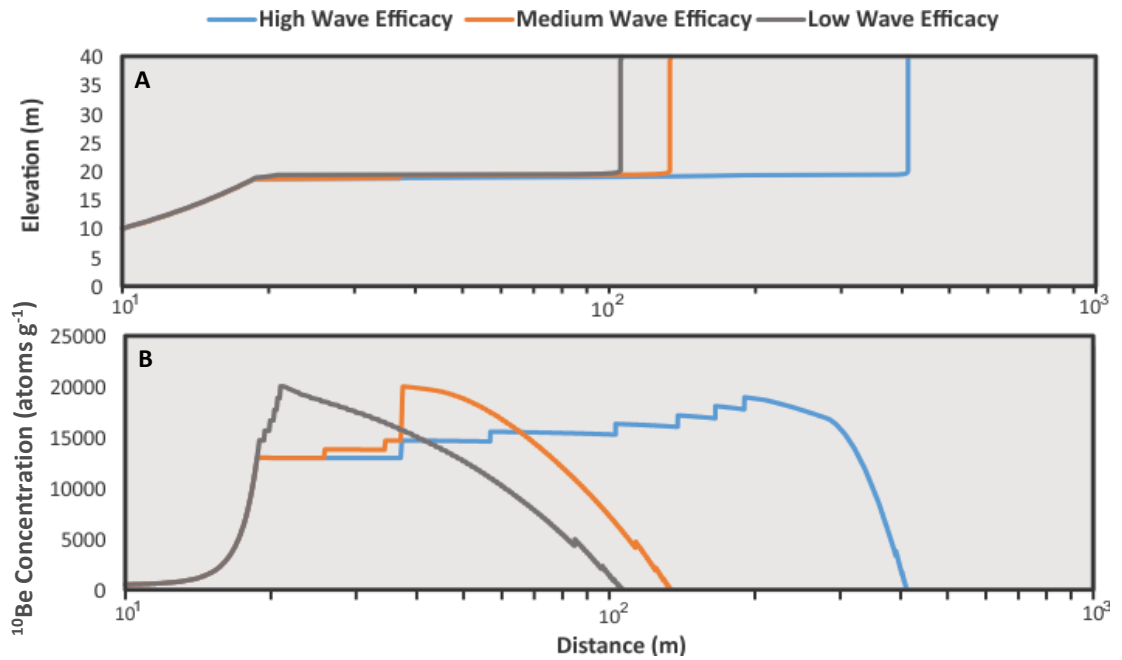


Figure 5.6: Final profiles after 8000yrs for the wave efficacy tests. Profiles are compared on logarithmic scale horizontal axes. The profiles for high wave efficacy are substantially longer than those for medium and slow weathering. All profiles reach similar nuclide concentrations. All the profiles also show re-incision of the seaward edge has lowered concentrations on the outer platform. Sea level is positioned at 20m.

5.2 RPM Scenario Testing

5.2.1 Sea Level Changes

The second set of model tests were based on scenarios of sea level rise, fall and tectonic movements as outlined in section 4.3.1. The first scenarios tested were continuously falling sea level over the entire model run and continuous sea level rise over the model run. The RPM allows for the direct input of rates of sea level rise in myr^{-1} . It is also possible to set up changes in the rate of sea level rise at set intervals during the model run. The tectonic uplift control is used to simulate sea level fall, as the sea level control only simulates sea level rise. The uplift control requires that values are specified for the number of tectonic uplift events, the iteration in which they occur and the magnitude of the event. For example a single uplift event may be: 1 event, occurring at iteration 5000, causing 1m of uplift. To simulate continuous sea level fall with this control, an array of very small events can be set up to occur at short time intervals for the duration of the model run.

For the continuous sea level fall tests, 0.0625m uplift events were set to occur every 50 iterations to produce a relative sea level fall rate of 0.00125m a^{-1} . This equates to 10m of total relative sea level fall over the 8000 iterations.

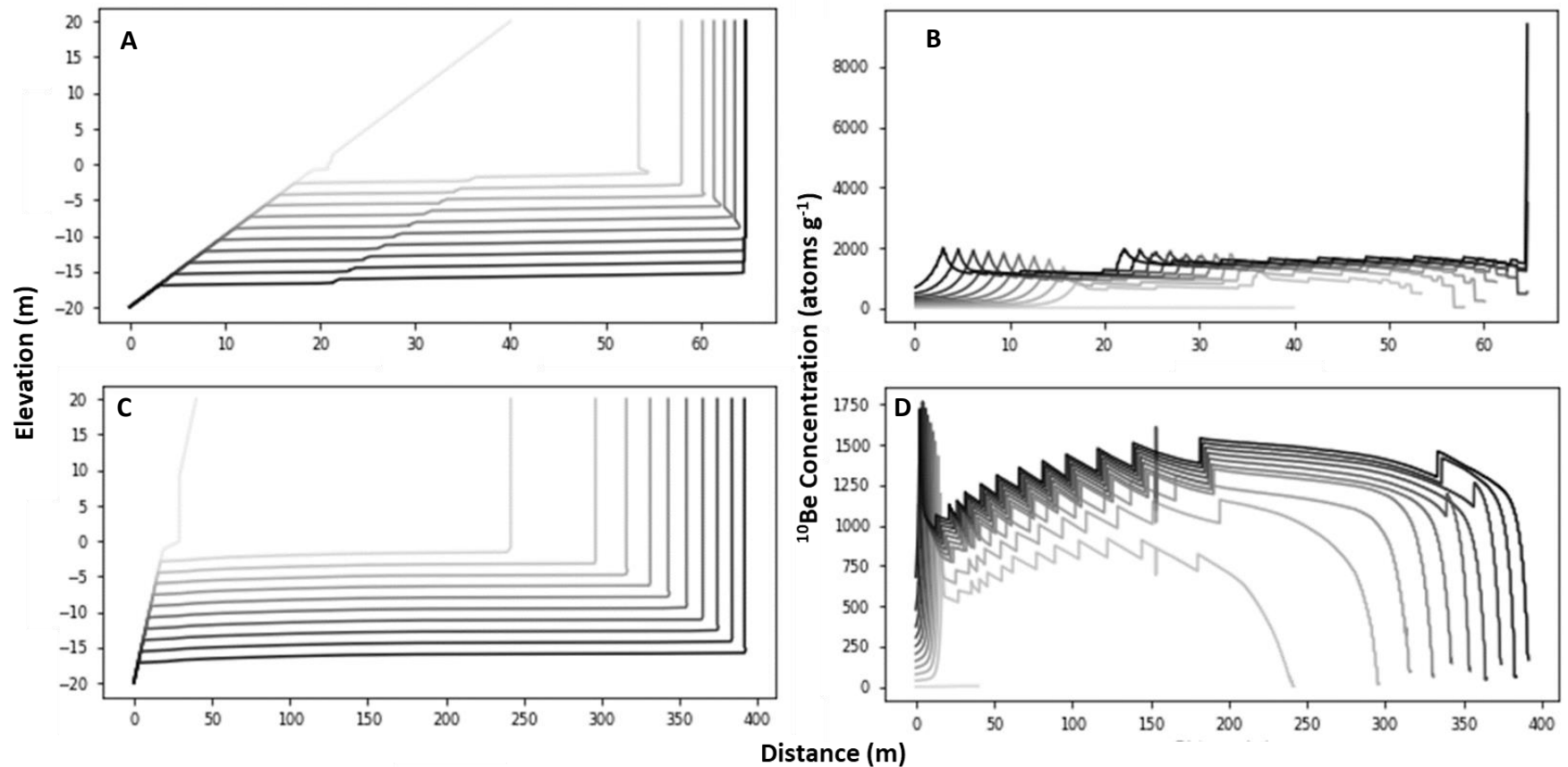


Figure 5.7: RPM outputs for falling sea level tests. Plots on the left show the evolving shore profile at intervals of 800 iterations. Plots on the right show the evolving profiles of the nuclide concentration across the shore profiles. (A,B) Sea level fall with hard rock. (C,D) Sea level fall with medium rock. Note that in the concentration plots there are some irregularities, specifically in (B) where the final profile shows a very high concentration at the cliff position. This is not likely to be real, indicating that the model has thrown an error in the output. In (D) there are also some abnormalities in the output. It is important to note that the output concentrations are similar for B and D, when accounting for the difference in the scale of the Y axes on the two plots.

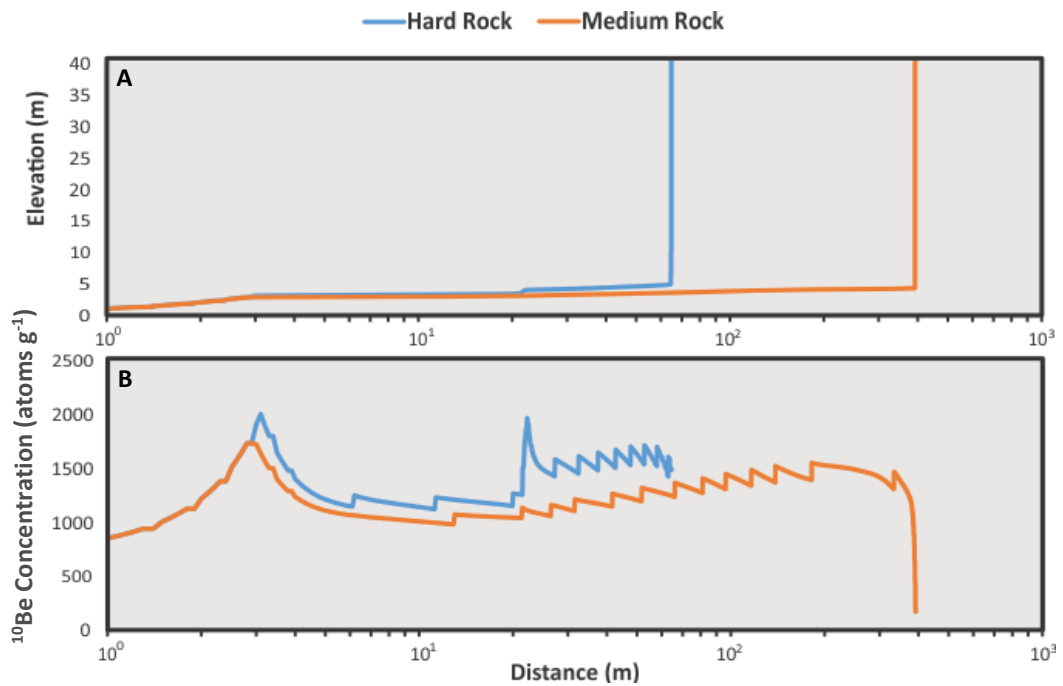


Figure 5.8: Final profiles for falling sea level RPM runs. The profiles are plotted on a logarithmic x axis. In the concentrations plot, the hard rock curve does not approach zero near the cliff juncture. This is due to the abnormality in the mode output, which had been removed for clarity of comparison in this figure. The line should curve down to zero where the rock of the platform is most recently exhumed. Sea level position is 20m at the beginning of model run.

This test was run both with medium and hard rock parameters for the material resistance. The two resistance values were used as they are more representative of the rock strength of the shore platforms being investigated in the two case studies for this thesis. The soft rock model runs (refer to section 5.1) formed platform widths substantially wider than platforms in these case studies. The outputs for these falling sea level model runs are given in *figure 5.7 and 5.8*. With both hard and medium resistance rock, the shore profiles appear to erode down to the new sea level, producing profiles at lower elevations. It also appears that the platforms have undergone re-incision of the seaward portions, visible from the step-down in concentrations. There are also peaks in the concentrations at the sea-ward margins of both profiles, indicating elevated rampart development. These sea level fall tests both produce very low concentrations (>2000 atoms g⁻¹).

Sea level rise tests were set up using the sea level control, so a continuous rate of sea level rise could be applied across all iterations. Once again the model was run twice, with hard and medium rock resistance. A rate of 0.00125m a⁻¹ was applied for the full duration. These outputs are shown in *figure 5.9 and 5.10*

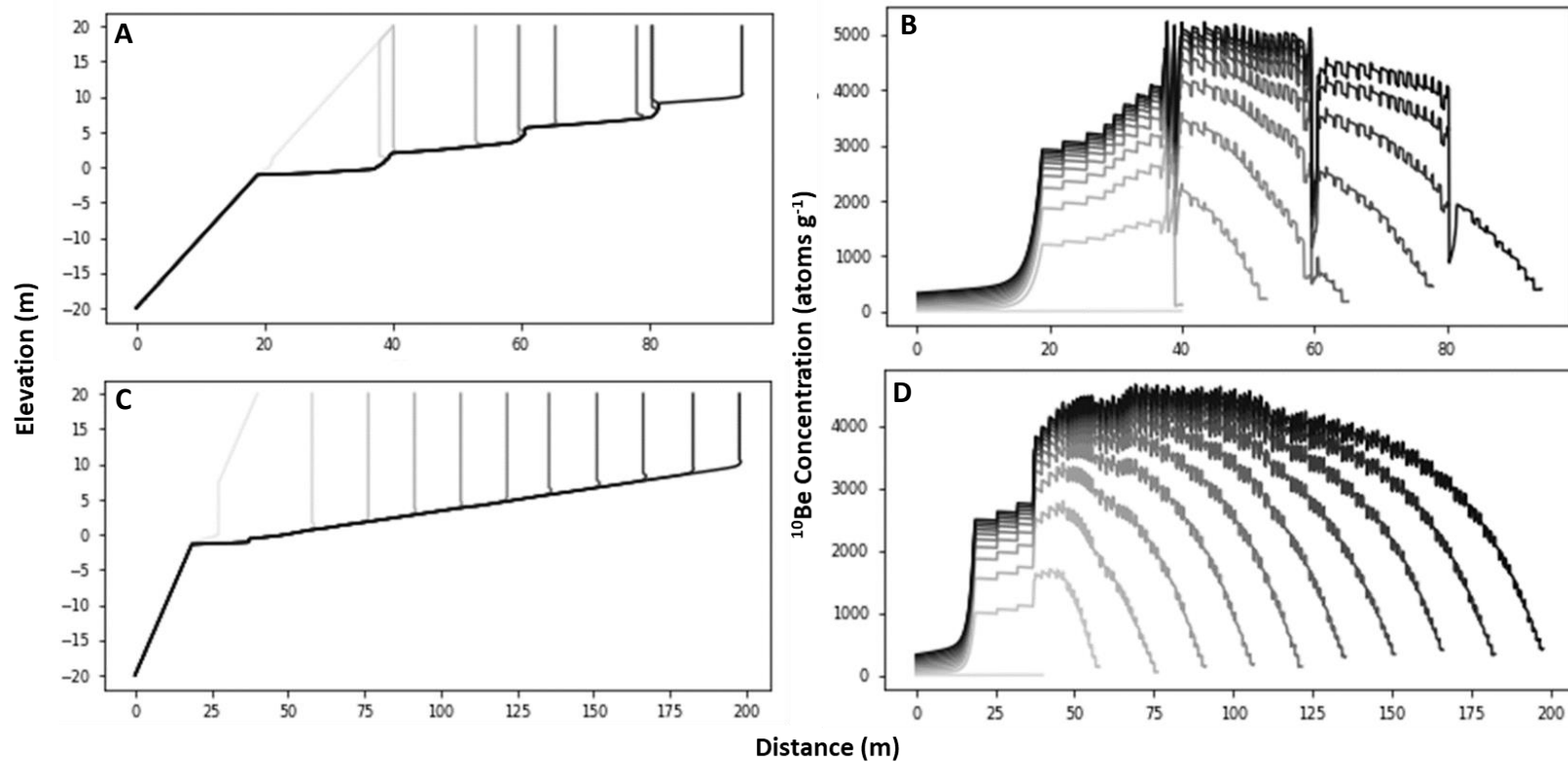


Figure 5.9: RPM outputs for the sea level rise. Plots on the left show the evolving shore profile at intervals of 800 iterations. Plots on the right show the evolving profiles of for the nuclide concentration across the shore profiles. (A,B) Sea level fall with hard rock. (C,D) Sea level fall with medium rock. The hard rock profile has developed into a stepped morphology, while the medium resistance profile had developed a sub-tidal slope. The concentrations of the stepped profile show four distinct changes in the concentrations across the platform, lining up with each step. In both runs there is a lack of a rampart, probably due to the drowning of the outer platforms.

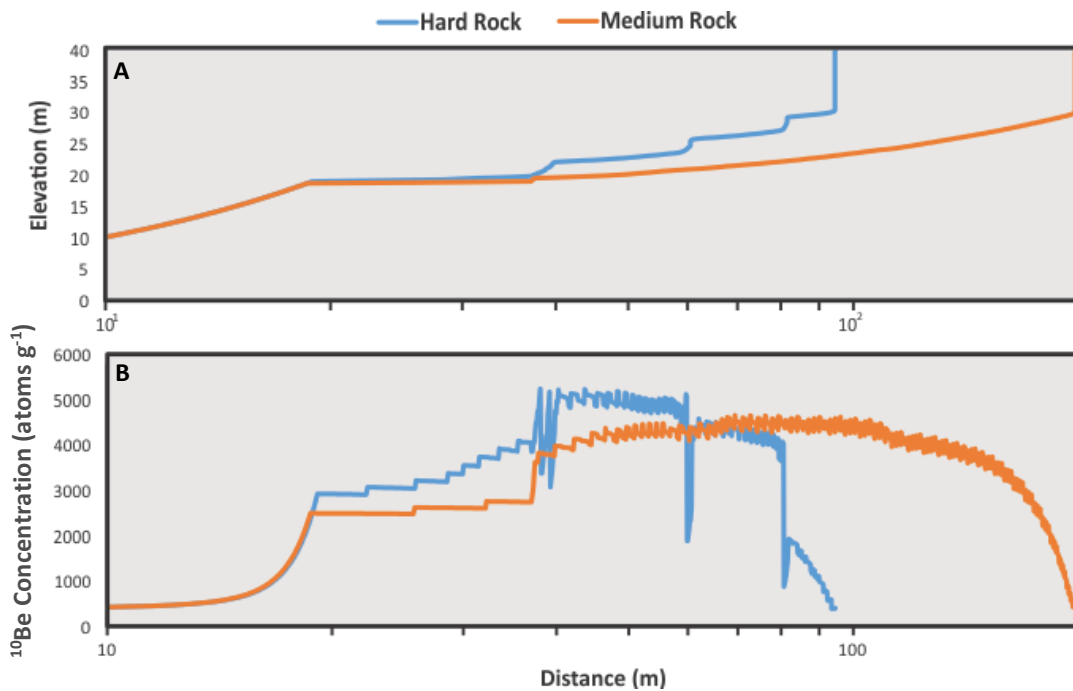


Figure 5.10: Final profiles for rising sea level RPM runs. The profiles are plotted on a logarithmic x axis. Note that the concentration profiles (B) are noisy. This indicates surface roughness of the platform profiles. Roughness is not visible in the platform profiles (A) due to the large scale used to show that entire profiles. Sea level position is 20m at beginning of model runs.

The model outputs for sea level rise are consistent with each other, both producing sub-tidal slopes as the sea level rises and causes the platform to cut back at higher elevations. The formation of the stepped profile with hard rock shows that sea level rise plays a role in the development of terraced rocky shore line.

5.2.2 Tectonic Perturbations

The next set of model runs were applied to test the impact of earthquakes which uplift the coastline relative to the sea level, driving relative sea level fall. These differ from the sea level fall simulations as few, large events are modelled as opposed to the regular small events used to mimic sea level fall (section 5.2.1). Here the events that are simulated are fewer and of a much larger magnitude (uplift >1m). The first set of model runs were aimed at testing the effect of step size (or magnitude) on the platform geometry, to evaluate if step size determines whether a platform surface becomes preserved above sea level or not. To test this potential control the models were run three times with the medium values set for all of the primary controls. In each run there were six uplift events which caused 0.5m, 1m and 2m of uplift for each successive run. The model outputs for these three runs is given in *Figures 5.11 and 5.12*.

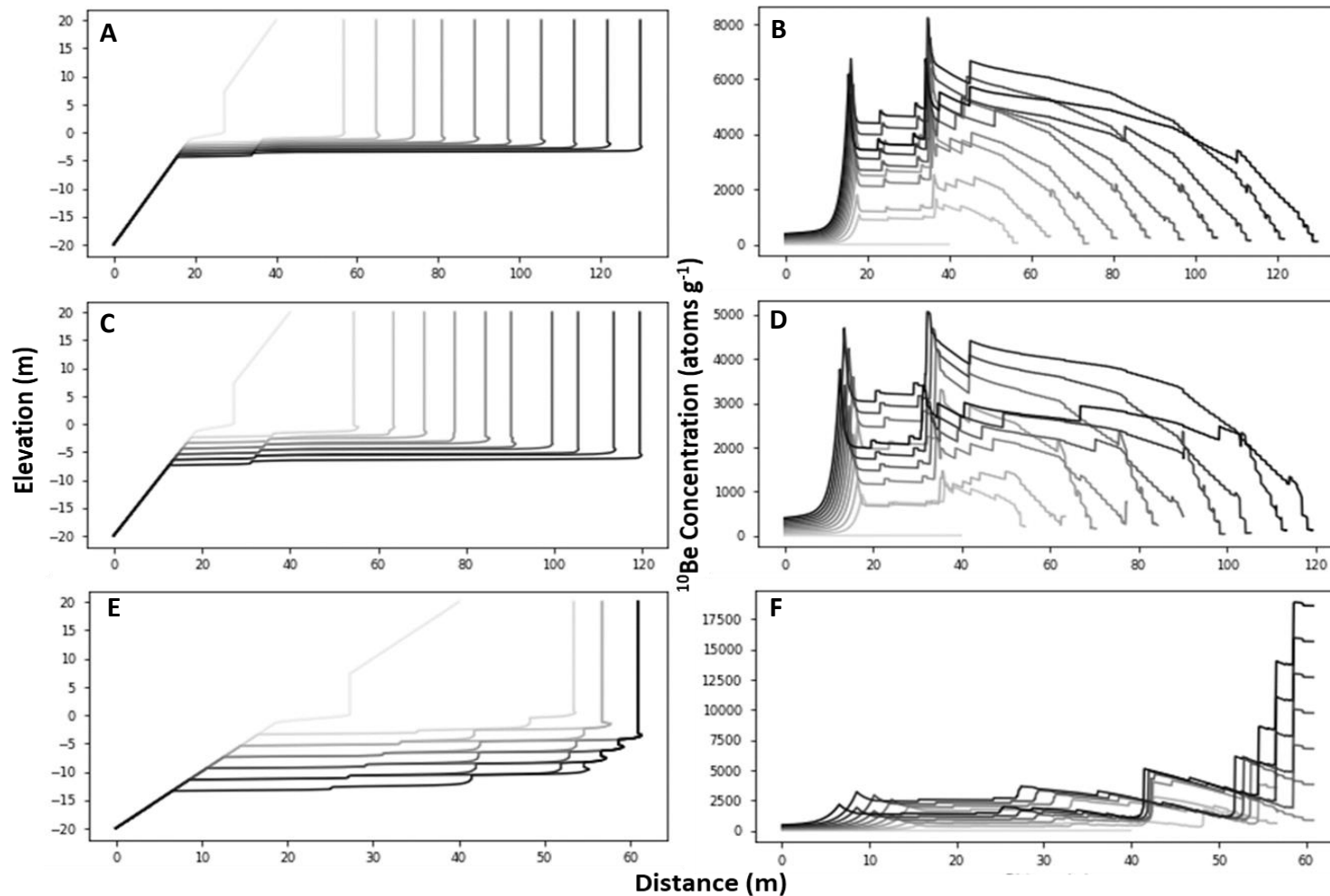


Figure 5.11: RPM model outputs for uplift step size tests. Plots on the left show the shore profiles, while plots on the right show nuclide concentrations across the platform. (A,B) step size of 0.5m, (C,D) step size of 1m, (E,F) step size of 2m. The outputs for the first two runs appear very similar, but E,F appear to have a large enough step size to cause stranding. The concentrations appear to be lower with higher step size. Some of the events also appear to be evident in the concentrations, where the concentration profile becomes lower and more spread out. This is seen best in the concentration plot for profile B.

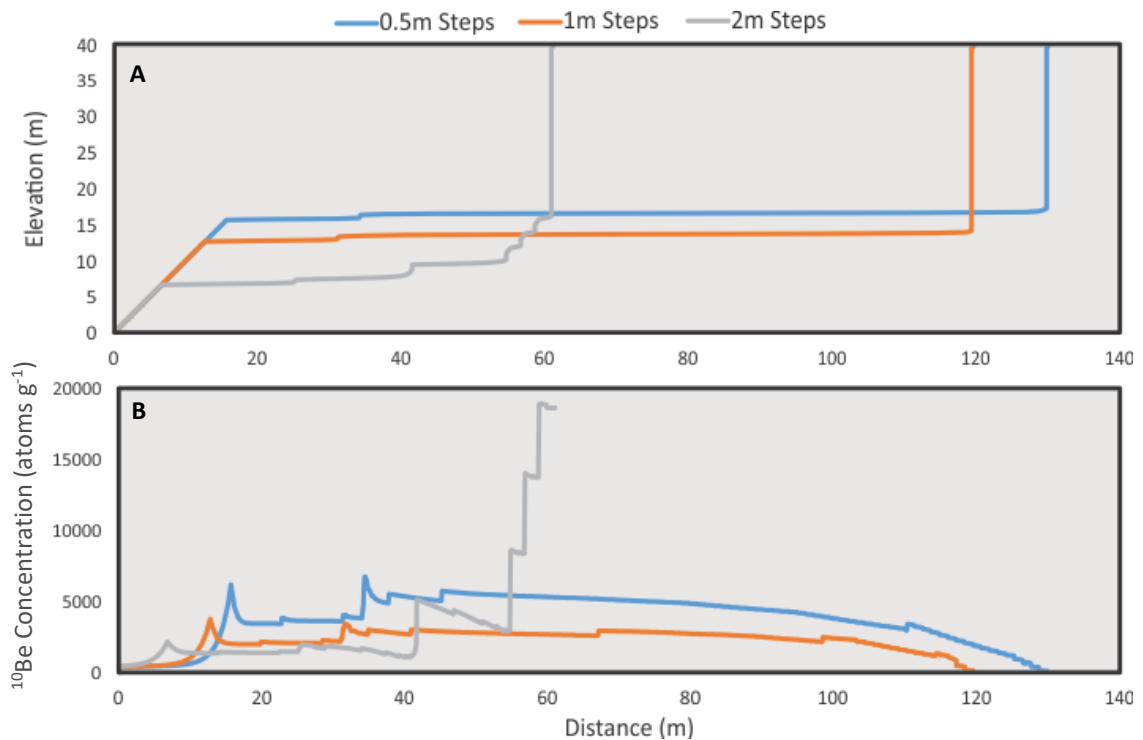


Figure 5.12: Final profiles for the step size RPM runs. The smaller sized steps have produced much wider platforms than the 2m step size. The concentrations on the 2m step size profile do reach much higher levels on the preserved steps than the other two profiles. This was probably caused due to the stranding of the steps followed by long-term exposure.

These step size tests reveal that the lower magnitude uplift events are not significant enough to strand a platform surface above sea level. After each successive uplift event the shore platform is incised again from a lower position, which eventually draws the platform surface back down to the sea level. However, with the 2m uplift step size the model is unable to completely planate off the surface after each event. This is why the profile for this model run was not as wide as the others, resulting in the development of a series of small steps, which are preserved above the sea level. These are not subsequently eroded as the model requires water to be inundating the rock surface for erosion to occur, so the steps have accumulated large nuclide concentrations. The active part of the platform has lower nuclide concentrations than the other two profiles, as it is eroded more significantly after each uplift event.

Finally the RMP was also run to investigate the effect of uplift event recurrence interval. In the previous test the interval between each uplift event was 1500 iterations. This was not based on any known fault rupture recurrence intervals. For this test the magnitude is set as equal for all runs at 1m. This magnitude is chosen simply to emulate the level of uplift observed in the M_w 7.8 Kaikoura earthquake in 2016.

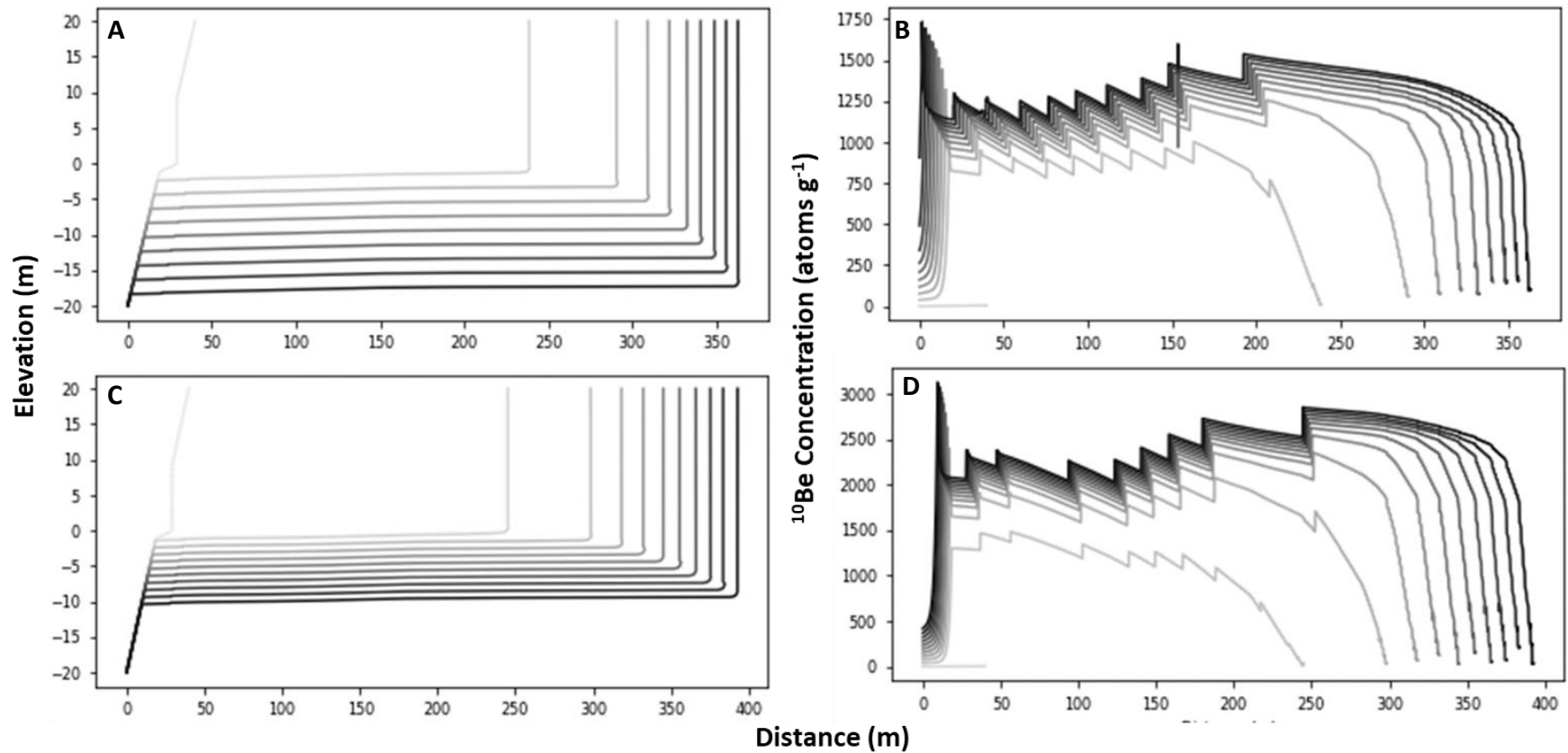


Figure 5.13: RPM outputs for the uplift recurrence interval tests. The plots on the left show the shore profiles. Plots on the right show nuclide concentration profiles. (A,B) is the output for a recurrence interval of 400 iterations, totalling 20 events of 1m uplift. (C,D) is the output for a recurrence interval of 800 iterations, totalling 10 events of 1m uplift. The profiles and concentrations look nearly identical, however, in a there are more events, which has resulted in more down wear and lower ^{10}Be concentrations overall.

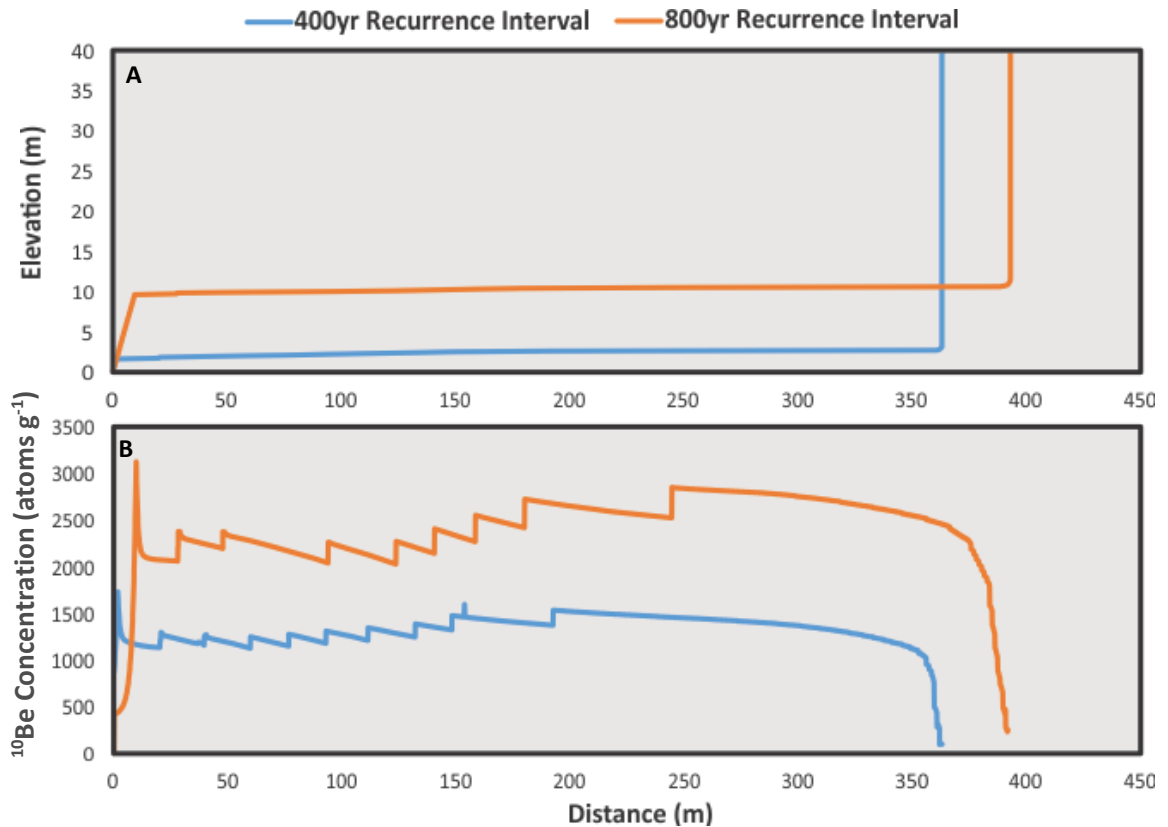


Figure 5.14: Final profiles for RPM uplift recurrence tests. The main difference between the short and long recurrence intervals is the width and elevation of the platforms they produce. The shorter recurrence interval produces a narrower and lower elevation profile with low nuclide concentrations. The longer recurrence interval produces a slightly wider, higher elevation platform with higher ¹⁰Be concentrations. The difference in the concentrations comes from the degree to which the two platforms have been eroded.

The number of events is based on the recurrence interval that is applied. Two recurrence intervals were selected for this test. A short interval of 400 iterations (years) was based on the fault rupture recurrence interval for the Kekerengu Fault, one of the major faults responsible for uplift near Kaikoura (Little et al., 2018). The recurrence interval reported in Little et al., (2018) was 376 ± 32 years; this interval has been rounded up to 400 years for simplicity in the model. The previous step size tests used a recurrence of 1500 years, so a recurrence interval of 800 years is used in here as a midpoint between this longer interval and the short one based on the Kekerengu fault. These outputs are shown in *figures 5.13* and *5.14*. Ultimately the recurrence interval effects the erosion on the shore platform. Higher frequency of uplift events results in more down wearing and lower nuclide concentrations.

Chapter 6: Wakatu Point, Results and Discussion

Tectonics have had a significant impact on the development of landforms on Kaikoura peninsula. A series of well-defined marine terraces, set against a back drop of the Kaikoura mountain ranges, one major fault and several smaller active faults define this story. Wakatu point, one of many shore platforms on the flanks of the stepped peninsula is linked with this story. Here, the results of the cosmogenic analysis of this shore platform and subsequent modelling work are presented, followed with a discussion of these results.

6.1 Results

The total station profile survey conducted at Wakatu Point, which runs north-east, revealed that the platform there is wide and sloping gently with a slope angle of 1.04° . The platform is, however, very irregular on a meter by meter scale, with many topographic highs and low due to the tight folding of the geology present. The survey profile is shown in *Figure 6.1*. It shows that a large high point disrupts the sloping direction of the shore platform at the seaward edge of the profile. This high point is discontinuous in the NW and SE directions and is likely a feature of geological control. Due to the loss of three samples that were collected on the outer platform there is only one sample (AD07) from which to gain information of the seaward section, and no samples remain that were taken from the high point at the edge. Also important, is that the cliff is not in this profile. The cliff is roughly another 120m back from the active platform, behind a developed area. The wide area between the cliff and active platform points to the likely case that the cliff has been abandoned by wave action. Thus, the sampled area represents the outer portion of the platform which is incising back into the original platform.

The samples, processed with the Accelerator Mass Spectrometer at PRIME lab, all returned $^{10}\text{Be}/^9\text{Be}$ ratios well above the blank ratio from the second sample set (AD09), indicating that sample processing was successful. From the $^{10}\text{Be}/^9\text{Be}$ ratios, the total concentration of ^{10}Be atoms per sample has been calculated, correcting for the lab blank. The blank that was processed with these samples, AD08, was returned from the AMS with a $^{10}\text{Be}/^9\text{Be}$ ratio that was high relative to other lab blanks from the lab the

samples were processed in. This was indicative of blank contamination sometime during the isotope isolation steps in the clean lab, potentially due to a beaker contamination that would not affect the other samples. Because the Wakatu blank was compromised, the Okakari blank has been used instead, to correct for the ^{10}Be concentration. Both blanks were processed under the same lab conditions with the same procedures. The Okakari blank ratio was low in comparison to the samples and represented similar ^{10}Be counts to other blanks processed in the large accelerator mass spectrometers from this lab.

The blank corrected concentrations for each sample are plotted in *Figure 6.2*. By using the lower blank, total errors are kept to a minimum within 13.2%. However, these cannot be considered low errors. *Figure 6.2* shows that there is no apparent trend across the platform in the Wakatu data.

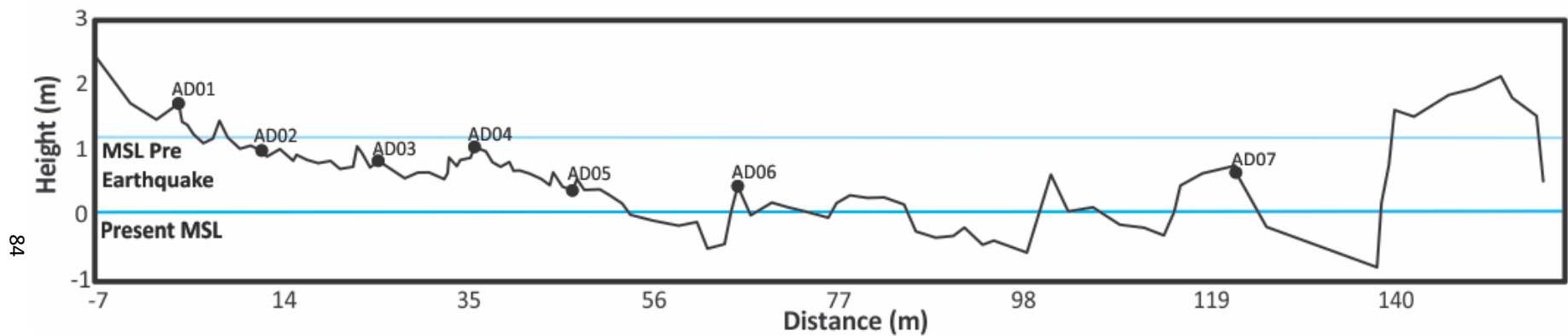


Figure 6.1: Shore Profile surveyed at Wakatu Point across widest part of the platform, lining up with sample transect. Survey was taken during low tide to capture as much of the profile as possible, however satellite imagery shows a submerged portion of this platform continues past this profile. The positions of the samples that were processed are given as the black dots. The positions of mean sea level in the present day and the mean sea level prior to the November 2016 Kaikoura Earthquake are also given.

Table 6.1: Measured $^{10}\text{Be}/^9\text{Be}$ ratios for Wakatu, after AMS and total concentration of ^{10}Be atoms in each sample. Calculated using KNSTD07 lab standard.

Sample	Location	Location	Shielding Factor	Thickness Scaling Factor	$^{10}\text{Be}/^9\text{Be}$ ratio	Error	Mass Dissolved	Mass ^9Be added by carrier	^9Be added by carrier	^{10}Be sample Conc	^{10}Be sample Conc error	Total Error
Label	Lat	Lon				%	g	g	atoms	atoms/g	atoms/g	%
AD01	-42.414624	173.705561	0.9623	0.9303	4.01E-14	12.4	62.622	0.00029	1.96E+19	12100	1590	13.20%
AD02	-42.414588	173.705696	0.9935	0.9377	3.44E-14	9.4	68.997	0.00029	1.96E+19	9310	960	10.30%
AD03	-42.41451	173.705794	0.9911	0.923	4.27E-14	7	59.881	0.00029	1.96E+19	13500	1040	7.70%
AD04	-42.414463	173.705880	0.9949	0.9157	3.61E-14	8.3	61.685	0.00029	1.97E+19	11000	1000	9.20%
AD05	-42.414441	173.706042	0.9652	0.9303	2.82E-14	9.4	67.264	0.00029	1.97E+19	7770	831	10.70%
AD06	-42.414371	173.706265	0.9770	0.9014	2.80E-14	9.4	52.363	0.00029	1.97E+19	9900	1060	10.70%
AD07	-42.414276	173.707820	0.9869	0.9303	3.02E-14	9.4	62.434	0.00029	1.97E+19	9010	951	10.60%

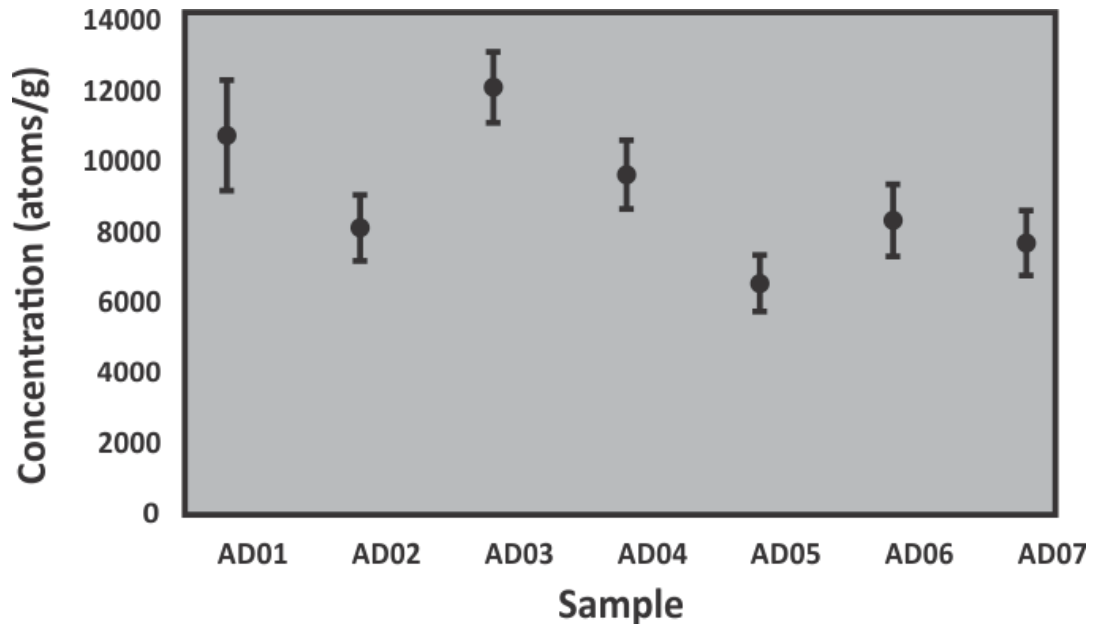


Figure 6.2: Concentrations in total atoms per gram of quartz for Wakatu Samples, plotted in the order they occur on the shore platform from the landward to the seaward.

Topographic shielding was calculated using the former CRONUS earth calculator version 2.3 (Balco et al., 2008). Figure 6.3 shows the view shed obstructed by the topography surrounding each of the samples. Because the cliff at Wakatu point is located ~200m landward it does not significantly shield the cosmic ray flux, hence all of the samples are only shielded a small amount by the topography. The most significant obstructions to the horizon were small scale localised topography, which were the main cause of slightly higher shielding factor. The Seaward Kaikoura ranges, which climb to over 2600m asl to the west-north west of the sample site also played a role in the topographic shielding.

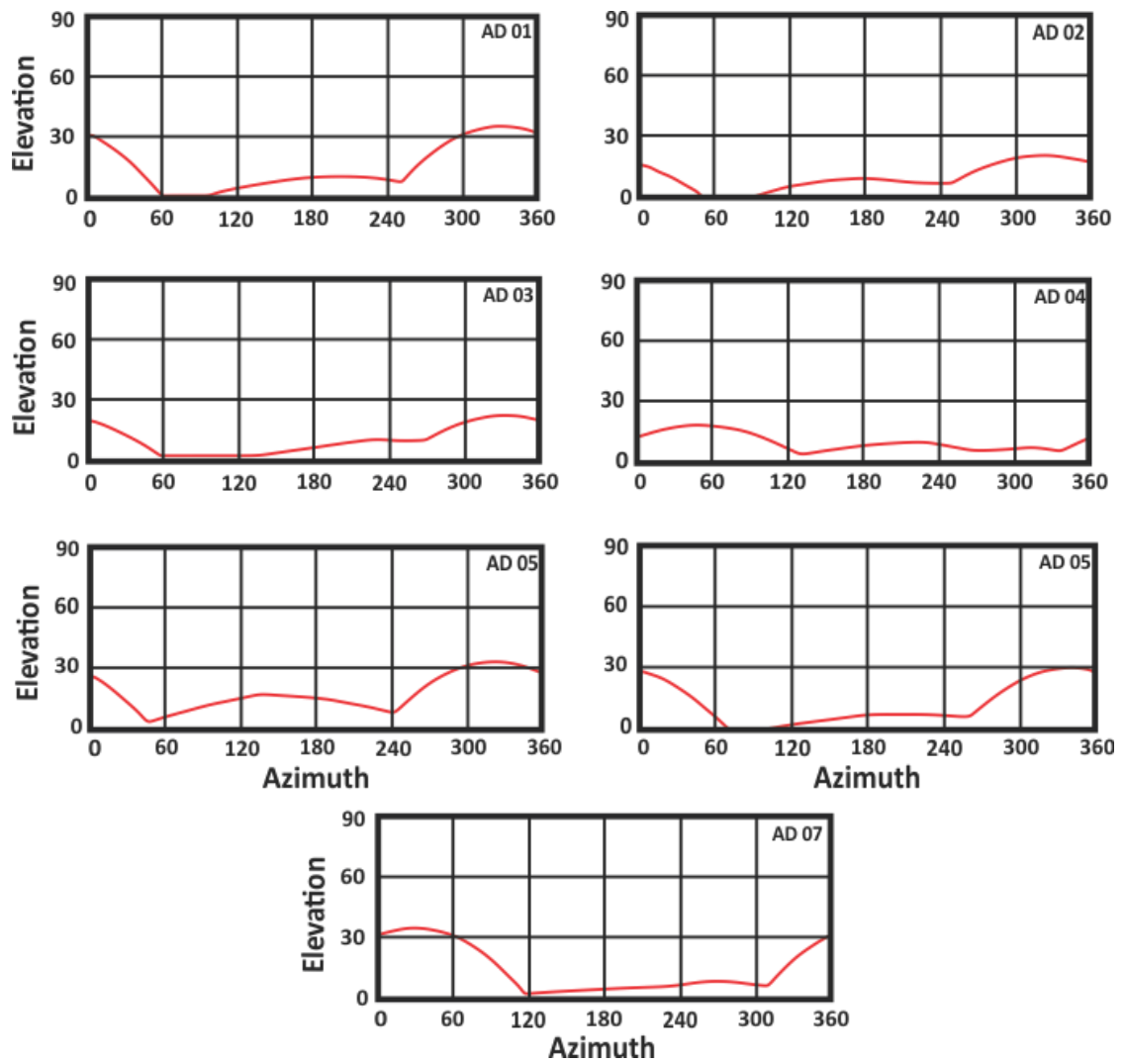


Figure 6.3: Obstructed portion of the view shed by topography (red line) for each of the samples at the position they were extracted. Sample ID is in top left of each plot.

Exposure ages for each of the samples were then calculated with the former CRONUS calculator version 2.3, using the above shielding factors. The calculator requires that a surface erosion rate is input in order to calculate the exposure ages. The erosion rate used to calculate these exposure ages was 0mm a^{-1} . Zero erosion was used as we do not know the long-term erosion rates on this shore platform at this stage. A 'no erosion' scenario will obtain the lowest possible exposure ages for the samples which enables the identification of a minimum age of initiation for this shore platform, i.e. the platform formed no later than $\sim 2\text{-}3\text{ka}$. The outputs for this model calculation are plotted in *Table 6.2*, which shows the production rate for each of the 7 samples after correction for shielding.

Table 6.2: Surface exposure ages for Wakatu Point samples calculated with the former CRONUS earth calculator using the Stone (2000) scaling scheme.

Sample ID	Thickness scaling factor	Shielding Factor	Production rate (muons) (atoms/g/yr)	Internal Uncertainty (years)	Exposure age (years)	External Uncertainty (years)	Production Rate (Spallation) (atoms/g/yr)
AD01	0.9303	0.9623	0.075	401	3052	479	3.51
AD02	0.9377	0.9935	0.075	233	2258	302	3.66
AD03	0.923	0.9911	0.075	257	3334	384	3.59
AD04	0.9157	0.9949	0.075	248	2727	340	3.57
AD05	0.9303	0.9652	0.075	209	1953	267	3.52
AD06	0.9014	0.977	0.075	272	2537	348	3.46
AD07	0.9303	0.9869	0.075	234	2217	301	3.6

Table 6.3: Exposure age results for four different time averaged scaling schemes.

Scaling scheme for spallation	Desilets and others (2003, 2006)		Dunai (2001).		Lifton and others (2005).		Time-dependent Lal (1991)/Stone(2000)	
Sample ID	Exposure age (yr)	External Uncertainty (yr)	Exposure age (yr)	External Uncertainty (yr)	Exposure age (yr)	External Uncertainty (yr)	Exposure age (yr)	External Uncertainty (yr)
AD01	3307	588	3280	576	3316	575	3132	504
AD02	2450	387	2432	379	2453	375	2320	322
AD03	3607	514	3575	500	3618	495	3419	413
AD04	2959	445	2937	434	2966	430	2800	364
AD05	2116	340	2098	332	2116	329	2009	285
AD06	2753	442	2733	433	2758	430	2605	369
AD07	2405	384	2387	375	2407	372	2277	320

Uncertainties in table 6.2 are internal and external. Internal uncertainty relates to the scaling scheme applied, and is derived from the uncertainty in reference production rates for spallation and muons of the scheme (Balco et al., 2008). External uncertainty, which is used for error calculation for these ages, is related to the measurement error in calculating nuclide concentrations (Balco et al., 2008).

The exposure ages were also calculated for four time dependent scaling schemes (table 6.3). These schemes use changing production rates through time taking into account variations in the magnetic field (Desilets et al., 2006; Dunai, 2001; Lifton et al., 2005) and the solar variability (Lifton et al., 2005). The scaling scheme used by the CRONUS calculator to produce Table 6.2 simply describes the variation in the spallogenic production rates with latitude and atmospheric pressure, assuming that the rates remain static through time (Balco et al., 2008).

The exposure ages calculated with CRONUS have been plotted in figure 6.4. Sample ages across the shore platform show no clear trend, with the 7 data points exhibiting a scattered range of ages. There is some clumping of the data points, with the distribution exhibiting a saw-toothed pattern. The oldest sample (AD03) shows an exposure age of 3334 ± 257 yrs BP. As this is a no erosion scenario, this represents the earliest time that the shore platform could have been exposed to the cosmic ray flux. Constraining a maximum bound for the exposure age of this platform is not possible as the samples may have reach secular equilibrium, where the sample is saturated with ^{10}Be . If this was the case, no age information could be gained from the nuclide concentration. It seems more likely that the samples are not at secular equilibrium and that the concentrations are simply low due to various types of surface erosion.

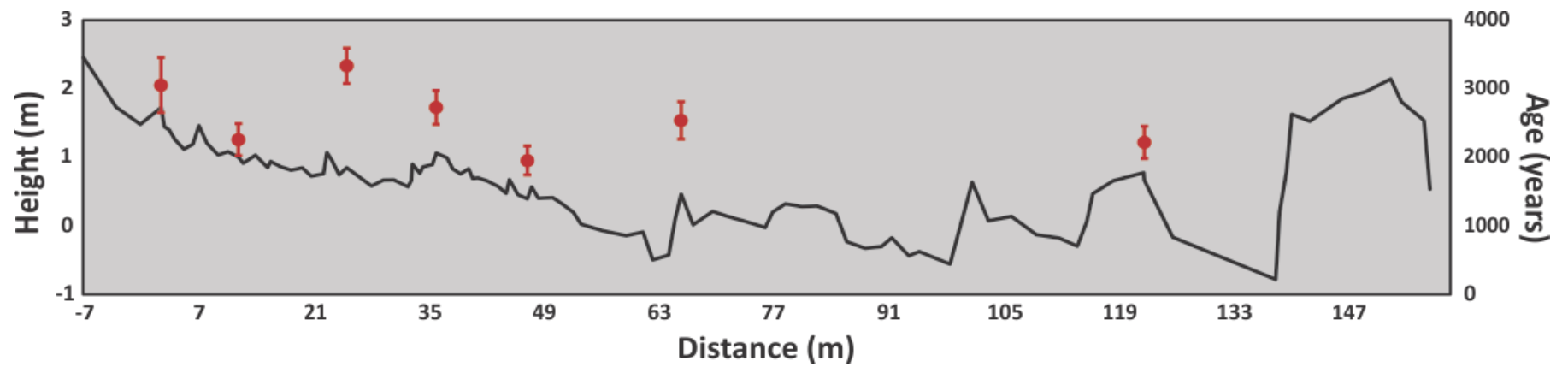


Figure 6.4: Exposure ages (right axis) of each Wakatu sample from the CRONUS output, plotted against profile of the shore platform. The left Y axis is the height above mean sea level position, which is at zero meters. MSL is the based on the Littleton harbour datum.

To determine the rates of platform surface erosion, nuclide concentration is plotted against exposure age for different erosion rates (as in *Figure 2.3* in chapter 2). Erosion rates that are possible on the shore platform are those which intersect with the full range of measured concentrations in this plot (*Figure 6.5*). Faster erosion rates would yield maximum nuclide concentrations that are lower than those measured. *Figure 6.5* shows that the highest possible erosion rate for the Wakatu platform would be $\sim 0.2\text{mm a}^{-1}$. However, if this were the case then the oldest sample (AD03) could have been exposed upwards of 16ka in the past. The true erosion rate for the Wakatu site likely lies somewhere between 0 erosion and 0.2mm a^{-1} .

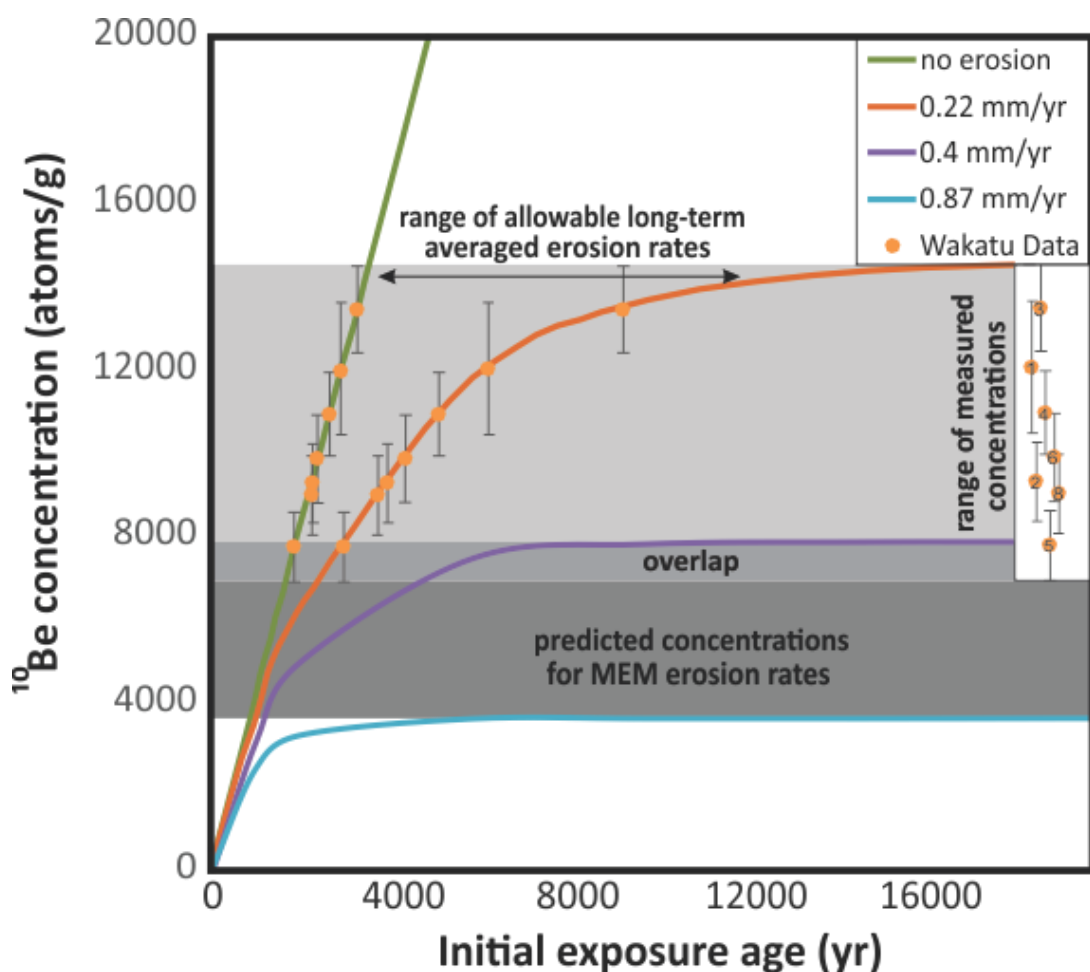


Figure 6.5: Erosion rates plot for Wakatu point showing the range of the samples concentrations (right) greyed out. Erosion rate curves which fully intersect this area of the plot represent realistic erosion rates that could have produced the measured range of concentrations. The sample concentrations are also plotted on the line which intersect the grey zone to show how old the samples would be with each rate. Two higher erosion rates are also plotted, these are known modern lowering rates from Stephenson et al., (2010). The curve for the slower of the two rates (0.4mm a^{-1}) just intersects with the sample concentration range before it reaches equilibrium. The 'no erosion' line represents that data plotted in figure 6.2.

6.2 Best Fit Model Result

The RPM model was applied with a parameterization that best reflected the conditions during which it was estimated that the Wakatu platform was cut. In simulating a 'best-fit' model scenario for this platform a better inference can be made about the drivers and style of platform development which has occurred at Wakatu point. The basic model set up was the same as the medium values set up in each of the three sensitivity test cases. On top of that there is a tectonic simulation and a sea level simulation. Sea level is set up to mimic the New Zealand sea level changes in Clement et al., (2016). So sea level is set to be stable until 4000 years into the run, after which sea level falls at a rate of 0.66 mm a^{-1} , resulting in 2 meters of sea level fall. The uplift set up for this run is based on the Little et al., (2018) recurrence interval of 400 years and each event produces 1m of uplift, based on the uplift recorded following the Mw 7.8 Kaikoura Earthquake.

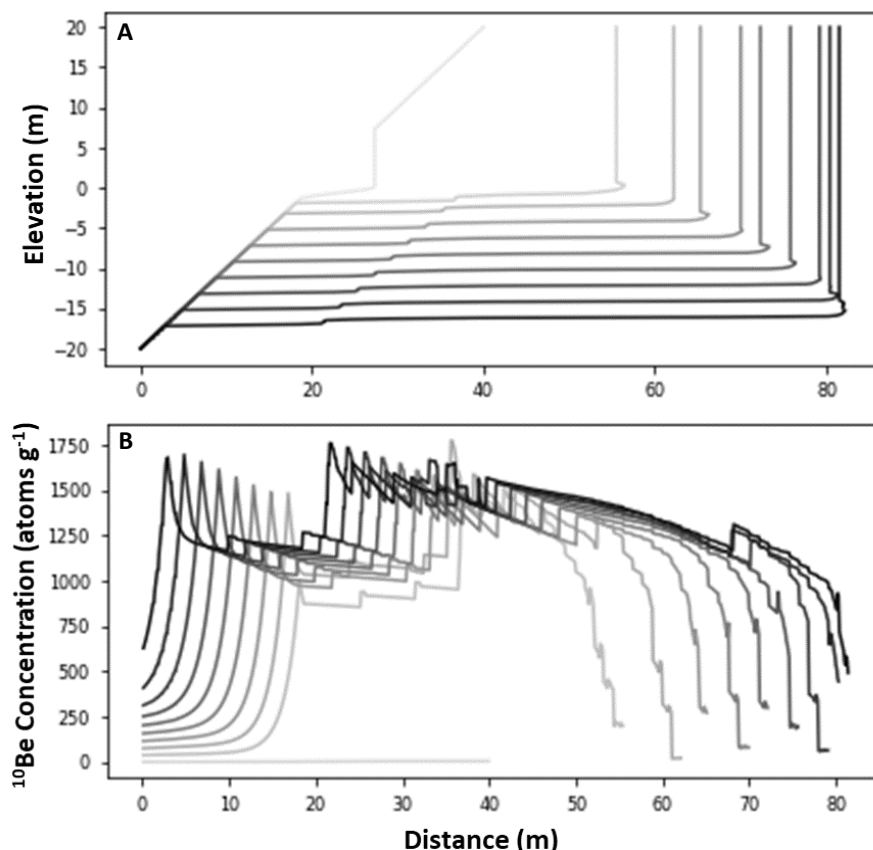


Figure 6.6: RPM_CRN model outputs for the Wakatu Point best-fit scenario. Uplift events of 1m set to recurrence of 400 years. (A) Shore profiles at 800 year intervals, (B) nuclide concentration profiles at 800 year intervals. Sea level fall is initiated after 4000 years. The platform is wide and heavily eroded, this is reflected with the low nuclide concentrations accumulated on the platform. The concentrations show a saw-toothed distribution, very similar to the measured concentrations at Wakatu Point.

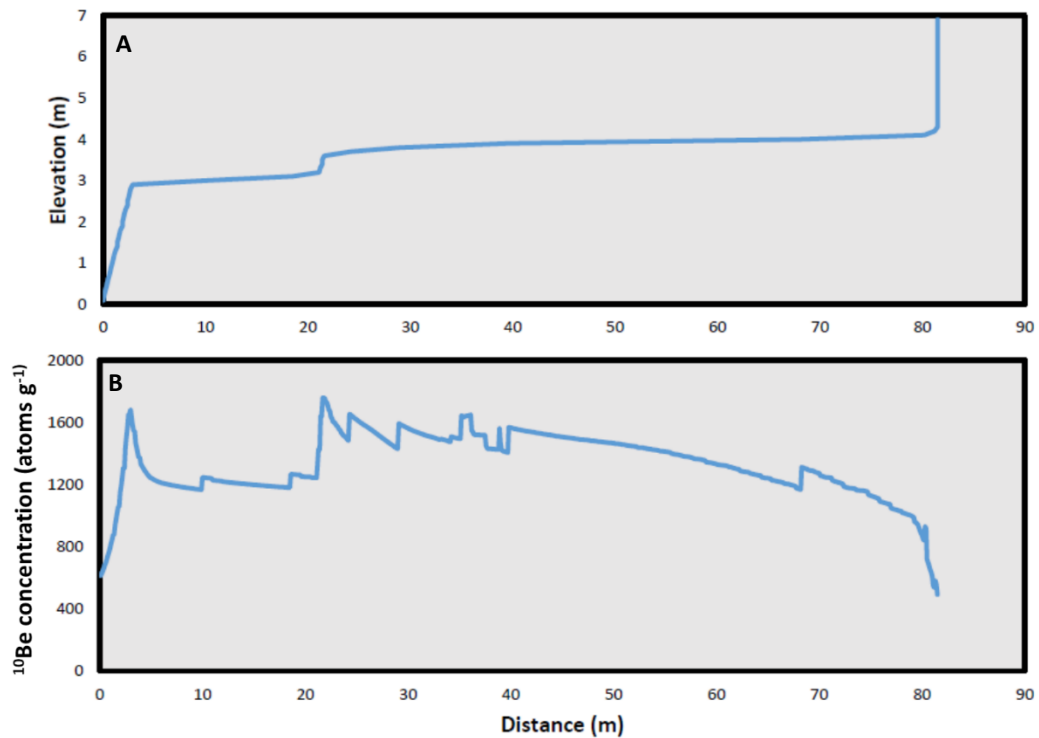


Figure 6.7: Final output profiles for the Wakatu best-fit model run. (A) The shore profile is shown with a shortened y axis to show the platform morphology. The platform is relatively smooth and gently sloping. (B) The nuclide concentration profile shows that there is a lot of irregularity in the concentrations across the platform, indicating that the surface may be rougher than can be seen at this resolution. The saw tooth like trend fits well with the data from Wakatu point, suggesting that this model set up is representative of this platform. Sea level position was at 20m at the beginning of the run, so relative sea level has lowered significantly.

The output of this model run is presented in *figure 6.6* showing the evolution of the platform over the 8000 year run period, which simulates the entire late-Holocene. The platform that has been produced is quite similar to the Wakatu point shore platform to which the model was being fit against. Some differences exist; first, the ^{10}Be concentrations are several thousand atoms g^{-1} lower than those measured on the platform and second, the simulated platform is narrower than Wakatu. This will be discussed in section 6.3.6.

6.3 Discussion

In-situ ^{10}Be surface exposure analysis of the Wakatu point shore platform has successfully produced seven exposure ages across a profile of the platform. Analysis of exposure dates for Wakatu point has been used in order to assess the developmental lifetime of this shore platform. It presents as a useful case study through which to examine shore platform formation within the context of active tectonics.

6.3.1 ^{10}Be Concentrations

The expected case for the nuclide concentrations on a platform, based on that of Hurst et al., (2017) and Regard et al., (2012) indicates that an across shore trend in the concentrations of ^{10}Be would show a 'hump shaped' distribution. This scenario is where the lowest concentrations occur next to the cliff following recent exhumation and the highest concentrations occur somewhere across the mid-section of the platform. This effect is due to more efficient erosion and deeper tidal inundation on the outer platform, lowering the concentrations there (see section 1.6.1). In contrast, the Wakatu point concentrations show a large degree of variance across the platform. This is not an unexpected outcome for this platform due to the geological structure present. The tight folding of the limestone beds have contributed to an irregular platform surface, demonstrated in the profile survey. Within a tight range of space the rock surfaces can be flat or steeply tilted so that erosion can directly exploit the skyward facing bedding plains. Where it was possible the samples were taken only from the flattest positions over the platform to avoid overly weathered material and locally shielded material.

The variable topography is likely a controlling factor in driving differential erosion patterns across the platform surface. Stephenson and Kirk (2000a) looked at the weathering of the Kaikoura shore platforms. They noted that water layer levelling, salt weathering and chemical weathering were particular forces operative on these platforms. These are all associated with the level of the water and the frequency of wetting and drying cycles. The limestone that makes up the Wakatu platform is not particularly prone to water layer weathering and due to the irregular shape this process is unlikely to occur. The blocky structure of the rock on the platform does

expose material to plucking from compressive wave action, which could be a major reason for the development of a rough platform surface.

Chemical weathering is also important on limestone platforms, which tend to be susceptible to salt water solution processes. Stephenson and Kirk (2001) also identified that the limestones at Kaikoura were susceptible to swelling due to the absorption of water during wet periods, which contributed to a weakening of the rock. The topographic roughness of the Wakatu shore platform results in different levels of water inundation across the shore platform, with some areas remaining high and dry all of the time. Other positions would experience regular and consistent cycles of wetting and drying (weathering), contributing to faster removal of material (erosion). This pattern of differential erosion across the surface of the shore platform would directly impact the ^{10}Be accumulation at different positions of the platform irrespective of the level of shielding.

The chert nodules which were targeted for sampling are much harder and less soluble than the limestone surrounding it. In many instances it was clear that the nodules persisted at the surface, holding higher positions than where there was no nodule. This phenomena indicated that the presence of a nodule had impacted the surface topography. By targeting the nodules for sampling, it was ensured that the less eroded portions of the platform were sampled. This provides the clearest possible signal of exposure ages on the very irregular platform surface.

In regarding the variance identified in the concentrations across the Wakatu platform, we can challenge the expected 'hump shaped' distribution model from Regard *et al.*, (2012) and later Hurst *et al.*, (2017). Regard *et al.* (2012) demonstrate that tidal range affects the magnitude and position of the highest concentration or 'hump'. The general relationship is that lower tidal range places the 'hump' closer to the cliff, with more prominence, while higher tidal range places the 'hump' more towards the sea, with less prominence. At Kaikoura, where the tidal range is very small, it is thus expected that a significant 'humped' trend in the concentrations across the shore platforms should arise (refer to section 1.6.1).

The Wakatu point shore platform with a slope angle of 1.04° only just comes under the classification of a sloping platform going by Sunamura's (1992) description; $<1^\circ$ are

horizontal type B platforms. Given that the slope of the Wakatu platform is so gentle, the 'hump shaped' distribution model, which was conceived in sloping (type A) platform settings, may not be applicable to this setting. Very low slope angle results in even water depth inundating across the platform during high tides, so the effect of the tide in controlling different rates of ^{10}Be production in the rock would be less significant. Under these conditions we expect to see a trend of increasing ^{10}Be concentration moving away from the cliff-platform juncture. At Wakatu point the cliff juncture is no longer active and samples were taken far from the juncture, therefore this is not apparent. The erosive signal from the sampled area appears to be predominantly that of down-wearing processes. Taking all of the above into account, it seems reasonable to get the variance and general lack of a directional trend from the ^{10}Be concentrations that have been observed at this site.

6.3.2 Exposure Ages

If the exposure ages ascertained in section 6.1 are taken as the correct age for this shore platform's development, it would place the development phase in the late (recent) Holocene. This time period is well after the post-glacial marine transgression, during a period of either slowly falling or stable sea level known as the Holocene still stand (Gibb, 1986). It is accepted that shore platforms do develop during periods of sea level stability, however these ages imply that the ~250m wide Wakatu shore platform complex formed rapidly during a period where sea level fell by ~2m to present day. This is an unlikely scenario and therefore supports the interpretation that erosion is a factor, lowering nuclide concentrations through the removal of material, so that the measured exposure ages are artificially young.

In section 3.1.1 it was implied that the flat area behind the shore platform, between Avoca Point and Armers Beach and up to the base of the cliff, was a multi-leveled Holocene aged terrace, based on Ota *et al.* (1996). In Figure 3.3, this area is classified as covered by beach sand and gravel. One possibility is that this low terrace feature which extends back to the sea cliff is a part of the Wakatu point shore platform, which has been abandoned by waves and is now preserved with overlying beach and gravel deposits. Another possibility is that it is indeed an uplifted Holocene terrace, with the modern platform cutting back into it. With the former interpretation of this platform

complex, the profile of the platform that was surveyed would represent only the outer half of the platform. This is the portion that has not yet been abandoned by waves and tide so it still undergoing surface erosion to lower the surface, but is not actively widening. Some coastal armouring between Wakatu point and the next platform protrusion to the east (*Figure 6.8*) suggests that relative sea level rise was beginning to re occupy some of the abandoned platform. This re-occupation of the coast has likely now stopped, due to the 1m gain in land surface elevation which occurred during the Kaikoura Earthquake in November 2016. Based on the latter interpretation, the sampled section constitutes a completely new late-Holocene platform.

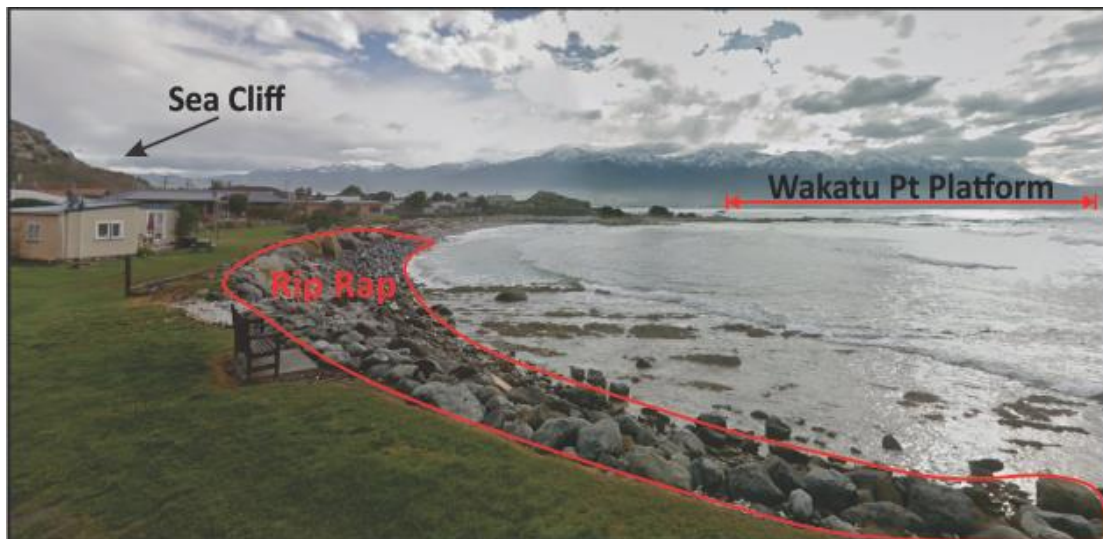


Figure 6.8: Image taken from Avoca St looking NW towards Wakatu Point. The presence of rip rap in foreground indicates that costal erosion was active around the time this photo was taken. Also shows plan view of Wakatu platform and the built up terrace area between the active platform and sea cliff. Image Source: Google Street View 2012.

Based on the first interpretation, that there is an abandoned and an active component to this shore platform, it could be expected that the ^{10}Be concentrations on the outer platform would be lower due to the continued removal of surface material. We were not able to collect samples from the landward section of this complex due to the build-up of sediments on top of the bedrock, and the fact that most of the area is private property. Without any ages from the landward terrace surface it cannot be confirmed if this surface is indeed a part of the same complex. To attempt to identify which assumption is more likely the RPM_CRN model was applied. This approach was used to test if wide platform geometries with pronounced steps along their profiles could be

created with a parameter set-up based on local Kaikoura conditions. A step would indicate that the platform and the raised terrace could be part of the same system. However, a lack of a step or a narrower geometry would suggest that the terrace is part of a separate feature that is now being eroded.

6.3.3 Surface Erosion Rates

An analysis of different surface erosion rates was conducted to determine a possible range of realistic erosion rates. By reproducing the concentrations over an increasing time scale with a range of apparent, steady-state erosion rates, it was possible to identify which erosion rates produce concentrations similar to the samples. The measured samples' ^{10}Be concentrations ranged from 13500 ± 1040 atoms g^{-1} to 7770 ± 831 atoms g^{-1} . Modelled erosion rates which completely intersect the range of concentrations are taken as possible rates. Below that threshold, the erosion rates would be too rapid, stripping ^{10}Be out of the system. The results in nuclide production that is as secular equilibrium with erosion so no more build up can occur. Once this occurs it is impossible to determine the age and erosion rate associated with that concentration (Lal, 1991).

This analysis showed that the fastest erosion rate that could be applied to the data and still produce the full range of measured concentrations was 0.22mm^{-1} . This is not similar to the MEM erosion rates reported in Stephenson (1997), Stephenson and Kirk (2000b) and Stephenson et al., (2010). This is discussed in depth in the following sections. This rate is, however, comparable to some of the down-wear rates measured in Porter et al., (2010). Porter *et al.* (2010), measured down wear rates of $\sim 0.2\text{mm a}^{-1}$ at mid-tide and low-tide positions on sloped platforms at Salmon River, Scots Bay and Mount Louis in Eastern Canada. These sites all differed in their geology to Wakatu Point; however, the Salmon River site consisted of sandstone which has a density of $\sim 2463 \text{ kg/m}^3$, similar to limestone with 2484 kg/m^3 (Tenzer *et al.*, 2011). Similar material densities point to why these platforms may have similar erosion rates. At the Salmon River these rates were recorded below the mid-tide position, so that the rock was submerged for a longer portion of the tidal period. The significance of the duration of submergence with relation to samples from this analysis are discussed later in this chapter (section 6.3.5 i).

Based on an erosion rate of 0.22mm^{-1} , *figure 6.5* shows us that the exposure age for the sample with the largest ^{10}Be concentration, AD03, would be $>\sim 9\text{ka}$. This places the expected period for platform formation during and following the post glacial marine transgression (PGMT), with a possible initiation time during a short stillstand around 9000yrs BP, which punctuates the PGMT (using the New Zealand eustatic sea level curve) (Gibb, 1986). This scenario is very plausible as the rapid continuous sea level rise during the latter part of the PGMT would drive fast coastal retrogradation. However the magnitude of the sea level rise during the last 1000yrs of the post-glacial marine transgression was significant, with $\sim 20\text{m}$ of sea level rise. This would likely form a drowned coastal slope rather than a wide planation along the rocky coast based on the negative feedback response of the SCAPE model (Ashton et al., 2011). For this reason it is more reasonable to argue that the true steady state erosion rate for Wakatu Point lies between 0 and 0.22mm^{-1} as demonstrated in *figure 6.5*.

6.3.4 Erosion Rates Disparity

As noted above, there is a disparity between MEM derived erosion rates and cosmogenically-derived erosion rates at Kaikoura. The MEM studies of Stephenson and Kirk (1996) provide us with precise decadal rates of platform denudation for Kaikoura. While the Wakatu platform has never been included in their record (probably due to its topography), other limestone platforms (including one bolt site (KMZ) on the Avoca point platform) provide a good constraint on the erosion rates for the limestone platforms. Lowering rates for the limestone platforms were attained from Stephenson *et al.* (2010). The slower rate of 0.4mm^{-1} applied in *Figure 6.5* is the two year average for bolt KMZB, one of Kirk's original MEM deployments. The second lowering rate (0.87mm^{-1}) that is plotted is the average of all the two year deployment rates for only the limestone platforms. These were from KM4 and KM7 transects (*figure 6.9*).

When looking at the 0.87mm^{-1} erosion rate plotted in *figure 6.5* it is apparent that the concentrations approach secular equilibrium rapidly. This rate fails to produce concentrations within the range recorded for the samples. This failure means that this

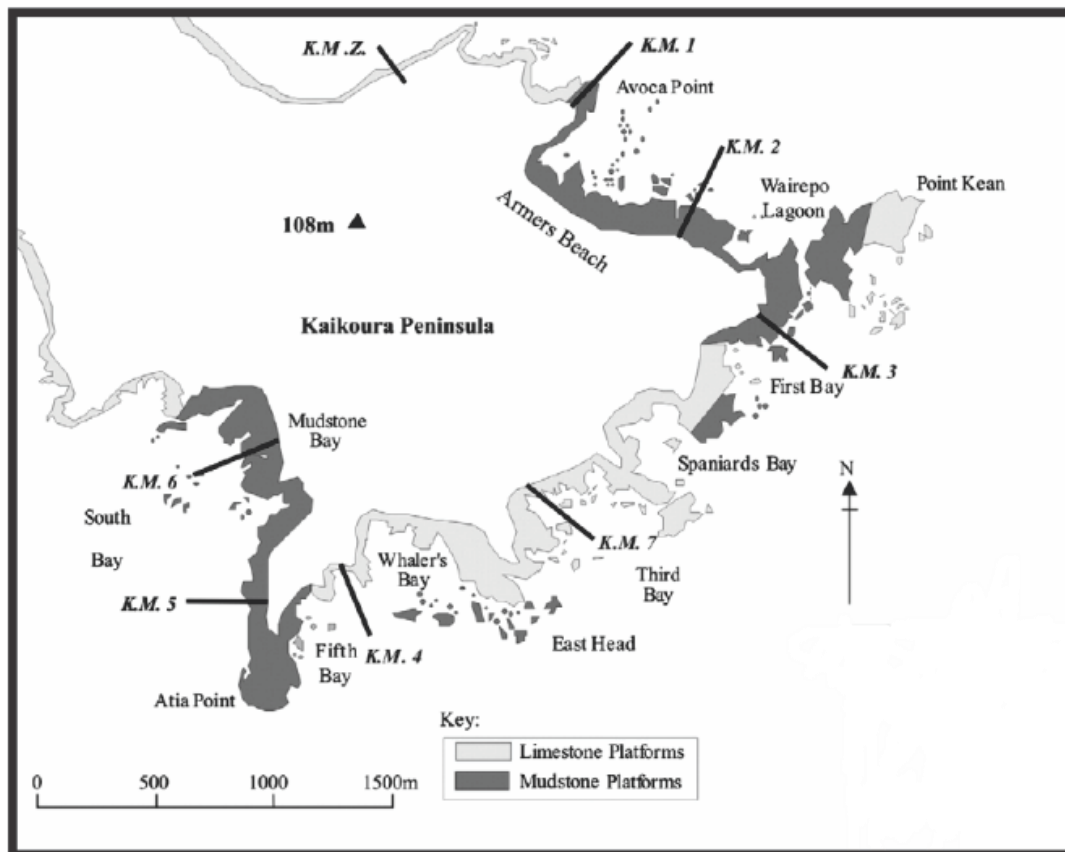


Figure 6.9: MEM bolt profiles from Stephenson et al., (2010). Shows the locations where MEM measurements are recorded and what rock type the platform is formed in. Source: Stephenson et al., (2010).

average for the modern decadal erosion rates on the limestone platforms is not possible over a longer timescale, based on the measured concentrations. Similarly, the 0.4mm^{-1} erosion rate, which represents the minimum rate recorded on a limestone platform, also reaches secular equilibrium too early. For this rate, however, the concentrations produced do overlap with the measured concentrations, but do not cover the full range. Therefore neither of the observed limestone lowering rates can be taken as reasonable long-term rates, as they are not consistent with the range of apparent erosion rates inferred from ^{10}Be analyses. This suggests a disparity between the long-term and the short term lowering rates.

6.3.5 Reconciling the Lowering Rates Disparity

In order to reconcile the disparity between these rates I present two separate interpretations in this section. The first looks at a geomorphic solution to the problem based on the role of tectonics and some relatively well defined process relationships. The second interpretation considers the theoretical impact that timescales of measurement can have on an investigation of process rates such as this.

6.3.5 i Geomorphic Solution

The recent 7.8 (Mw) Kaikōura earthquake on 14 November 2016, which resulted in 1.1m of uplift of the coast at the Kaikōura peninsula (Stephenson et al., 2017) has provided some insights into process regimes on Kaikōura shore platforms. Stephenson et al., (2017) discuss how the process regime can shift on a shore platform through changes to relative sea level. This comes about through the role of wetting and drying cycles in the weathering of the platform surface. The zone of maximum wetting and drying cycles, which Stephenson and Kirk (2000b) found to be between 0.6 and 0.9m above MSL at Kaikōura, contributes to the most efficient surface weathering. The authors state that the recorded lowering rates from MEMs in this zone on the Kaikoura platforms were at least an order of magnitude larger than those recorded at lower positions on the platform (Stephenson et al., 2017). The rates recorded by Porter et al., (2010) reveal the same trend. The MEMs which recorded rates similar to those based of the measured ^{10}Be concentrations in this study tended to be at lower positions on the platform, but those in the mid-high tide range weathered much faster. At Kaikoura the uplift has significantly altered the elevations of the shore platforms. The net result is the moving of the zone of maximum wetting and drying to new positions on the platform. Stephenson *et al.* (2017) predict that over the next few years the lowering rates on these surfaces will increase significantly.

A solution for this disparity between the long-term and the short term lowering rates is that a similar event or events in the past have promoted the same kind of regime shift, driving the lowering rate up to those in the decadal record. This suggests that both the long-term and the short term rates for this platform could be correct; they need not be identical. With initiation of platform development sometime around the end of the PGMT, the platform would have been cut rapidly through the combined action of waves and weathering. At this time, backwearing is likely to have been a more dominant process than downwearing, because narrow platforms would have done little to dissipate wave action (Dickson et al., 2013; Ogawa et al., 2011; Trenhaile, 2001). More recently, the platform has been uplifted in at least one uplift event. It is known that there has been active uplifting at Kaikoura during the Holocene. The event identified in Duckmanton (1974) as discussed in section 3.1.3 is evidence of this. Also mentioned in section 3.1.3 were the sea caves stranded well above the modern sea

level position at various positions around the peninsula. This uplifting is likely the reason that the landward half of the platform is now abandoned by sea level. The more recent events, such as the ~2m uplift identified in Duckmanton (1974) could have lifted the platform (that which was sampled) and others around the peninsula into a zone where wetting and drying was more frequent. This would increase the lowering rates on the platforms to come in line with the rates that are observed over recent decades.

The benefit of this interpretation is that it holds that the decadal scale MEM erosion rates and the exposure analysis inferred range of apparent erosion rates can both be correct. The disparity between rates in this case is due to tectonically-driven process regime shifts around the late-Holocene. This interpretation fits in well with the overall story of the Kaikoura peninsula as being heavily influenced by the regional tectonics. However, other factors may be at play in causing this disparity. Therefore a second possible interpretation is outlined below.

6.3.5 ii Effect of Timescale

An important consideration for interpreting these data is the impact the timescale of measurement has on the rates we record. The ^{10}Be exposure analysis aims to capture the entire lifetime of the shore platform from its initiation to present form. MEM measurements are employed to capture the small scale behaviours in weathering processes over deployment periods of months to decades. In this case we are trying to reconcile rates from surface exposure analysis on the order of thousands of years with rates from MEM studies on the order of tens of years. An important relationship that has been identified and well documented in studies of sedimentation rates is that from Sadler (1981). This is the relationship where sediment accumulation rates are inversely related to the timespan for which they are determined Sadler (1981). In other words, measured rates of deposition tend to decrease systematically with measurement duration for virtually all depositional environments in which there are sufficient data for time intervals ranging from minutes to millions of years (Schumer & Jerolmack, 2009). Schumer and Jerolmack (2009) term this the 'Sadler effect'. This relationship also holds for erosional systems (Schumer & Jerolmack, 2009; Willenbring & Jerolmack, 2016).

Schumer and Jerolmack (2009) find that this relationship occurs as a result of hiatuses in deposition through time. Depositional and erosional systems are inherently stochastic, and nonlinearities in sedimentation and erosion occur as thresholds are reached. For example, on a shore platform, erosion into the cliff may occur rapidly for a time, but the erosion will eventually cease as the erosive power of waves is dissipated over the ever lengthening shore profile. When hiatuses in these processes occur they reduce the rates substantially. For this reason erosion and sedimentation rate will always vary significantly through time, even under steady-state forcing (Schumer & Jerolmack, 2009). By measuring these processes over longer time-scales we will capture more of these periods of erosional or depositional hiatuses in that rate. The net result of which is that the rates will become slower with increasing time of measurement. This relationship is captured quite well in *figure 6.10*.

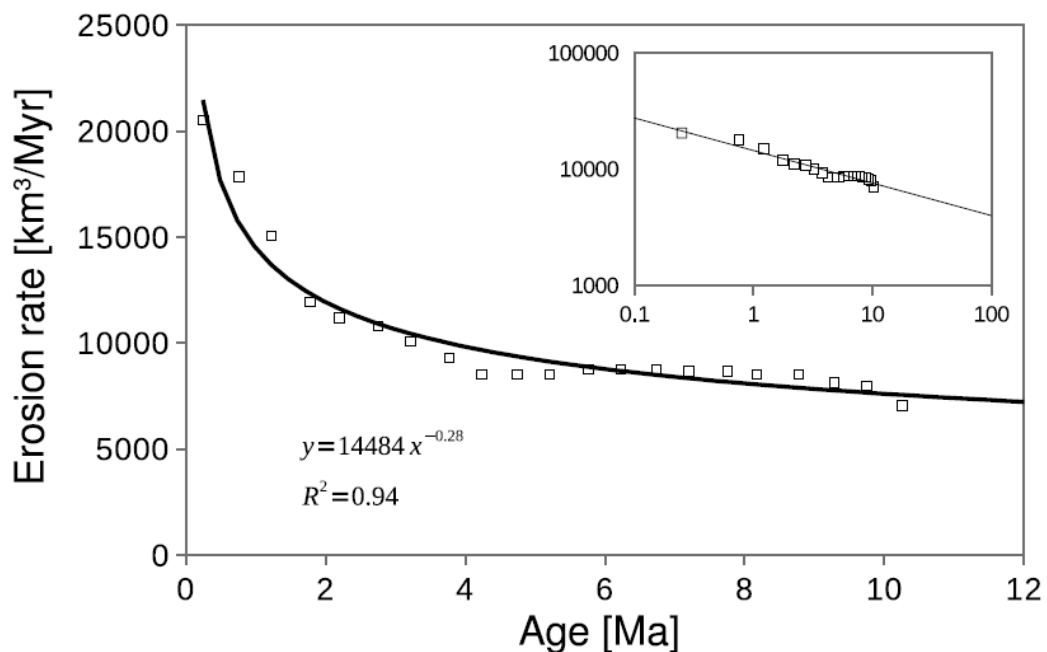


Figure 6.10: This figure from Schumer and Jerolmack (2009) shows volumetric erosion rates for the last 10Ma for the Eastern Alps. The rates are based on measurements of sediment accumulation in basins around the Alps, which have been corrected for compaction. The figure clearly shows that the erosion rates calculated for the younger ages a substantially faster than those for much older ages. This relationship can be represented as a power law function.

This relationship would influence MEM records as well. Stephenson *et al.* (2000b) described how on mudstone platforms at Kaikoura, slaking-like processes weakened the surface rocks. This occasionally caused large pieces of rock to dislodge and in some cases this resulted in the loss of MEM bolts. The result of this process for would be a significant jump in the average erosion rate measured on the platform. Removal of significant amounts of material in this way is almost impossible to quantify with MEM records, because the stochastic nature of this slaking-like material shearing means there is little uniformity in the timing and scale of erosion. When slaking occurs, it represents a step change in the erosion rate at a point on the platform. During the interim periods regular surface erosion is very slow to almost negligible (Stephenson *et al.*, 2010; Stephenson, 1997; Stephenson & Kirk, 2000b). Averaging MEM rates of over short periods (year to tens of years) would amplify the signal of these significant material losses, while averaging over longer geological timescales would reduce the signal of larger scale stochastic mass losses.

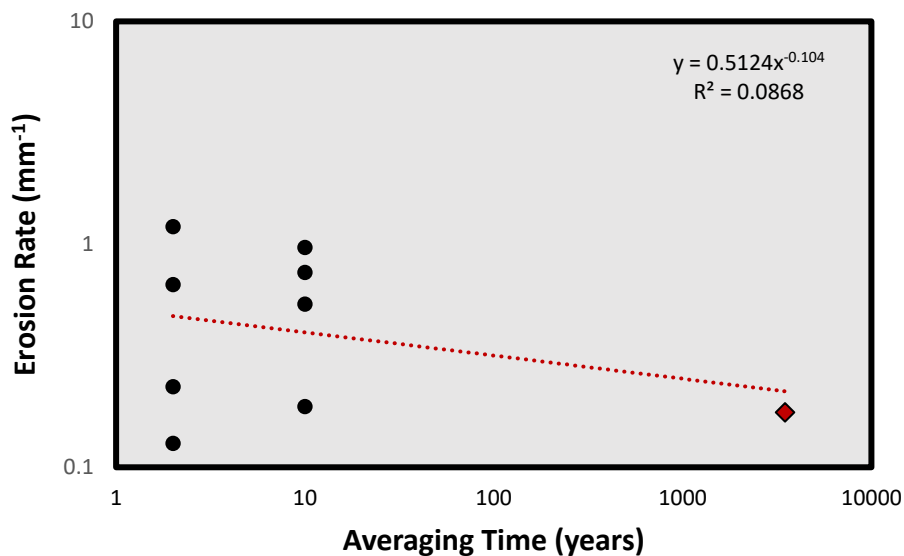


Figure 6.11: Plot showing relationship between time scale and erosion rate. The erosion rates used for the two and ten year time scales are taken from Stephenson *et al.* (2010) as rates on limestone platforms at Kaikoura that were measured by MEMs over two then ten years; these are the black dots. The red diamond is a mid-range erosion rate that sits in the range of allowable erosion rates calculated from the cosmogenic nuclides. A power function is used to produce the trend line, which gives a poor correlation that shows a small decreasing trend.

Based on the Sadler effect it would be a reasonable assumption that this relationship was a factor for the rates calculated at Wakatu point in the short term and the long-term. This can be tested in the same way that the Alps erosion rates were calculated in

Schumer and Jerolmack (2009). In figure 6.11, surface erosion rates are plotted against averaging time to see if there is a significant biasing effect due to the time scale. There is a very weak correlation with a power-law exponent of ~ -0.1 , significantly different from the -0.5 that would be expected from a random walk event. This suggests that there is, at most, a small degree of bias associated with the time scale of measurement, indicating that the geomorphic solution to this rates disparity is the more important source of separation.

6.3.6 Interpreting Best Fit RPM Simulation

The best fit model simulation for Wakatu point produces a medium width profile with a rough surface and 'saw toothed' distribution of nuclide concentrations. The model output is a reasonably good fit for the platform. The model profile is narrower than the real platform, which is consistent with the interpretation that the exposed area that was sampled is a new, young platform that is currently incising into an earlier Holocene terrace. The low ^{10}Be concentrations in the model output, while they showed a very similar distribution to the real concentrations, indicated that the parameterization was not completely representative of the actual drivers on the platform. However, the goal of this modelling was to explore the most likely drivers and their interactions in developing a similar geometry to the real platform. This parameterization, therefore, does well to simulate Wakatu.

The likely cause of the lower ^{10}Be concentrations are the uplift event recurrence interval and the uplift magnitude. With a longer recurrence interval, the ^{10}Be concentrations would be higher. It is possible, then, that the recurrence interval of earthquakes which cause uplift of the Kaikoura peninsula is longer than the average recurrence interval of ruptures on the Kekerengu Fault. This is reasonable, as not all fault ruptures cause uplift to occur. Alternatively (or additionally), the regular magnitude of uplift may be lower than one meter each time there is an uplift event.

Chapter 7: Okakari Results and Discussion

The Okakari Point shore platform contrasts in its evolutionary history with that of Kaikoura. This is a tectonically quiescent coastline, very much affected by the fluctuations in eustatic sea level, which have left markers behind in the shore platforms along this coast. This chapter will present the results of field and laboratory procedures, along with the modelling conducted for this site, followed with a discussion of these results for Okakari Point.

7.1 Results

The profile of Okakari point shows that the only major unconformity in the profile is the step, or raised surface at the back of the platform, below the cliff. The profile also shows there is a rampart (slightly higher elevation) on the outer (seaward) portion of the platform. The samples that were processed from this platform capture the area at the back of the platform and the more seaward portion. Samples AD12, AD14 and AD15 lie above the high water mark on this platform, but would be exposed to wave action during exceptional spring tides and storm events.

Figure 7.1 does not show sample AD13 as it is not located on this profile. However the sample is take from a small sea cave at the same elevation as sample AD15, which appears to still be actively forming. This cave sample was intended for use in this analysis to correct for an inheritance signal of ^{10}Be if such a signal existed, as was done in Hurst et al., (2016). However, it was determined that the concentration of this sample did not represent inherited nuclides and most likely came from muogenic production.

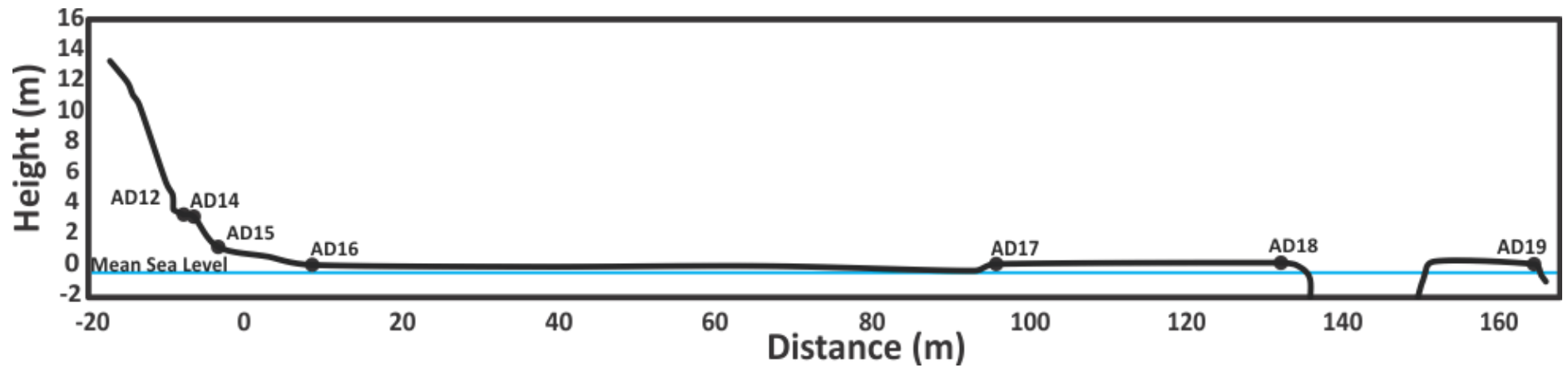


Figure 7.1: Shore platform profile surveyed at Okakari Point. The 13m cliff is captured on the left. The profile extends across the entire width of the shore platform including a small semi-detached portion on the seaward side. The platform is $\sim 0.8\text{m}$ above MSL, shown with the blue line. Overall this profile represents a typical type B platform morphology with the exception of the raised surface at the back of the platform, where sample AD12 and AD14 were taken.

Table 7.1: Measured $^{10}\text{Be}/^9\text{Be}$ ratios and total concentration of ^{10}Be atoms in each sample from Okakari. Calculated using KNSTD07 lab standard.

Sample	Location	Location	Shielding Factor	Thickness scaling factor	$^{10}\text{Be}/^9\text{Be}$ ratio	Error	Qtz mass dissolved	Weight ^9Be added by Carrier	^9Be added by Carrier	^{10}Be Sample Conc.	^{10}Be sample Conc. error	Total error
Label	Lat	Lon				%	g	g	atoms	atoms/g	atoms/g	%
AD12	-36.260919	174.767314	0.9521	0.976	2.35E-15	21	44.447	0.000308	2.06E+19	8227	2281	28%
AD13	-36.261581	174.768742	0.2680	0.9682	8.72E-15	11	14.352	0.000271	1.81E+19	3755	1484	40%
AD14	-36.260903	174.767322	0.9528	0.9605	1.39E-14	7	22.143	0.000307	2.05E+19	7580	1093	14%
AD15	-36.260872	174.767328	0.9343	0.9605	7.27E-15	11	7.524	0.000271	1.81E+19	3672	2435	66%
AD16	-36.260797	174.767428	0.9820	0.9605	1.35E-14	27	28.219	0.000308	2.06E+19	5624	2722	48%
AD17	-36.260164	174.767967	0.9977	0.9839	1.34E-14	8	14.678	0.000271	1.81E+19	9483	1540	16%
AD18	-36.259911	174.768169	0.9981	0.9682	1.43E-14	10	10.993	0.000270	1.81E+19	14065	2606	19%
AD19	-36.259597	174.768.092	0.9992	0.9839	2.53E-14	6	19.165	0.000283	1.89E+19	19296	1644	9%

The AMS processing returned $^{10}\text{Be}/^9\text{Be}$ ratios for all of the samples that were sent away, these are presented in *table 7.1*. The lab blank (AD09) that was sent with this sample set returned and $^{10}\text{Be}/^9\text{Be}$ ratio of $5.74 \pm 0.66\text{E}^{-15}$. This ratio was compared with other blank ratios returned from the large AMS labs (ETH and ANU) and found to be within a normal range. The concentrations listed in *table 7.1* are blank corrected against the AD09 blank. An important thing to note about these results in *table 7.1* are the substantial errors, up to 66% total error for AD15. The errors are high in this sample set due to the small amounts of quartz material that was isolated and dissolved for many of the samples and the low concentrations.

These concentrations have been plotted in *figure 7.2*. This visualisation shows that the concentrations measured on the raised surface at the back of the cliff are higher than those immediately seaward. The samples on the main platform surface show linear increase in concentration away from the cliff.

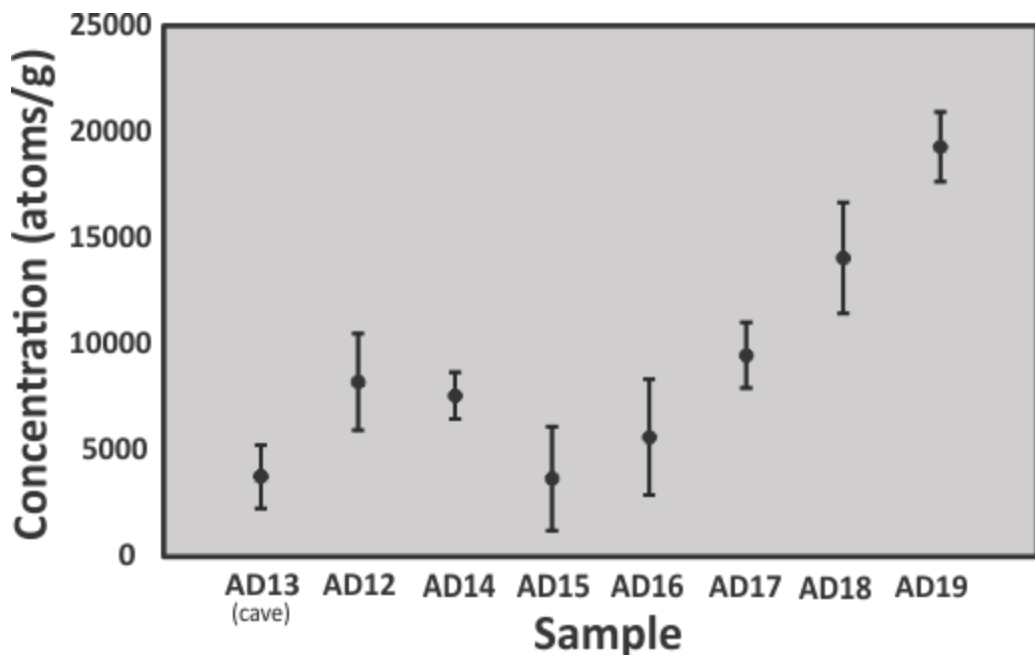


Figure 7.2: Concentrations of total atoms per gram of material for the Okakari Samples, plotted in the order they occur on the shore platform from cliff to sea.

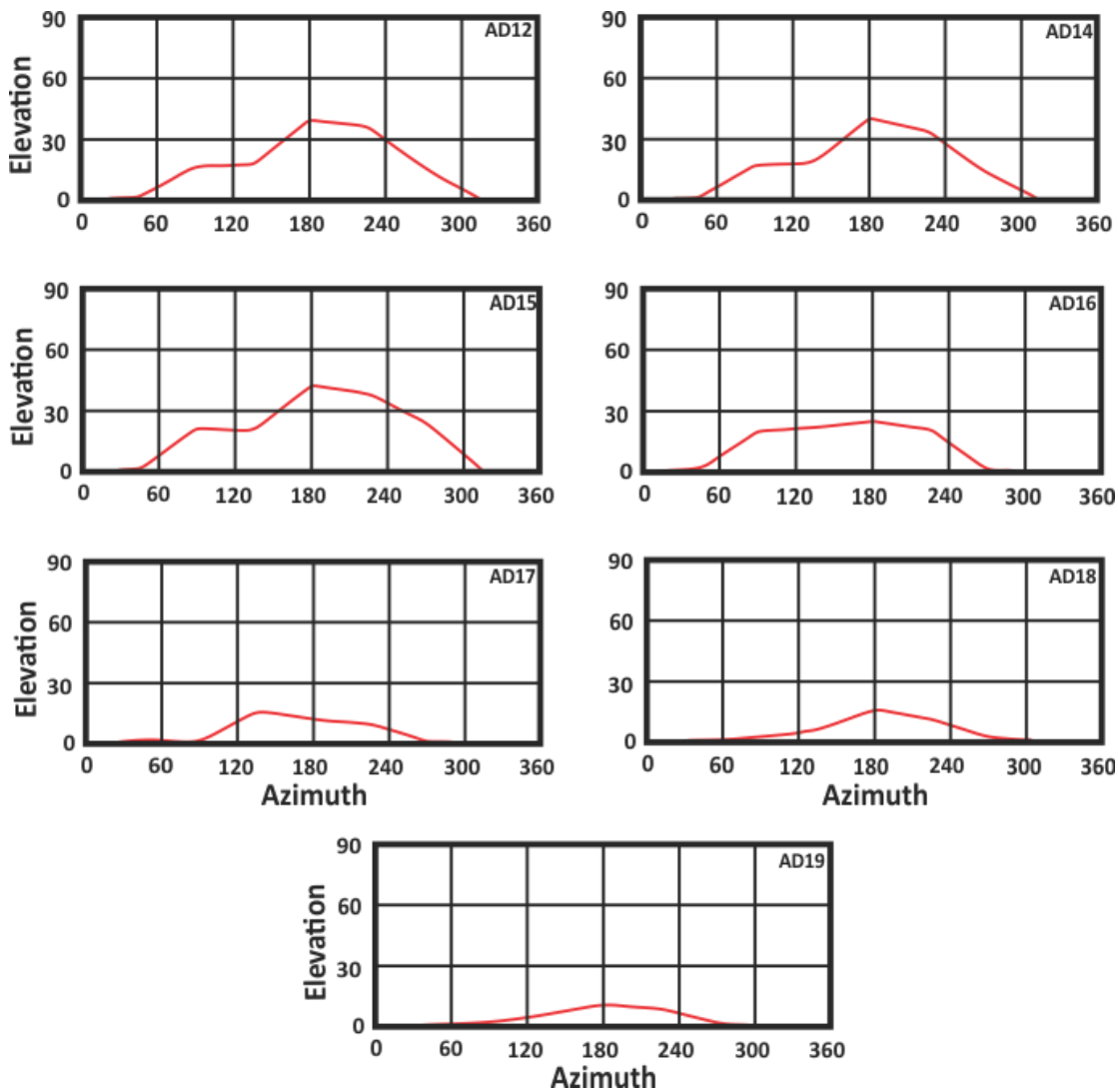


Figure 7.3: Obstructed portion of the view-shed at the positions from which samples were extracted. Sample IDs in top right of plots.

In order to calculate sample exposure ages, topographic shielding for each sample was first calculated using CRONUS version 2.3. The topographic shielding at each sample is shown by the obstructed view-shed plots in *figure 7.3*. This shore platform was sampled from the cliff to the sea, therefore the samples nearest the cliff are shielded from the cosmic ray flux more effectively. This is evident in *figure 7.3* with the more landward samples all showing significant obstruction about the south facing azimuths.

With the topographic shielding values, exposure ages were calculated also using the CRONUS calculator. The exposure age results are given in *table 7.2*. This shows that the sample AD15 is ~1006 years old, with an error of 670 years which means it could be much older or very recently exposed. The exposure ages based on the time-varied production rate scaling are also plotted in *table 7.3*.

In *figure 7.4* the exposure age results from *table 7.2* are plotted along the profile of the shore platform. This figure shows more clearly the trend in *figure 7.2*; the exposure ages on the main platform surface become steadily older, moving away from the cliff platform juncture. As these ages are calculated with no erosion, the oldest sample, in this case AD19 at the edge of the platform, indicates the minimum exposure age for this shore platform. This is 4284yrs BP \pm 411yrs, placing it in the midst of the Holocene high-stand. These minimum ages are based on the assumption of no erosion, however erosion is a factor and is assessed below.

To assess a possible range of ages accounting for erosion, the same erosion rate analysis as for the Wakatu dataset was conducted. Erosion rate curves are plotted in *figure 7.5* along with the measured concentrations from Okakari point. This highest erosion rate which is still able to produce the full range of measured concentrations at Okakari is 0.147mm a⁻¹. Therefore, the down wear rate for this platform is between 0 and 0.147mm a⁻¹. The age of the outer shore platform based on this rate of down wear could be ~10ka, however it may be as old as ~16ka when accounting for the upper bound of the error in *figure 7.5*. The curve for the erosion rate 0.1mm a⁻¹ is based on a more realistic timing for the initiation of the platform based on the localised sea level curve for the Auckland Region after Clement et al., (2016), this is elaborated on in the discussion in section 7.3.3.

Table 7.2: Surface exposure ages for Okakari point samples. Calculated with the former CRONUS calculator version 2.3 using the Stone (2000) scaling scheme.

Sample	Thickness Scaling Factor	Shielding Factor	Production rate (muons) (atoms/g/yr)	Internal Uncertainty (years)	Exposure Age (years)	External Uncertainty (years)	Production rate Spallation (atoms/g/yr)
AD12	0.976	0.952121	0.075	603	2174	618	3.35
AD14	0.9605	0.952822	0.075	294	2035	318	3.3
AD15	0.9605	0.934262	0.075	670	1006	670	3.23
AD16	0.9605	0.982036	0.075	709	1464	713	3.4
AD17	0.9839	0.997733	0.075	385	2364	415	3.55
AD18	0.9682	0.998092	0.075	662	3564	709	3.5
AD19	0.9839	0.999248	0.075	411	4814	548	3.55

Table 7.3: Table 6.4: Exposure age results for four different time averaged scaling schemes.

Scaling scheme for spallation	Desilets and others (2003, 2006)		Dunai (2001).		Lifton and others (2005).		Time-dependent Lal (1991/Stone(2000)	
Sample ID	Exposure age (yr)	External Uncertainty (yr)	Exposure age (yr)	External Uncertainty (yr)	Exposure age (yr)	External Uncertainty (yr)	Exposure age (yr)	External Uncertainty (yr)
AD12	2457	742	2384	717	2486	745	2246	657
AD14	2298	431	2227	414	2325	427	2103	361
AD15	1127	762	1069	723	1139	769	1041	699
AD16	1645	821	1580	787	1664	827	1514	747
AD17	2671	540	2595	520	2702	536	2441	458
AD18	3972	878	3853	845	4019	874	3662	760
AD19	5342	786	5154	745	5406	766	4910	619

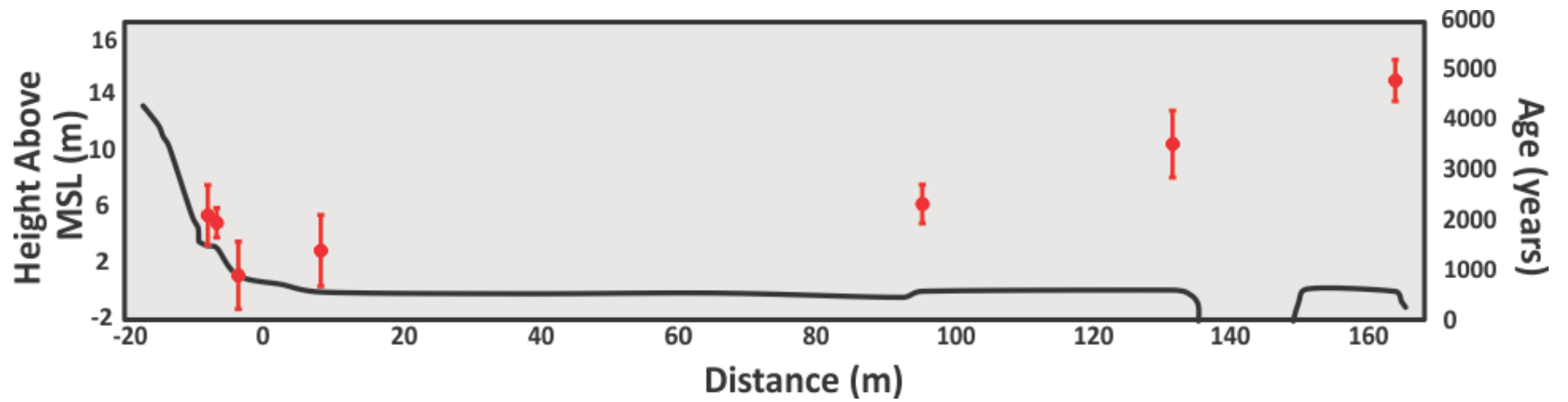


Figure 7.4: Exposure ages of the Okakari point samples from the CRONUS calculator, plotted on the shore platform profile.

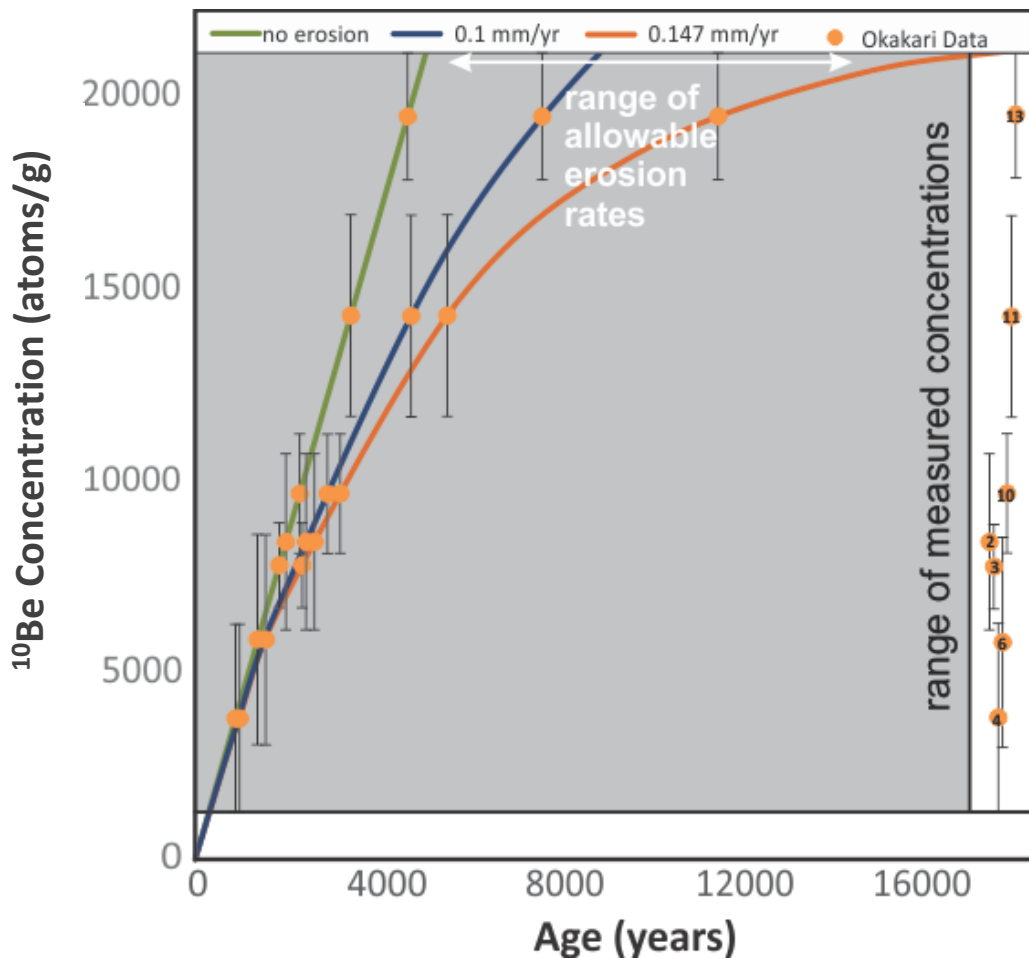


Figure 7.5: Erosion rates plot for Okakari point, showing the range of the sample concentrations (right) greyed out. The samples are numbered with their original sample numbers. Erosion rate curves which fully intersect this area of the plot represent erosion rates that could have produced the measured range of concentrations. The sample concentrations are also plotted on the three erosion curves to show how old the samples would be with each rate. Any erosion rate faster than 0.147mm a^{-1} results in curves which reach secular equilibrium before they can accumulate ^{10}Be up to the upper level of the measured concentration range. The blue line for 0.1mm a^{-1} represents the erosion rate that results in platform initiation $\sim 7000\text{yrs BP}$.

7.2 Best Fit Model Results

A best fit RPM_CRN model simulation was also conducted. This was done to identify the best-fit parameters that produce a model that looks like the Okakari platform, in order to understand what drives platform evolution. It has been identified that sea level change has played an important role in the development of this platform, so this test aimed to confirm if the Auckland sea level curve produced a platform geometry and ^{10}Be concentrations consistent with the field and lab analysis. One important facet of the measured concentrations at Okakari point is the linearity in the trend from the base of the cliff to the seaward scarp, with the resistant rampart. In the sensitivity

analysis (refer to chapter 5), it was found that using a high wave attenuation constant, so that wave efficacy is low, the model will develop a medium width profile with linear concentration increasing from the cliff to the seaward scarp.

The parameter set up used for this best fit model run utilises the medium values for material resistance and weathering rate and applies the high wave attenuation constant. The sea level trend for Auckland/New Zealand is also applied, with stable sea level set until 4000 years, after which sea level falls for the remaining 4000 years at a rate of 0.66mm a^{-1} . The resulting model output is displayed in *Figure 7.6*, and the final profiles in *Figure 7.7*.

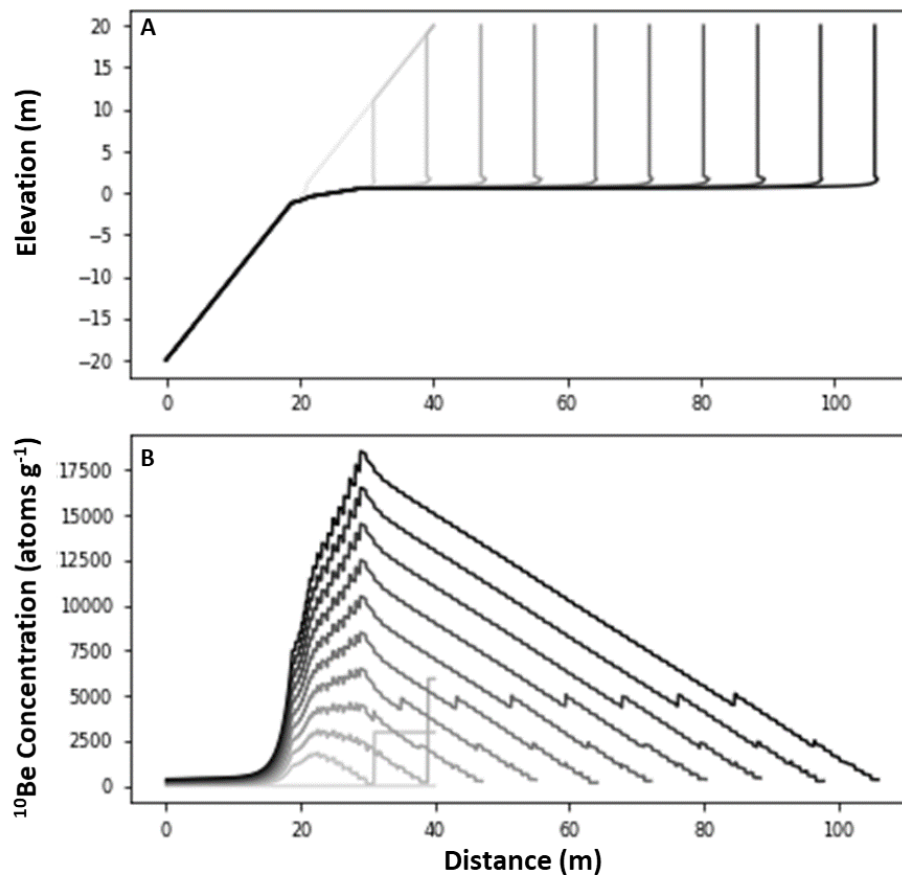


Figure 7.6: Model output for the Okakari point best fit test. (a) The platform profiles printed at intervals of 800 years. (b) The nuclide concentration profiles, printed at intervals of 800 years. This produces a medium width platform profile that is very flat. The concentration distribution shows very linear accumulation across the shore platform and a peak in concentrations at the sea ward scarp, indicating that the model has produced a rampart. Erosion beyond the rampart causes a rapid reduction in ^{10}Be concentrations.

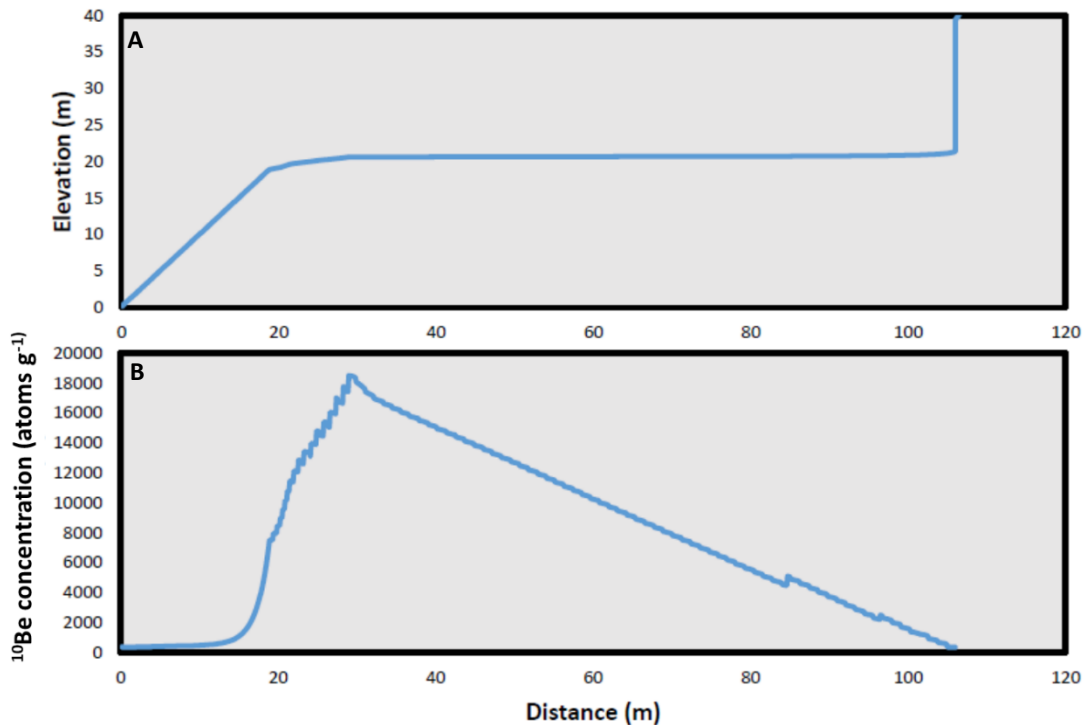


Figure 7.7: Final profiles for the Okakari best fit run. (a) The platform profile is near-horizontal, having produced a type-B platform, with some erosion of the scarp. This is very close in geometry to the Okakari shore platform. (b) The nuclide concentrations are also very similar to those measured at Okakari, showing not only a similar distribution, but also having roughly the same amount of nuclides accumulated. The rampart is also evident in the model run.

These outputs fit very well with the measured concentrations and profile geometry at Okakari point. The deviations from the real profile include the platform width, which is narrower in the model output, and the lack of a ledge at the back of the platform. The sea level fall also has not caused the whole platform to lower, leaving behind the rampart. In this simulation the rampart has formed early on in the run time and has developed into more of a point, rather than a bulge, as sea level fall has eroded the seaward scarp.

7.3 Discussion

From Okakari point we have successfully measured 8 samples for their ^{10}Be concentration and produced from these, 7 surface exposure dates ages. The concentrations measured here show a contrast to other concentrations measured at Kaikoura and other platforms around the world, meaning that the processes and

drivers operative in the formation of this platform differ somewhat from those at Kaikoura. In this section the concentrations and ages will be interpreted for what they can tell us about the history of development for the Okakari Point shore platform. This case study is a good example of platform formation in a quiescent setting, where the main influence has been eustatic sea level.

7.3.1 Concentrations

The sample concentrations presented in *figure 7.2* are in stark contrast to the ones measured at Wakatu point. Samples AD15 through AD19 at the cliff edge exhibit a very linear increasing trend in concentration away from the cliff. Outside of this group are three other samples: the two samples above the ledge, collected on the slightly raised platform just below the cliff, both have higher concentrations than the first two samples on the lower surface. The ^{10}Be concentration of AD15 is very low compared to all of the others, which indicates that it has been exhumed recently. It is likely that the platform is still being cut into the ledge and cliff during storm events.

An important thing to note with these concentrations is that the trend across the shore platform is a linear increase towards the sea. As at Wakatu this pattern is not representative of the 'hump shaped' distribution described in Regard *et al.* (2012) and Hurst *et al.* (2017). In the discussion of the Wakatu results it was suggested that the gradient of the platform may play a key role in regulating the distribution of concentrations across the shore platform. The Okakari shore platform is easily classified as a type-B platform, with a near flat surface across most of its profile. This case seemingly confirms that gradient plays an important role. With a flat surface, tidal inundation results in the platform being covered by the same depth of water across all of its profile (except where the profile deviates from flat). This means that the impact of water attenuation is equal across the shore platform through all tidal cycles.

In addition, there appears to be no evidence of differential weathering across the platform surface, except on the rampart. The raised ledge is also exempt from this as it would only erode during significant storm wave attack. The outcome of this lack of differential weathering is that erosion processes are not any more efficient at removing ^{10}Be -enriched material at the seaward edge than at the cliff base (base of the ledge). Therefore erosion is uniform across the platform.

7.3.2 Exposure Ages

The exposure ages were calculated with the former CRONUS calculator, again calculating the ages with zero erosion. Exposure ages range from 1006 ± 670 yrs BP to 4814 ± 411 yrs BP. The youngest sample is AD15 which could be a nearly fresh exposure. Based on these ages the platform has formed almost entirely during the mid to late Holocene highstand. According to Dougherty (2011), the mid-Holocene highstand reached peak sea level height of 2m above present mean sea level at about 4000 yrs BP, after which sea level began a gradual decline to present sea level. Based on this sea level history, the ages modelled for no erosion indicate that platform cutting occurred primarily during a time of gradually falling sea level. Platform cutting during falling relative sea level is not consistent with the current knowledge about the conditions under which platforms develop. With softer rock platforms, such as those of the Waitemata group, around Auckland, it is likely that platform formation continued during falling sea level, hence why platforms in the more southern parts of Auckland sit at lower elevations near low tide. However, for harder rock platforms like Okakari, platform formation is unlikely during falling sea level.

Another element in this exposure age data are the two sample ages taken from the raised ledge feature at the back of the platform. As expected, the ages for this feature are older than the first two ages from the main platform surface. How this feature came to be preserved, however, is somewhat enigmatic. One possibility is that this higher surface was the original elevation of the whole shore platform. If this were the case, we could infer that the platform has since been planated, probably as a result of the drop in sea level. This theory relies on the notion that the seaward scarp can be eroded back to planate a lower elevation surface.

This idea of planation is in conflict with the hypothesis Sunamura (1992), who proposes that near-horizontal shore platforms form through wave cutting, while the position of the seaward scarp is preserved, until the negative feedback relationship prevents the platform from widening. Additionally, the time frame for this planation of a pre-existing platform is likely insufficient to cut completely back to the present position of the raised surface. This scenario is especially likely, given that the rocks of the Pakiri formation are particularly hard compared to other flysch lithologies around

Auckland (Bell, 2007). Retreat rates for Auckland's hard rock cliffs were reported by Bell (2007), with rates ranging from 4mm a^{-1} to 20mm a^{-1} . With the former rate, planation would take $\sim 40,000$ years; with the latter, planation would take ~ 8000 years. These time frames are too long as they both exceed the period in which sea level has been stable over the Holocene. It would take a retreat rate of $>53\text{mm a}^{-1}$ to produce sufficient planation. Planation would need to have occurred within the last 3000 years, in which sea level has fallen to its present day position, to accept this theory. As will be discussed in section 7.7.3 the cliff retreat rate for Okakari point agrees with the rates reported by Bell (2007) and are not sufficiently fast to fit this scenario.

Another possibility for the preservation of this higher surface is that it is a remnant of the sea cliff position at the time sea level began to fall. The 3m wide surface would have been formed through subaerial cliff weathering and storm wave attack over a shorter duration, leaving the surface exposed along a bedding plane. The rest of the platform in this interpretation would have slowly worn down to its present level as sea level fell. It is likely that due to the hardness of the rock, any interpretation of this platform and its features would involve a longer time scale than what the 'zero erosion' exposure ages have shown. This suggests that surface erosion needs to be accounted for.

Before considering the rates of surface erosion on this platform, it is possible to ascertain a cliff back wear erosion rate based on the exposure ages. As mentioned earlier there is a linear increasing trend between the most landward sample's concentration (that is on the main platform surface) (AD15) and the most seaward AD19. Based on this trend, it is likely that during the platform cutting phase, that cliff back wear occurred at a steady rate. The exposure ages show that over ~ 3863 years the platform eroded back 168.5m. This equates to an average retreat rate of 43.6mm a^{-1} . This rate is much faster than the cliff recession rate for the nearby Leigh marine reserve observed by Bell (2007) of $18.48 \pm 0.22\text{mm a}^{-1}$. While this rate was only inferred from the width of the platform, it provides a benchmark with which to compare cliff retreat rates in the same rocks. However, in order to gain a more representative cliff retreat rate we need to infer a platform surface erosion rate.

7.3.3 Surface Erosion Rates

The surface erosion rates for Okakari point were assessed in the same way as the Wakatu samples. *Figure 7.5* shows that the wide distribution of measured ^{10}Be concentrations requires that the surface erosion rate be slow in order to produce concentrations of the magnitude recorded. This erosion rate 0.146mm a^{-1} at Okakari is slower than the fastest rate for Wakatu Point (0.22mm a^{-1}), possibly due to rock strength. Bell (2007) measured uniaxial compressive strength of shore platform rock, finding rock strength to be $79.02 \pm 14.08\text{MPa}$ at a shore platform formed in the Pakiri formation. Stephenson (1997) took measurements of compressive strength in the Kaikoura limestones of 57.251MPa and 21.75MPa (Stephenson, 1997); both are lower than the rock strength near Okakari based on Bell (2007). The true compressive strength of rock at Wakatu Point is likely even lower than those measured in Stephenson (1997) as the rocks are more heavily jointed and folded at Wakatu Point. Based on these compressive strengths, the difference between maximum erosion rates for these two sites makes sense.

If the maximum surface erosion rate of 0.147mm^{-1} at Okakari Point is applied, then the age of the most seaward sample would be $\sim 12\text{ka}$. This places platform development in the early stages of the PGMT (Gibb, 1986), and it is possible that the true long-term surface erosion rate is slower. Clement *et al.* (2016) find that the establishment of sea level similar to present in the Auckland area (the start of the mid-Holocene high-stand) occurred slightly earlier than in Gibb's (1968) estimate, so that platform cutting in Auckland probably commenced around 7ka . Assuming that this is a better initiation time for the shore platforms around Auckland, a third erosion rate was plotted in *figure 7.5*. The erosion rate 0.1mm^{-1} is the rate at which AD19 (the platform edge) is $\sim 7000\text{yrs}$ old. This is likely to be the surface erosion rate that is the best representation of the long term erosion at Okakari. Based on a platform initiation of $\sim 7000\text{yrs BP}$ and a surface erosion rate of 0.1mm a^{-1} , the rate of cliff back wear becomes 23.66mm a^{-1} . This is more similar to the 18.48mm a^{-1} measured by Bell (2007).

There have not been any surface erosion studies previously conducted at Okakari Point, like the MEM record that is available for Kaikoura. This means there is no modern down wear rates against which to compare this long-term signal. As such, we

do not know if there is a disparity between modern and long-term erosion rates at Okakari Point.

7.3.4 The Role of Rock Strength

One of the interesting elements of the Okakari Point shore platform is its elevation relative to mean sea level. The platform is currently 0.8m above MSL. The micro-tidal range at Okakari means that this is an intertidal platform; however, the zone at the back of the platform between AD15 and AD16 is only inundated during spring tides. The raised ledge would only be exposed to tidal inundation during extreme tides and storm surges. Sunamura (1991) made the distinction that rock strength was an important control on shore platform morphology. Flume-based testing revealed that increasing rock strength caused near-horizontal platforms to develop at higher elevations (Sunamura, 1991). This finding was confirmed using field-based measurements in Thornton and Stephenson (2006) and supported by Kennedy and Dickson (2007). The Okakari Shore platform sits at a relatively high elevation, which is expected given the compressive strength of rocks along this coast.

We know that the Okakari Point platform was previously situated at a higher elevation relative to its current position. This is known because there is clear evidence that the platform is actively down-wearing. This evidence is the water layered weathering morphologies present across the platform (*Figure 7.8a*); the rampart feature at the seaward margin (*Figure 7.8b*); and higher elevation irregularities in the platform surface (*Figure 7.8c*). This down-wearing signal implies that as sea level fell from ~4000yrs BP, the platform surface lowered as well. The lowering rates evaluated in the previous section indicate that this adjustment occurred slowly. We can validate this assumption by taking the difference between the top of the rampart and the platform surface and dividing this by the length of time that sea level was lowering, ~3000 years. This gives an erosion rate of 0.072mm a^{-1} , which is similar to the rate the 0.1mm a^{-1} from the previous section. The expectation would be that shore platforms with higher elevation than Okakari would have higher compressive strength so that they have been able to resist the lowering of sea level in the late-Holocene. When comparing the compressive strength of the Okakari platform with similar higher elevation platforms at Shag Point, Otago (Kennedy & Dickson, 2007) and the Otway

Coast, VIC, Australia (Thornton & Stephenson, 2006), this was found not to be the case. The compressive strength for high elevation platforms at Shag Point was $\sim 44\text{MPa}$ and at Otway, 58MPa and 70MPa ; all lower than the 79MPa at Okakari. This suggests that it may be more than just rock strength which demarcates whether the shore platform remains supra-tidal during sea level fall or becomes inter-tidal, such as at Okakari. One possibility is that the geological structure, as well as rock strength, controls the way the platform can adjust to falling sea level.

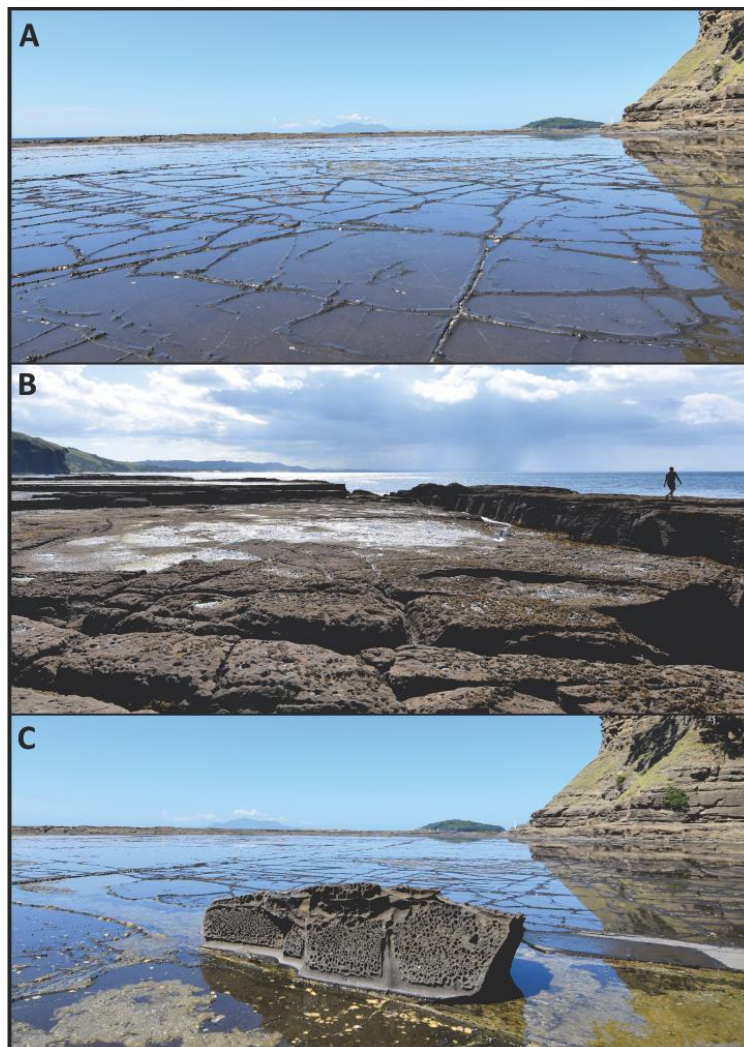


Figure 7.8: Photos of different platform morphologies that occur on the Okakari shore platform, which confirm down-wearing is occurring on this platform. (A) Water layered weathering morphology, represented by ridges and water pools. (B) Seaward rampart, slightly elevated from the rest of the platform. (C) Higher elevation irregularity on the main platform surface, heavily mottled with tafoni weathering. Image Credit: Martin Hurst (2017)

7.3.5 Interpreting Best Fit RPM Simulations

The best fit model simulation for Okakari produced a very similar platform geometry and nuclide concentration trend to the Okakari Platform. The low wave efficacy reduced the erosive force of the waves acting on the platform scarp and surface, allowing most of the accumulated nuclides to be retained in the rock. This behaviour is likely to be very similar to the erosive processes on the real Okakari platform. The erosion rates identified in section 7.3.4, show that the erosion on this surface is particularly slow, which is why we obtained higher nuclide concentrations on the outer platform. The low wave efficacy may also be responsible for the shorter modelled platform profile, so we can infer that wave efficacy is likely slightly higher on the real platform. This could alternately be due to the timing of sea level falling. The sea level was simulated to fall after 4000 years, following the Auckland sea level fluctuations identified in Clement et al., (2016). However, the exact timing of the drop in sea level is difficult to pinpoint. If the sea level remained high enough to actively erode the cliff until later than 4000yrs then the platform may have widened further before waves abandoned the cliff base. One of the model behaviours that deviates from the real platform is the response to the sea level fall. Section 7.3.4 suggests that the platform has likely down-worn since sea level began to fall, leaving behind the rampart and ledge features. This was not replicated in the model run, instead the erosion was only focused on the outside edge of the platform once sea level began to fall signalling the abandonment of the cliff by wave action.

Chapter 8: General Discussion

The case studies evaluated in Chapters 6 and 7 are detailed assessments of empirical measurements of the age and erosive history of two New Zealand shore platforms. In addition to these analyses and discussions, modelling was conducted with the Rocky Profile Model to assess the relative roles of different process drivers in shore platform development. This combination of methods enables the comparison of empirical measurements with modelled shore platform geometries to direct the interpretations of these features in the New Zealand coastal context. In this chapter the modelling work presented in Chapter 5 will be discussed along with the cosmogenic analysis in chapters 6 and 7. This discussion will address some of the assumptions involved with this model and the overall validity of this style of exploratory modelling in this thesis. I also discuss the relationships and trends that become evident from the sensitivity analysis of the drivers and scenario-based testing of sea level and tectonic activity. This chapter will also draw comparisons between the two case studies and attempt to evaluate them within the wider literature in the area of shore platform investigation. Finally directions for future work will be discussed with regard to this thesis.

8.1 Assumptions and Validity of the Rocky Profile Model

The RPM model framework is a significant simplification of the drivers of shore platform development (Matsumoto et al., 2016a). The benefit of treating the drivers in a simple modelling framework is that this model is able to produce a wide variety of shore profile geometries, as well as reducing computational demands (Matsumoto et al., 2016a). However this approach of exploratory modelling requires that numerous assumptions are made in the representation of processes. Notably the morphology building component of the model includes parameters that cannot be defined in real terms, such as the material resistance parameter. Other examples include the cliff height and the cliff failure mechanism. In the model, cliff failure or back wearing occurs only due to the formation of notches of a set depth at the base of the cliff, where in reality the cliff can fail also from subaerial processes of weathering. The height of the cliff would also generally change with the topography as the shore line is eroded. The inclusion of more detailed parameters, however, such as assigning values to critical rock strength and accounting for other mechanisms of cliff and platform erosion would be largely speculative. This is because many of the small scale process relationships

and drivers on shore platforms remain poorly understood and quantified (Stephenson, 2000).

The Rocky Profile Model takes a generally 'top-down', exploratory approach to the numerical modelling of shore platform development. This approach is well supported by Murray (2003), who discussed the benefits of taking this approach over more directed empirical modelling. Murray (2003) stated that if a modelling approach explicitly simulated processes at smaller scales, the large scale interactions produced in the model may not represent nature closely enough if the processes were not well defined. This outcome is because small inaccuracies tend to cascade up through the scales (Murray, 2003). When these small scale interactions are poorly understood, a top-down approach is more likely to produce morphologically accurate model behaviour (Murray, 2003). This is the case with the RPM_CRN model, where the model simulates a range of realistic platform geometries under reasonable process regimes. It is difficult to explicitly validate an exploratory model such as this, but based on the production of geometries comparable to the varied platform geometries found along the New Zealand coastline, it is reasonable to use this model for this thesis.

8.2 Insights from Platform Driver Sensitivity Analysis

The sensitivity analysis in Chapter 5 revealed that by and large, the three main drivers (material resistance, weathering rate, and wave efficacy) affected platform development in very similar ways. Each of the three sets of model runs for these drivers produced very similar platform geometries and trends in the nuclide concentrations across the shore platforms. Low resistance, fast weathering and high wave efficacy all resulted in the development of wide shore platforms. These three tests showed the geometries moving beyond the state of realistic platform widths for New Zealand, as platforms around New Zealand are typically narrower. These narrower platforms are a function of the smaller tidal ranges in New Zealand and the higher numbers of type B platforms that occur as a result. Based on the model's behaviour towards wider than expected platforms we can infer that in New Zealand, platforms are either, more often built in harder rocks, less active weathering systems lower wave energies, or some combination of these. However, local and regional scales are very important in determining which of these drivers are more important. In

most other cases where drivers were set up with medium value parameters or high resistance, slow weathering and low wave efficacy, the platform widths were narrower. More moderate weathering and wave conditions, or rock strength produce widths comparable to New Zealand platforms: at Kaikoura, platform widths do not exceed 200m (Stephenson et al., 2017). This is also the case at Shag Point (Kennedy & Dickson, 2006), Mahia Peninsula (Ogawa et al., 2012) and Okakari Point (Dickson & Pentney, 2012). The exception to this narrower platform type would be Tatapouri, at ~240m (Ogawa et al., 2011). These findings help to frame the suite of more realistic driver settings for producing more accurate platform geometries. Also demonstrating that New Zealand platforms develop within subdued process regimes.

One of the interesting behaviours identified from the sensitivity analysis was the erosion of the outer (or seaward) platform surfaces. In almost every case the modelled platforms would undergo surface erosion to some extent. However, the behaviour of this erosion was dominated by cutting into the seawards scarp and fresh planation of the platform surface from that position. Regular surface erosion usually occurs through processes of surface down wearing (Stephenson and Kirk, 2000b), rather than planation from the scarp. The latter behaviour (cutting into scarps) is generally refuted by Sunamura (1992), who argued that scarps do not migrate and platforms develop under a negative feedback regime. However, if sea level was changing, cutting from the scarp would be more likely.

One case of particular importance was the model run for low wave efficacy. This run produced a shoreline profile relatively similar to that measured at Okakari Point. The ^{10}Be concentration trend with distance across the platform was also very linear, showing steady accumulation of ^{10}Be towards the sea, very similar to the trend identified at Okakari. While the modelled nuclide concentrations were far higher than those observed, this helped to direct the interpretation and best-fit modelling of Okakari point. The implication here is that shore platforms that are harder, which tend to sit at higher elevations (like Okakari), are less prone to effective wave erosion action. This helps them to retain their elevation and maintain higher nuclide accumulations towards their seaward edges.

Generally, the sensitivity analyses helped to identify the way certain drivers influenced the platform geometry and guided the interpretation of the data from the case studies. The model runs on their own, however, did reflect very well the measured data attained from these cases studies. This was an expected outcome as the testing of drivers in their simplest terms was unlikely to yield completely realistic shore profiles and nuclide concentrations. In order to attain model outputs that were more directly reflective of real morphologies observed at the case study sites, the scenario based testing was applied.

8.3 Insights from Scenario Based Testing

The falling sea level tests in sections 5.2.1 reveal the primary response for a reasonably rapid and constant fall in sea level ($1.25 \times 10^{-4} \text{ myr}^{-1}$) was for the surface erosion to accelerate to keep pace with the fall; cliff back wear was also increased producing wider profiles. These rates of constant sea level fall (and for sea level rise, below) were not based on actual measured rates of sea level fall (rise) around New Zealand. However, these rates represent the pace of sea level change prior to the establishment of the Holocene high-stand. These scenarios were used to show how the sea level driver affected platform evolution in the model.

With a faster rate of sea level fall it may be possible to cause stranding of the platform surface, however this did not occur in these simulations, indicating that the parameterization may not have been optimal for stranding to occur. For the modelled outputs on hard and medium resistance rocks, the continuous erosion of the platform causes the nuclide concentrations to be low across the platform. If a slower rate of sea level fall was used it is likely that the nuclide concentrations would be less significantly reduced. The rate of sea level fall applied, $1.25 \times 10^{-4} \text{ myr}^{-1}$, is much faster than any rate of sea level change that has occurred around New Zealand during the mid to late-Holocene. Based on the New Zealand sea level indicators reviewed in Clement et al., (2016), sea level fell from $\sim 2\text{m}$ above present mean sea level to the present mean sea level from about 3ka. This constitutes an average rate of sea level fall of $6.6 \times 10^{-4} \text{ myr}^{-1}$. This rate of sea level falling was applied in the best fit modelling for the two case studies. The surface erosion relating to this rate of sea level fall was less extreme than what has been modelled in the scenario tests, allowing for higher nuclide

concentrations to occur on real New Zealand platforms. Sea level fall tests also show that ramparts at the platform edge tend to develop as the platforms lower. This is common of real Type B shore platforms and is evident at Okakari Point.

The simulations for constant sea level rise developed wide, sloping and stepped profiles. The sloping profile for medium resistance rock is a good representation of rocky coastline response to sea level rise. Where the rising sea level is a very efficient driver of cliff erosion the shore platforms are not flat as the sea continually initiates cutting at a higher elevations. This process produces a drowned coastal slope. This behaviour is consistent with Trenhaile (2001), where, during interglacial periods when sea levels rise, modelled shore platforms developed wider profiles, drawing them away from a state of static equilibrium. The hard rock sea level rise simulation exhibited very similar behaviour, however, the resultant morphology consisted of a series of narrow platform steps. An explanation for this is that the harder rock, coupled with the rapid rate of sea level rise, caused the abandonment of sections of the platform, with cutting resuming at higher elevations. This was the only scenario which produced notable stepped morphology.

Simulations of tectonic uplift events on the shore platforms were applied to this modelling. One aspect of these model runs was to determine if terraced morphology could be simulated by uplift. The three model runs using different magnitudes of event uplift were used to test for this signal of terrace formation. Only the largest step size of 2m produced terraces. However, following each successive event the terraces morphology was eventually destroyed by incision. This incision left behind only small ledge features below the cliff. This platform geometry does not result in marine terrace preservation.

Some previous modelling work has been conducted to assess the drivers behind marine terrace formation (e.g. Trenhaile, 2002). The inability of the Rocky Profile Model to clearly simulate terrace preservation under this parameterization points to the conclusion that uplift events (earthquakes) may not be significant drivers in marine terrace preservation. However, with a lower wave efficacy parameter, the best fit test for Okakari produced the initial stages of shoreline stranding, so in a setting with lower wave energies stranding may be more likely. Simulated earthquakes do appear to drive

the formation of small scale elevational features, such as ledges, on platforms. These features, however, are highly susceptible to erosion as the shore profile adjusts to the event.

This outcome does not completely preclude terrace formation through single event uplift. Some fault ruptures exhibit extreme vertical displacement, such as the 1855 Mw 8.2 Wairarapa Earthquake, which produced ~6.4m of uplift at its most significant point (Little et al., 2009). Events of a similar magnitude may be able to strand a shore platform high enough above mean high water to become a marine terrace. Assuming that most lower magnitude (<2m) uplift events tend not to be preserved in coastal morphology, the main driver for platform stranding and terrace formation is likely to be large scale (>10 meters) eustatic sea level fall. This is well supported in the existing literature on marine terraces (Berryman, 1993; Chappell, 1975; Ota et al., 1996; Pillans, 1983; Ward, 1988a, 1988b).

The final scenario testing around recurrence intervals for uplift events revealed a clear relationship. When uplifting occurred at a shorter recurrence interval, 400 years, the shore platform underwent more surface erosion. This increased erosion was due to the system adjusting to the lowered sea level. With uplift occurring frequently, the platform was unable to fully adjust before the next event, so surface erosion continued. Without the continued perturbations to the system the erosion would eventually reduce significantly or halt through negative feedback. With the longer recurrence interval, the platform is perturbed less often, so it is able to attain a wider profile, with a lesser degree of surface lowering. These recurrence interval tests, like the sea level fall tests showed that ramparts had developed on the sea-ward margins of the platforms, which is evident in the nuclide concentration plots. In fact, all of the model runs which simulated the relative lowering of sea level in some way developed ramparts, as well as fairly saw-toothed trends in the nuclide concentrations across their profiles. If this model is taken to be accurate in representing shore platform development then it can be interpreted that Wakatu point shore platform must have undergone relative sea level fall to produce the saw toothed concentrations measured. This is in line with the interpretation in chapter 6.

8.4 Linking to Previous Cosmogenic Platform Investigations

The previous three investigations of shore platforms using cosmogenic nuclides have helped to set a precedent for how to undertake this type of investigation. A useful numerical framework for interpreting cosmogenic nuclide results was developed by Regard *et al* (2012), and Hurst *et al.* (2017) improved the framework. One of the key developments in this earlier work was the identification of an expected trend in the nuclide concentrations that are measured across a shore platform. The ‘hump shaped’ distribution as termed by Regard *et al.* (2012), described in section 1.6.1, denotes that concentrations reach a maximum somewhere in the mid-section of an across shore profile and tail off further from the cliff. This trend was supported by three separate investigations in the northern hemisphere (Choi *et al.*, 2012; Hurst *et al.*, 2016; Regard *et al.*, 2012). In each of these independent investigations a hump shaped distribution was identified from the nuclide concentrations attained from platform sampling.

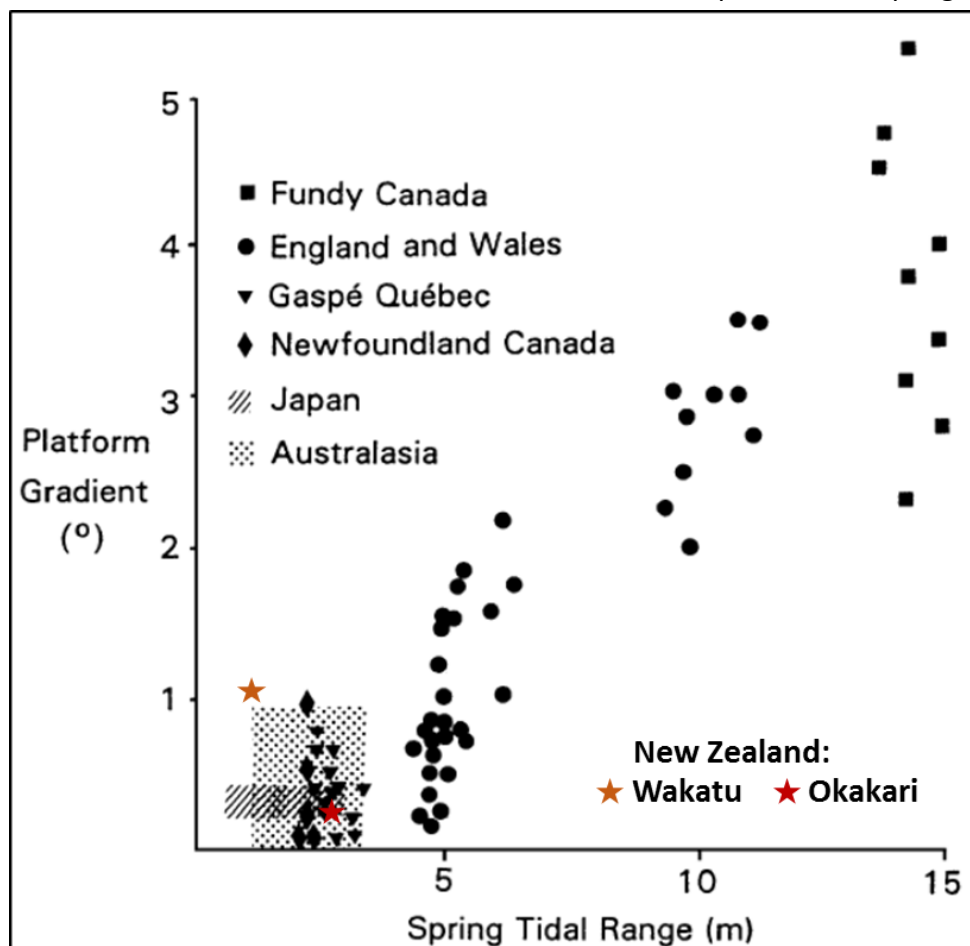


Figure 8.1: Plot from Trenhaile (2002) shown in section 1.5.1, illustrating the relationship between tidal range and platform slope. Now including the two New Zealand case studies, represented by the stars.

A key control on the magnitude of this humped distribution was identified in Regard *et al.* (2012) to be tidal range. All three of these earlier studies investigated shore platforms with macro-tidal ranges; subsequently these platforms are all sloping (type A) and very wide. The two case studies investigated for this thesis are very different shore platforms than these other three examples. The tidal settings of the two New Zealand platforms are both micro-tidal and subsequently the slope of these platforms are very low (*Figure 8.1*). In Regard *et al.* (2012) they predict that on platforms of micro-tidal range, the magnitude of the hump will be more accentuated and closer to the sea cliff. In both of the New Zealand case studies, this is not the case. The absence of this trend in both the Okakari and Wakatu data sets indicate that the model of hump shaped distribution may not be a good fit on platforms of micro-tidal ranges.

The humped distribution model is generally applicable on wide, sloped platforms because the relationships associated with the distribution are optimised for these types of platforms. The reasons that expected nuclide concentrations are lower on the seaward part of the shore platforms are: firstly, sloped platforms are more efficiently weathered on the outer surface due to lower attenuation of wave activity and wetting and drying processes; secondly, the outer platforms are inundated at greater depths, effectively attenuating the cosmic ray flux to the surface more of the time. In lower tidal ranges, we know from the relationship in *figure 8.1* that platforms tend to develop towards the sub-horizontal, type B morphology. As mentioned in chapter 7, on these flatter surfaces the depth of the attenuating water column at high tide is the same across the platform and weathering rates are generally also similar across the profile. Therefore there is not any more efficient material removal or attenuation at the seaward edge than near the cliff. As such, the humped distribution is unlikely to be applicable on low tidal range platforms.

Another advantage to using the exploratory modelling approach of Matsumoto *et al.* (2016a) in the coupled Rocky Profile Model is its ability to simulate more diverse geometries and nuclide distributions than just fitting to the humped distribution. The RPM does in some cases produce a humped distribution of concentrations, notably in the sensitivity tests for medium weathering and slow weathering in section 5.1. However, it also produces concentrations trends completely at odds with the hump,

i.e. the best fit simulation for Okakari point. This diversity of outputs makes the RPM_CRN a useful framework for interpreting cosmogenic nuclides on shore platforms.

8.5 Future Work

One of the main outcomes of this work was the addition of two new shore platform chronologies to the very small set of three other works that precede it, while also applying the first ever application of this approach in New Zealand. Through the application of this method we have identified that trends associated with shore platforms in macro-tidal settings are not persistent on lower tidal range platforms. This separation indicates that on platforms with different tidal ranges, the drivers of change on the platforms are likely to be different. This difference demonstrates a need to produce more cosmogenic nuclide derived chronologies on other micro and meso-tidal shore platforms. With more cases to draw from it will be possible to make determinations about how long-term platform evolution is affected by the platform type and the balance of drivers in their respective settings and how this is expressed in nuclide production trends. Low angle platforms such as those in Australia and Japan would be good areas for future cosmogenic nuclide analysis. It would also be useful to attain nuclide concentrations on other shore platforms where short-term rates of platform erosion and/or cliff erosion have been assessed. Doing this will allow for better understanding of any discrepancies between long-term and short-term erosion rates, if they exist. It is important to understand this relationship as it has implications for how we come to assess erosion hazards on rocky coastlines.

The modelling work provided useful insights into the process regimes operative on different platform geometries. In this work the RPM_CRN model was applied in simple fashion only using a few variations on the different values of the parameters to test factors that were likely to differ between the two platform sites. There is wider scope within this model to apply vastly different parameterizations from those used in this study to investigate other hard coast morphologies. This simple style of analysis could be expanded upon in future studies which used this model as a means to evaluate shore platform formation and nuclide accumulation trends.

Conclusion

In-situ cosmogenic ^{10}Be exposure age dating successfully established two shore platforms in New Zealand as being late-Holocene features and identified long-term surface denudation rates on the platforms at Kaikoura Peninsula and Cape Rodney, New Zealand. Denudation rates obtained from these locations showed that they have eroded at similarly slow rates during the late-Holocene, $<0.22\text{mm a}^{-1}$ at Wakatu Point, Kaikoura and $\sim 0.1\text{mm a}^{-1}$ at Okakari Point, Cape Rodney.

At Kaikoura the long-term erosion rates were significantly different from the modern erosion rates measured with micro erosion meters indicating a recent shift in the process regime to affect the rates of weathering on the platform surface. This shift is attributed to the tectonic regime in the area, suggesting earthquakes have driven this change on the platform. This was assessed by modelling this platform with 1 meter of uplift at 400 year recurrence intervals, which produced geometry and ^{10}Be concentrations which upheld this interpretation.

The morphological structure of the shore platform at Okakari point has been shown to be primarily influenced by late-Holocene sea level changes, mostly due to the lowering of the local sea level over the last 3-4ka. Geomorphic markers on the platform, such as the rampart, and weathering morphologies point to continuous slow lowering of the platform. The nuclide concentrations obtained from this platform also allowed for a cliff erosion rate to be ascertained ($\sim 23\text{mm a}^{-1}$), due to the linear trend in the accumulated nuclides across the platform.

The coupled exploratory RPM_CRN model was used to identify how the drivers of platform development had influenced these shore platforms. Key findings from this modelling were, firstly, that simulated relative sea level changes were instrumental in replicating the measured platform geometries and concentrations. Secondly, that platforms in New Zealand tend to be developed in coastlines with higher rock strength, lower weathering rates and lower wave efficacy, with the regional setting determining the degree to which this holds true.

Finally, one of the most significant outcomes of this research was the observation that type B platforms (measured in this thesis) exhibit significantly different trends in the distribution of nuclide concentrations across shore than type A platforms, measured in

earlier works. This work has demonstrated that platforms at low tidal ranges and shallow slopes may operate with different processes than their high slope counterparts. This shows that models based on type A platforms are not capable of modelling processes on type B platforms.

Reference List

- Ackermann, M., Ajello, M., Allafort, A., Baldini, L., Ballet, J., Barbiellini, G., ... Zimmer, S. (2013). Detection of the Characteristic Pion-Decay Signature in Supernova Remnants. *Science*, 339(6121), 807–811.
- Adams, P. N., Anderson, R. S., & Revenaugh, J. (2002). Microseismic measurement of wave-energy delivery to a rocky coast. *Geology*, 30(10), 895–898.
- Adams, P. N., Storlazzi, C. D., & Anderson, R. S. (2005). Nearshore wave-induced cyclical flexing of sea cliffs. *Journal of Geophysical Research: Earth Surface*, 110(F2), F02002.
- Allen, S. R. (2004). The Parnell Grit beds revisited: Are they all the products of sector collapse of western subaerial volcanoes of the Northland Volcanic Arc? *New Zealand Journal of Geology and Geophysics*, 47(3), 509–524.
- Ashton, A. D., Walkden, M. J. A., & Dickson, M. E. (2011). Equilibrium responses of cliffed coasts to changes in the rate of sea level rise. *Marine Geology*, 284(1–4), 217–229.
- Balco, G., Stone, J. O., Lifton, N. A., & Dunai, T. J. (2008). A complete and easily accessible means of calculating surface exposure ages or erosion rates from ¹⁰Be and ²⁶Al measurements. *Quaternary Geochronology*, 3(3), 174–195.
- Ballance, P. F. (1974). An inter-arc flysch basin in northern New Zealand: Waitemata Group (upper Oligocene to lower Miocene). *The Journal of Geology*, 82(4), 439–471.
- Bartrum, J. A. (1926). "Abnormal" Shore Platforms. *The Journal of Geology*, 34(8), 793–806.
- Bell, J. E. (2007). *Towards a Better Understanding of Coastal Cliff Erosion in Waitemata Group Rock; Auckland, New Zealand*. (Thesis). The University of Waikato.

- Berryman, K. R. (1993). Distribution, age, and deformation of Late Pleistocene marine terraces at Mahia Peninsula, Hikurangi Subduction Margin, New Zealand. *Tectonics*, 12(6), 1365–1379.
- Bird, E. C. F. (2011). *Coastal Geomorphology: An Introduction*. John Wiley & Sons.
- Borchers, B., Marrero, S., Balco, G., Caffee, M., Goehring, B., Lifton, N., Nishiizumi, K., Phillips, F., Schaefer, J. and Stone, J. (2016) Geological calibration of spallation production rates in the CRONUS-Earth project. *Quaternary Geochronology*, 31, 188-198.
- Bradley, W. C., & Griggs, G. B. (1976). Form, genesis, and deformation of central California wave-cut platforms. *Geological Society of America Bulletin*, 87(3), 433–449.
- Brooke, B. P., Young, R. W., Bryant, E. A., Murray-Wallace, C. V., & Price, D. M. (1994). A pleistocene origin for shore platforms along the Northern Illawarra Coast, New South Wales. *Australian Geographer*, 25(2), 178–185.
- Bruun, P. (1954). Coast Erosion and the Development of Beach Profiles. *U. S. Army Beach Erosion Board Technical Memorandum 44*, 44, 79pp.
- Budetta, P., Santo, A., & Vivenzio, F. (2008). Landslide hazard mapping along the coastline of the Cilento region (Italy) by means of a GIS-based parameter rating approach. *Geomorphology*, 94(3–4), 340–352.
- Carter, R. W. G., & Woodroffe, C. D. (1997). *Coastal Evolution*. Cambridge, UK: Cambridge University Press.
- Chandra, S. (1968). *The Geomorphology of the Kaikoura Area, Thesis Presented in Partial Fulfilment of the Requirements for the Degree of Master of Arts in Geography. Department of Geography. University of Canterbury, Canterbury, New Zealand.*
- Chappell, J. (1974). Late Quaternary glacio- and hydro-isostasy, on a layered earth. *Quaternary Research*, 4(4), 405–428.

- Chappell, J. (1975). Upper Quaternary warping and uplift rates in the Bay of Plenty and west coast, North Island, New Zealand. *New Zealand Journal of Geology and Geophysics*, 18(1), 129–154.
- Chappell, J., Omura, A., Esat, T., McCulloch, M., Pandolfi, J., Ota, Y., & Pillans, B. (1996). Reconciliation of late Quaternary sea levels derived from coral terraces at Huon Peninsula with deep sea oxygen isotope records. *Earth and Planetary Science Letters*, 141(1), 227–236.
- Chappell, J., & Shackleton, N. J. (1986). Oxygen isotopes and sea level. *Nature*, 324(6093), 137.
- Chappell, P. J. (2013). *The Climate and Weather of Auckland* (NIWA Science and Technology Series No. 60) (p. 40pp). NIWA. Retrieved from <https://www.niwa.co.nz/static/Auckland%20ClimateWEB.pdf>
- Chmeleff, J., von Blanckenburg, F., Kossert, K., & Jakob, D. (2010). Determination of the ^{10}Be half-life by multicollector ICP-MS and liquid scintillation counting. *Nuclear Instruments and Methods in Physics Research Section B: Beam Interactions with Materials and Atoms*, 268(2), 192–199.
- Choi, K. H., Seong, Y. B., Jung, P. M., & Lee, S. Y. (2012). Using Cosmogenic ^{10}Be Dating to Unravel the Antiquity of a Rocky Shore Platform on the West Coast of Korea. *Journal of Coastal Research*, 282, 641–657.
- Church, J. A., Clark, P. U., Cazenave, A., Gregory, J. M., Jevrejeva, S., Levermann, A., ... Unnikrishnan, A. S. (2013). Sea Level Change. In *Climate Change 2013: The Physical Science Basis. Contribution of Working Group I to the Fifth Assessment Report of the Intergovernmental Panel on Climate Change*. Cambridge, UK and New York, NY, USA.: Cambridge University Press.
- Claessens, L., Veldkamp, A., ten Broeke, E. M., & Vloemans, H. (2009). A Quaternary uplift record for the Auckland region, North Island, New Zealand, based on marine and fluvial terraces. *Global and Planetary Change*, 68(4), 383–394.

- Clement, A. J. H., Whitehouse, P. L., & Sloss, C. R. (2016). An examination of spatial variability in the timing and magnitude of Holocene relative sea-level changes in the New Zealand archipelago. *Quaternary Science Reviews*, *131*, 73–101.
- Coelho, C., Silva, R., Veloso-Gomes, F., & Taveira-Pinto, F. (2009). Potential effects of climate change on northwest Portuguese coastal zones. *ICES Journal of Marine Science: Journal Du Conseil*, *66*(7), 1497–1507.
- Dana, J. D. (1894). *Manual of Geology Fourth Edition*. New York, Cincinnati and Chicago: American Book Company.
- de Lange, W. P., & Moon, V. G. (2005). Estimating long-term cliff recession rates from shore platform widths. *Engineering Geology*, *80*(3–4), 292–301.
- Desilets, D., Zreda, M., & Prabu, T. (2006). Extended scaling factors for in situ cosmogenic nuclides: New measurements at low latitude. *Earth and Planetary Science Letters*, *246*(3), 265–276.
- Dickson, M. E., Ogawa, H., Kench, P. S., & Hutchinson, A. (2013). Sea-cliff retreat and shore platform widening: steady-state equilibrium? *Earth Surface Processes and Landforms*, *38*(9), 1046–1048.
- Dickson, M. E., & Pentney, R. (2012). Micro-seismic measurements of cliff motion under wave impact and implications for the development of near-horizontal shore platforms. *Geomorphology*, *151–152*, 27–38.
- Dickson, M. E., & Stephenson, W. J. (2014). Chapter 13 The rock coast of New Zealand. *Geological Society, London, Memoirs*, *40*(1), 225–234.
- Dorman, L. I., Valdés-Galicia, J. F., & Dorman, I. V. (1999). Numerical simulation and analytical description of solar neutron transport in the Earth's atmosphere. *Journal of Geophysical Research: Space Physics*, *104*(A10), 22417–22426.
- Dougherty, A. J. (2011). *Evolution of prograded coastal barriers in northern New Zealand* (PhD Thesis) University of Auckland, Auckland, NZ.
- Dougherty, A. J., & Dickson, M. E. (2012). Sea level and storm control on the evolution of a chenier plain, Firth of Thames, New Zealand. *Marine Geology*, *307–310*, 58–72.

- Duckmanton, N. M. (1974). *The Shore Platforms of the Kaikoura Peninsula* (MA Thesis). University of Canterbury, Christchurch, NZ.
- Dunai, T. J. (2001). Influence of secular variation of the geomagnetic field on production rates of in situ produced cosmogenic nuclides. *Earth and Planetary Science Letters*, 193(1), 197–212.
- Dunai, T. J. (2010). *Cosmogenic nuclides: principles, concepts and applications in the earth surface sciences*. Cambridge; New York: Cambridge University Press.
- Dunne, J., Elmore, D., & Muzikar, P. (1999). Scaling factors for the rates of production of cosmogenic nuclides for geometric shielding and attenuation at depth on sloped surfaces. *Geomorphology*, 27(1), 3–11.
- Emery, K. O., & Kuhn, G. G. (1982). Sea cliffs: Their processes, profiles, and classification. *Geological Society of America Bulletin*, 93(7), 644–654.
- Flemming, N. C. (1965). Form and Relation to Present Sea Level of Pleistocene Marine Erosion Features. *The Journal of Geology*, 73(5), 799–811.
- Fyfe, J. C. (2003). Extratropical Southern Hemisphere cyclones: Harbingers of climate change? *Journal of Climate*, 16(17), 2802–2805.
- Gibb, J. G. (1986). A New Zealand regional Holocene eustatic sea level curve and its application to determination of vertical tectonic movements. *Royal Society of New Zealand Bulletin*, 24, 377–395.
- Gornitz, V. (1991). Global coastal hazards from future sea level rise. *Palaeogeography, Palaeoclimatology, Palaeoecology*, 89(4), 379–398.
- Gosse, J. C., & Phillips, F. M. (2001). Terrestrial in situ cosmogenic nuclides: theory and application. *Quaternary Science Reviews*, 20, 1475–1560.
- Griggs, G. B., & Trenhaile, A. S. (1997). Coastal cliffs and platforms. In R. W. G. Carter & C. D. Woodroffe, *Coastal Evolution: Late Quaternary Shoreline Morphodynamics*. Cambridge University Press.

- Heisinger, B., Lal, D., Jull, A. J. T., Kubik, P., Ivy-Ochs, S., Knie, K., & Nolte, E. (2002). Production of selected cosmogenic radionuclides by muons: 2. Capture of negative muons. *Earth and Planetary Science Letters*, *200*(3–4), 357–369.
- Hemmingsen, S. A., Eikaas, H. S., & Hemmingsen, M. A. (2007). The influence of seasonal and local weather conditions on rock surface changes on the shore platform at Kaikoura Peninsula, South Island, New Zealand. *Geomorphology*, *87*(4), 239–249.
- Hilton, M. J. (1995). Sediment Facies of an Embayed Coastal Sand Body, Pakiri, New Zealand. *Journal of Coastal Research*, *11*(2), 529–547.
- Hurst, M. D., Rood, D. H., & Ellis, M. A. (2016). Controls on the distribution of cosmogenic ^{10}Be across shore platforms. *Earth Surface Dynamics Discussions*, 1–38.
- Hurst, M. D., Rood, D. H., & Ellis, M. A. (2017). Controls on the distribution of cosmogenic ^{10}Be across shore platforms. *Earth Surface Dynamics*, *5*(1), 67–84.
- Hurst, M. D., Rood, D. H., Ellis, M. A., Anderson, R. S., & Dornbusch, U. (2016). Recent acceleration in coastal cliff retreat rates on the south coast of Great Britain. *Proceedings of the National Academy of Sciences*, *113*(47), 13336–13341.
- Inman, D. L., & Nordstrom, C. E. (1971). On the tectonic and morphologic classification of coasts. *The Journal of Geology*, 1–21.
- Ivy-Ochs, S., Poschinger, A. v., Synal, H.-A., & Maisch, M. (2009). Surface exposure dating of the Flims landslide, Graubünden, Switzerland. *Geomorphology*, *103*(1), 104–112.
- Kennedy, D. M., & Dickson, M. E. (2006). Lithological control on the elevation of shore platforms in a microtidal setting. *Earth Surface Processes and Landforms*, *31*(12), 1575–1584.
- Kennedy, D. M., & Dickson, M. E. (2007). Clifed coasts of New Zealand: Perspectives and future directions. *Journal of the Royal Society of New Zealand*, *37*(2), 41–57.

- Kennedy, D. M., Paulik, R., & Dickson, M. E. (2011). Subaerial weathering versus wave processes in shore platform development: reappraising the Old Hat Island evidence. *Earth Surface Processes and Landforms*, 36(5), 686–694.
- Kirk, R. M. (1975). Aspects of Surf and Runup Processes on Mixed Sand and Gravel Beaches. *Geografiska Annaler. Series A, Physical Geography*, 57(1/2), 117–133.
- Kirk, R. M. (1977). Rates and forms of erosion on intertidal platforms at Kaikoura Peninsula, South Island, New Zealand. *New Zealand Journal of Geology and Geophysics*, 20(3), 571–613.
- Kohl, C. P., & Nishiizumi, K. (1992). Chemical isolation of quartz for measurement of in-situ produced cosmogenic nuclides. *Geochimica et Cosmochimica Acta*, 56, 3583–3587.
- Lal, D. (1991). Cosmic ray labeling of erosion surfaces: in situ nuclide production rates and erosion models. *Earth and Planetary Science Letters*, 104(2), 424–439.
- Lambeck, K., & Chappell, J. (2001). Sea Level Change Through the Last Glacial Cycle. *Science*, 292(5517), 679–686. <https://doi.org/10.1126/science.1059549>
- Lifton, N. A., Bieber, J. W., Clem, J. M., Duldig, M. L., Evenson, P., Humble, J. E., & Pyle, R. (2005). Addressing solar modulation and long-term uncertainties in scaling secondary cosmic rays for in situ cosmogenic nuclide applications. *Earth and Planetary Science Letters*, 239(1–2), 140–161.
- Lim, M., Rosser, N. J., Petley, D. N., & Keen, M. (2011). Quantifying the Controls and Influence of Tide and Wave Impacts on Coastal Rock Cliff Erosion. *Journal of Coastal Research*, 46–56.
- Lingenfelter, R. E., & Flamm, E. J. (1964). Solar Neutrons and the Earth's Radiation Belts. *Science*, 144(3616), 292–294.
- Little, T. A., Dissen, R. V., Kearsse, J., Norton, K., Benson, A., & Wang, N. (2018). Kekerengu Fault, New Zealand: Timing and Size of Late Holocene Surface Ruptures. *Bulletin of the Seismological Society of America*, (Advance Online Publication).

- Little, T. A., Dissen, R. V., Schermer, E., & Carne, R. (2009). Late Holocene surface ruptures on the southern Wairarapa fault, New Zealand: Link between earthquakes and the uplifting of beach ridges on a rocky coast. *Lithosphere*, 1(1), 4–28.
- Manabe, S., Stouffer, R. J., Spelman, M. J., & Bryan, K. (1991). Transient Responses of a Coupled Ocean–Atmosphere Model to Gradual Changes of Atmospheric CO₂. Part I. Annual Mean Response. *Journal of Climate*, 4(8), 785–818.
- Masarik, J., & Reedy, R. C. (1995). Terrestrial cosmogenic-nuclide production systematics calculated from numerical simulations. *Earth and Planetary Science Letters*, 136(3), 381–395.
- Masselink, G., & Hughes, M. G. (2003). *Introduction to Coastal Processes & Geomorphology* (First). Great Britain: Hodder Education.
- Matsumoto, H., Dickson, M. E., & Kench, P. S. (2016a). An exploratory numerical model of rocky shore profile evolution. *Geomorphology*, 268, 98–109.
- Matsumoto, H., Dickson, M. E., & Kench, P. S. (2016b). Modelling the Development of Varied Shore Profile Geometry on Rocky Coasts. *Journal of Coastal Research*, 75(sp1), 597–601.
- McGranahan, G., Balk, D., & Anderson, B. (2007). The rising tide: assessing the risks of climate change and human settlements in low elevation coastal zones. *Environment and Urbanization*, 19(1), 17–37.
- Michel, R., Leya, I., & Borges, L. (1996). Production of cosmogenic nuclides in meteoroids: accelerator experiments and model calculations to decipher the cosmic ray record in extraterrestrial matter. *Nuclear Instruments and Methods in Physics Research Section B: Beam Interactions with Materials and Atoms*, 113(1), 434–444.
- Mii H. (1962). Coastal Geology of Tanabe Bay. *The science reports of the Tohoku University. Second series, Geology*, 34(1), 1-A14.
- Moore, L. J., Benumof, B. T., & Griggs, G. B. (1999). Coastal Erosion Hazards in Santa Cruz and San Diego Counties, California. *Journal of Coastal Research*, 121–139.

- Mortimer, N., Campbell, H. J., Tulloch, A. J., King, P. R., Stagpoole, V. M., Wood, R. A., ... Seton, M. (2017). Zealandia: Earth's Hidden Continent. *GSA Today*, 27–35.
- Mullan, B., Carey-Smith, T., Griffiths, G., & Sood, A. (2011). *Scenarios of Storminess and Regional Wind Extremes Under Climate Change* (NIWA Client Report No. WLG2010-31) (pp. 1–80). Wellington, N.Z.: National Institute of Water & Atmospheric Research Ltd.
- Murray, A. B. (2003). Contrasting the Goals, Strategies, and Predictions Associated with Simplified Numerical Models and Detailed Simulations. In P. R. Wilcock & R. M. Iverson (Eds.), *Prediction in Geomorphology* (pp. 151–165). American Geophysical Union.
- Murray, A. B. (2007). Reducing model complexity for explanation and prediction. *Geomorphology*, 90(3), 178–191.
- Naylor, L. A., Stephenson, W. J., & Trenhaile, A. S. (2010). Rock coast geomorphology: Recent advances and future research directions. *Geomorphology*, 114(1–2), 3–11. <https://doi.org/10.1016/j.geomorph.2009.02.004>
- Nishiizumi, K., Imamura, M., Caffee, M. W., Southon, J. R., Finkel, R. C., & McAninch, J. (2007). Absolute calibration of ^{10}Be AMS standards. *Nuclear Instruments and Methods in Physics Research Section B: Beam Interactions with Materials and Atoms*, 258(2), 403–413.
- Nishiizumi, K., Lal, D., Klein, J., Middleton, R., & Arnold, J. R. (1986). Production of ^{10}Be and ^{26}Al by cosmic rays in terrestrial quartz in situ and implications for erosion rates. *Nature*, 319(6049), 134–136.
- Ogawa, H., Dickson, M. E., & Kench, P. S. (2011). Wave transformation on a sub-horizontal shore platform, Tatapouri, North Island, New Zealand. *Continental Shelf Research*, 31(14), 1409–1419.
- Ogawa, H., Kench, P., & Dickson, M. (2012). Field Measurements of Wave Characteristics on a Near-Horizontal Shore Platform, Mahia Peninsula, North Island, New Zealand. *Geographical Research*, 50(2), 179–192.

- Ota, Y., Pillans, B., Berryman, K., Beu, A., Fujimori, T., Miyauchi, T., ... Climo, F. M. (1996). Pleistocene coastal terraces of Kaikoura Peninsula and the Marlborough coast, South Island, New Zealand. *New Zealand Journal of Geology and Geophysics*, 39(1), 51–73.
- Owen, L. A., Caffee, M. W., Bovard, K. R., Finkel, R. C., & Sharma, M. C. (2006). Terrestrial cosmogenic nuclide surface exposure dating of the oldest glacial successions in the Himalayan orogen: Ladakh Range, northern India. *Geological Society of America Bulletin*, 118(3–4), 383–392.
- Pillans, B. (1983). Upper Quaternary marine terrace chronology and deformation, South Taranaki, New Zealand. *Geology*, 11(5), 292–297.
- Porter, N. J., Trenhaile, A. S., Prestanski, K., & Kanyaya, J. I. (2010). Patterns of surface downwearing on shore platforms in eastern Canada. *Earth Surface Processes and Landforms*, 35(15), 1793–1810.
- Rattenbury, M. S., Townsend, D. B., & Johnston, M. R. (2006). Geology of the Kaikoura Area. Institute of Geological and Nuclear Sciences 1:250000 geological map 13. *GNS Science. Lower Hutt, New Zealand*, 1 sheet +70p.
- Regard, V., Dewez, T., Bourlès, D. L., Anderson, R. S., Duperret, A., Costa, S., ... Maillet, G. M. (2012). Late Holocene seacliff retreat recorded by ¹⁰Be profiles across a coastal platform: Theory and example from the English Channel. *Quaternary Geochronology*, 11, 87–97.
- Rosser, N. J., Petley, D. N., Lim, M., Dunning, S. A., & Allison, R. J. (2005). Terrestrial laser scanning for monitoring the process of hard rock coastal cliff erosion. *Quarterly Journal of Engineering Geology and Hydrogeology*, 38(4), 363–375.
- Sadler, P. M. (1981). Sediment Accumulation Rates and the Completeness of Stratigraphic Sections. *The Journal of Geology*, 89(5), 569–584.
- Schaefer, J. M., Denton, G. H., Kaplan, M., Putnam, A., Finkel, R. C., Barrell, D. J. A., ... Schlüchter, C. (2009). High-Frequency Holocene Glacier Fluctuations in New Zealand Differ from the Northern Signature. *Science*, 324(5927), 622–625.

- Schumer, R., & Jerolmack, D. J. (2009). Real and apparent changes in sediment deposition rates through time. *Journal of Geophysical Research: Earth Surface*, 114(F3), F00A06.
- Schumm, S. A. (1979). Geomorphic Thresholds: The Concept and Its Applications. *Transactions of the Institute of British Geographers*, 4(4), 485–515.
- Sharma, P., Bourgeois, M., Elmore, D., Granger, D., Lipschutz, M. E., Ma, X., ... Vogt, S. (2000). PRIME lab AMS performance, upgrades and research applications. *Nuclear Instruments and Methods in Physics Research Section B: Beam Interactions with Materials and Atoms*, 172(1), 112–123.
- Smart, D. F., Shea, M. A., & Flückiger, E. O. (2000). Magnetospheric Models and Trajectory Computations. *Space Science Reviews*, 93(1–2), 305–333.
- Statistics New Zealand. (2009). Are New Zealanders living closer to the coast? Retrieved November 3, 2016, from http://www.stats.govt.nz/browse_for_stats/population/Migration/internal-migration/are-nzs-living-closer-to-coast.aspx
- Stephenson, W. J. (1997). *Development of Shore Platforms on Kaikoura Peninsula, South Island, New Zealand*. (PhD thesis) University of Canterbury, Canterbury, New Zealand.
- Stephenson, W. J. (2000). Shore platforms: a neglected coastal feature? *Progress in Physical Geography: Earth and Environment*, 24(3), 311–327.
- Stephenson, W. J., Dickson, M. E., & Denys, P. H. (2017). New insights on the relative contributions of coastal processes and tectonics to shore platform development following the Kaikōura earthquake. *Earth Surface Processes and Landforms*, 42(13), 2214–2220.
- Stephenson, W. J., & Kirk, R. M. (2000b). Development of shore platforms on Kaikoura Peninsula, South Island, New Zealand: II: The role of subaerial weathering. *Geomorphology*, 32(1–2), 43–56.

- Stephenson, W. J., & Kirk, R. M. (2000a). Development of shore platforms on Kaikoura Peninsula, South Island, New Zealand: Part One: The role of waves. *Geomorphology*, 32(1–2), 21–41.
- Stephenson, W. J., & Kirk, R. M. (1996). Measuring erosion rates using the micro-erosion meter: 20 years of data from shore platforms, Kaikoura Peninsula, South Island, New Zealand. *Marine Geology*, 131(3), 209–218.
- Stephenson, W. J., & Kirk, R. M. (2001). Surface swelling of coastal bedrock on intertidal shore platforms, Kaikoura Peninsula, South Island, New Zealand. *Geomorphology*, 41(1), 5–21.
- Stephenson, W. J., Kirk, R. M., Hemmingsen, S. A., & Hemmingsen, M. A. (2010). Decadal scale micro erosion rates on shore platforms. *Geomorphology*, 114(1–2), 22–29.
- Stephenson, W. J., & Thornton, L. E. (2005). Australian Rock Coasts: review and prospects. *Australian Geographer*, 36(1), 95–115.
- Stirling, M. W., Litchfield, N. J., Villamor, P., Van Dissen, R. J., Nicol, A., Pettinga, J., ... Zinke, R. (2017). The Mw7.8 2016 Kaikōura earthquake: Surface Fault Rupture and Seismic Hazard Context. *Bulletin of the New Zealand Society for Earthquake Engineering*, 50(2), 73–84.
- Stone, J. (1998). A Rapid Fusion Method for Separation of Beryllium-10 From Soils and Silicates. *Geochimica et Cosmochimica Acta*, 62(3), 555–561.
- Stone, J., Lambeck, K., Fifield, L. K., Evans, J. t., & Cresswell, R. G. (1996). A lateglacial age for the main rock platform, western Scotland. *Geology*, 24(8), 707–710.
- Stone, J. O., Ballantyne, C. K., & Fifield, L. K. (1998). Exposure dating and validation of periglacial weathering limits, northwest Scotland. *Geology*, 26(7), 587–590.
- Sunamura, T. (1978). Mechanisms of Shore Platform Formation on the Southeastern Coast of the Izu Peninsula, Japan. *The Journal of Geology*, 86(2), 211–222.
- Sunamura, T. (1991). The Elevation of Shore Platforms: A Laboratory Approach to the Unsolved Problem. *The Journal of Geology*, 99(5), 761–766.

- Sunamura, T. (1992). *The Geomorphology of rocky coasts* (Vol. 3). John Wiley & Sons, Chichester, UK.
- Tenzer, R., Sirguey, P., Rattenbury, M., & Nicolson, J. (2011). A digital rock density map of New Zealand. *Computers & Geosciences*, 37(8), 1181–1191.
- Thornton, L. E., & Stephenson, W. J. (2006). Rock Strength: A Control of Shore Platform Elevation. *Journal of Coastal Research*, 22(1), 224–231.
- Trenhaile, A. S. (1974). The Geometry of Shore Platforms in England and Wales. *Transactions of the Institute of British Geographers*, (62), 129.
- Trenhaile, A. S. (1987). *The Geomorphology of Rock Coasts*. Oxford University Press. USA.
- Trenhaile, A. S. (1999). The Width of Shore Platforms in Britain, Canada, and Japan. *Journal of Coastal Research*, 15(2), 355–364.
- Trenhaile, A. S. (2001). Modelling the Quaternary evolution of shore platforms and erosional continental shelves. *Earth Surface Processes and Landforms*, 26(10), 1103–1128.
- Trenhaile, A. S. (2002). Modeling the development of marine terraces on tectonically mobile rock coasts. *Marine Geology*, 185(3), 341–361.
- Trenhaile, A. S. (2002). Rock coasts, with particular emphasis on shore platforms. *Geomorphology*, 48(1), 7–22.
- Trenhaile, A. S. (2010). The effect of Holocene changes in relative sea level on the morphology of rocky coasts. *Geomorphology*, 114(1–2), 30–41.
- van der Woerd, J., Klinger, Y., Sieh, K., Tapponnier, P., Ryerson, F. J., & Mériaux, A.-S. (2006). Long-term slip rate of the southern San Andreas Fault from ¹⁰Be-²⁶Al surface exposure dating of an offset alluvial fan. *Journal of Geophysical Research: Solid Earth*, 111(B4),
- Ward, C. M. (1988a). Marine terraces of the Waitutu district and their relation to the late Cenozoic tectonics of the southern Fiordland region, New Zealand. *Journal of the Royal Society of New Zealand*, 18(1), 1–28.

- Ward, C. M. (1988b). New Zealand marine terraces: uplift rates. *Science*, 240(4853), 803–804.
- Wells, S. G., McFadden, L. D., Poths, J., & Olinger, C. T. (1995). Cosmogenic ³He surface-exposure dating of stone pavements: Implications for landscape evolution in deserts. *Geology*, 23(7), 613–616.
- Wheeler, B. W., White, M., Stahl-Timmins, W., & Depledge, M. H. (2012). Does living by the coast improve health and wellbeing? *Health & Place*, 18(5), 1198–1201.
- Willenbring, J. K., & Jerolmack, D. J. (2016). The null hypothesis: globally steady rates of erosion, weathering fluxes and shelf sediment accumulation during Late Cenozoic mountain uplift and glaciation. *Terra Nova*, 28(1), 11–18.
- Wolman, M. G., & Miller, J. P. (1960). Magnitude and Frequency of Forces in Geomorphic Processes. *The Journal of Geology*, 68(1), 54–74.
- Woodroffe, C. D. (2002). *Coasts: Form, Process and Evolution*. Cambridge University Press. Cambridge, UK.
- Wright, L. W. (1969). Shore platforms and mass movement: a note. Retrieved from <https://researchcommons.waikato.ac.nz/handle/10289/9141>
- Young Adam P., Adams Peter N., O'Reilly William C., Flick Reinhard E., & Guza R. T. (2011). Coastal cliff ground motions from local ocean swell and infragravity waves in southern California. *Journal of Geophysical Research: Oceans*, 116(C9).